1916 - 2026

An Acad Bras Cienc (2026) 98(4): e20260029 DOI 10.1590/0001-3765202620260029
Anais da Academia Brasileira de Ciências | *Annals of the Brazilian Academy of Sciences*
Printed ISSN 0001-3765 I Online ISSN 1678-2690
www.scielo.br/aabc | www.fb.com/aabcjournal

HEALTH SCIENCES

Thiosemicarbazone-based Molecular Hybrids as Prototypes for Antitumor Drugs: Recent Advances in the Last Decade

CAIO VICTOR S. SOARES, JOÃO PEDRO P. GOMES, ANTONIO MIGUELSINHO M. DE SOUSA FILHO, LUIZ VITOR O. LIMA, CIDLA S. MARINHO, ANA KAROLINE R. NOVAIS, MARIA DO CARMO A. DE LIMA & JAMERSON F. DE OLIVEIRA

Abstract: Molecular hybridization is used in the development of drug prototypes through the combination of bioactive compounds, being useful in the development of new drugs with antitumor action, given the high complexity of the disease. Thiosemicarbazones are interesting structures for the development of hybrids, enabling the discovery of unexplored mechanisms of action and new alternatives in cancer treatment. In this study, we report data on new thiosemicarbazone hybrids from the last 10 years (2015-2025), identifying the main bioactive groups, pharmacological targets, and cell lines of interest. The study indicates a strong trend towards hybridization with nitrogenous heterocycles (52%), with emphasis on indole, quinoline, and pyridine groups. Regarding targets, VEGFR-2 (Vascular Endothelial Growth Factor Receptor 2) and different topoisomerases are particularly prominent. The main cell lines used in cytotoxicity studies were MCF-7 (36 studies), MDA-MB-231 (21 articles), A549 (21 articles), and HepG-2 (20 articles). Only 20 compounds showed IC_{50} values below 2 μM, with emphasis on those hybridized with nitrogenous groups. Thus, thiosemicarbazone hybrids, especially those conjugated with nitrogenous compounds, show promise for exploration in the development of antitumor prototypes.

Key words: Thiosemicarbazone, Molecular Hybridization, Antitumor Activity, Molecular Fragments, Molecular Targets.

INTRODUCTION

Molecular hybridization is a classic strategy for developing new drug candidates, in which structures from different pharmacophore subunits of bioactive compounds are integrated into a single molecule. This combination can offer numerous advantages, leading to synergistic effects that can increase efficacy and reduce side effects associated with the original compounds (Viegas-Junior et al. 2007, Pinheiro et al. 2024).

This strategy for obtaining compounds can be classified as drug-drug, when it results from the direct combination of different drugs, or pharmacophoric, when it involves the union of pharmacophoric groups from different substances. There are four different ways to obtain a hybrid compound, in which distinct pharmacophores can be incorporated into a single molecular structure. Conjugated hybrids are those in which two distinct moieties are connected by a linker; conjugated hybrids with a metabolically cleavable linker are designed to release the active moieties into the biological system; fused hybrids feature a direct bond

between the components, but without overlap between them; and blended hybrids are obtained by fusing two pharmacophores, with the aim of developing small molecules with favorable physiological properties (Nepali et al. 2014, Singh & Agrawal 2022).

The molecular hybridization strategy is widely used in the development of anticancer drugs, including candidates currently in clinical trials or already approved by the FDA (Food and Drug Administration). Notable examples include the drugs Lapatinib (Tykerb®) and Tucatinib (Tukysa®) (Figure 1), quinazoline-based hybrids that utilize the strategy of combining pharmacophore groups to obtain molecules with activity against breast cancer. In addition to these, Panobinostat (Farydak®) and Quisinostat (Figure 1) — hybrids derived from indole and hydroxamic acid — act as HDAC inhibitors in the treatment of multiple myeloma (Shalini & Kumar 2021, Singh et al. 2022).

In addition to indole, quinazoline, and hydroxamic acid, other promising molecular scaffolds present themselves as pharmacophore alternatives of interest for molecular hybridization strategies, capable of providing broad and innovative mechanisms of action. Among these, thiosemicarbazones stand out — a molecular fragment characterized by the presence of two structural moieties, an imino-hydrazinyl (HC=N–NH–) and a thioamide (S=C–N–), both of which confer multifunctionality to the structure, from both a chemical and biological perspective (Singh et al. 2022, Hassan et al. 2025).

Thiosemicarbazones are characterized by the high degree of electronic delocalization present in this group, which is responsible for establishing the tautomeric equilibrium between the thiol (–SH) and thione (S=C) forms of the molecule. As for the synthesis method, direct synthetic routes are employed that allow for the introduction of different substituent groups into their structure, enabling the production of compounds with distinct chemical and biological properties. Thus, the biological activity of thiosemicarbazones is strongly related to structural aspects, such as the nature of the aldehyde or ketone used in the synthesis and the specific properties of the terminal amino group. This increase in efficacy can be explained by the considerable conformational flexibility of the structure, which favors a greater number

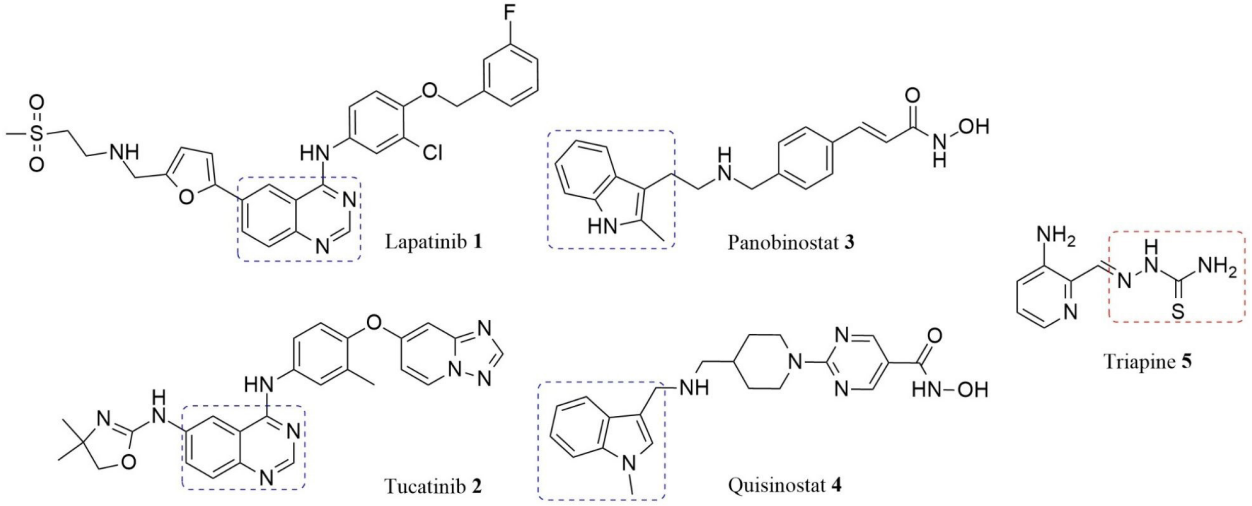


Figure 1. Structural representations of molecules obtained from the molecular hybridization strategy (1-4) and the most promising thiosemicarbazone structure (5) aimed at antitumor action.

of interactions with amino acid residues of the receptor (Hassan et al. 2025, Ucar et al. 2025).

Regarding antitumor activity, the main thiosemicarbazone derivative with clinical results is Triapine (Figure 1), a promising ribonucleotide reductase inhibitor capable of inducing apoptosis and increasing sensitivity to radiation therapy. Among the studies conducted, the Phase I and II clinical trials that evaluated the use of Triapine in synergistic combination with fludarabine in patients with refractory acute leukemias and aggressive myeloproliferative syndromes (MPS) stand out, demonstrating favorable results and moderate toxicity. The most robust clinical trial involving this derivative is the Phase III study that evaluated the combination of Triapina with cisplatin-based chemoradiotherapy (CRT) for the treatment of locally advanced cervical and vaginal cancer. However, the results were unfavorable, with no benefits observed compared to standard chemotherapy (Karp et al. 2008, McDevitt et al. 2011, Leath et al. 2025).

METHODOLOGY

It was proposed to conduct an integrative review of studies involving the development and evaluation of new hybrids containing the thiosemicarbazone fragment, with a focus on antitumor activity. Consequently, an understanding was established of the molecular profile observed among the hybrids, the *in silico*, *in vitro*, and *in vivo* biological results, as well as the SAR (structure-activity relationship) studies and the potential mechanisms of action of the compounds that stood out. Thus, the aim was to provide an overview of the molecular patterns involving thiosemicarbazone hybrids, as well as to highlight the main findings associated with these compounds, given the scarcity of studies elucidating current perspectives on the strategy of molecular hybridization with thiosemicarbazone as a key pillar for obtaining innovative compounds with promising antitumor activity.

Accordingly, scientific articles published between January 2015 and March 2025 — covering a 10-year period — were collected using the keywords "thiosemicarbazone," "hybrids," "molecular hybridization," "synthesis," and "cancer," as well as the Boolean operators 'AND' and "OR," in five different databases: Web of Science, PubMed, ScienceDirect, SciELO, and the Virtual Health Library (BVS), resulting in an initial total of 1,793 articles.

Subsequently, all the articles collected were uploaded to the *Rayyan* platform (https://www.rayyan.ai/), a free web-based tool that assists in the selection of references for reviews. This made it possible to analyze and remove duplicate articles, leaving 1,563 studies.

Regarding the inclusion criteria, only original studies published in peer-reviewed journals, reported within the selected time frame, and written in English, Portuguese, or Spanish were accepted. Additionally, studies were selected that investigated thiosemicarbazone hybrids evaluated for antitumor activity using at least one methodology, which could be through *in silico*, *in vitro*, or *in vivo* studies. Furthermore, regarding the exclusion criteria, any review articles, editorials, and abstracts were disregarded, as were studies that were not available for free access or that contained incomplete or insufficient data for analysis. In addition, studies that did not clearly and descriptively state the use of a molecular hybridization strategy or that involved the evaluation of metal complexes alone were also excluded.

Thus, a final total of 75 articles was obtained, all of which underwent further evaluation to confirm their compliance with the inclusion

and exclusion criteria. This allowed each study to be analyzed individually to identify which compounds exhibited the best activity, as well as the respective cell lines studied; which targets were most frequently evaluated; and what the overall outlook is for the antitumor potential of thiosemicarbazone hybrids (Figure 2).

RESULTS AND DISCUSSION

When analyzing the 75 articles obtained, they were divided into six main groups, namely: nitrogen-containing heterocycles (n: 39 articles), sulfur-containing heterocycles (n: 3 articles), oxygen-containing heterocycles (n: 4 articles), various heterocycles (n: 12 articles), steroid analogs (n: 6 articles), and various aromatic compounds (n: 11 articles). Furthermore, it is worth noting that, over the past 10 years, nitrogen nuclei have been given clear priority in hybridization processes with thiosemicarbazones, with the indole, quinoline, and pyridine groups being the most targeted, accounting for 41.33% of the studies evaluated and 36.12% of the hybrids discussed in this review.

Furthermore, it should be noted that sulfur- and oxygen-containing heterocycles and steroid analogs account for a small number of studies, together totaling 17.33% of the analyzed studies and representing only 5.51%, 7.58%, and 6.20% of the hybrids presented throughout the text, respectively. Among the various heterocycles, no specific ring stood out, but a significant percentage of studies was observed, representing 16% of the collected articles and 16.55% of the highlighted hybrids. Similarly, the "various aromatics" did not feature any core system that stood out among the nine analyzed, with one to two hybrids per molecular fragment reported

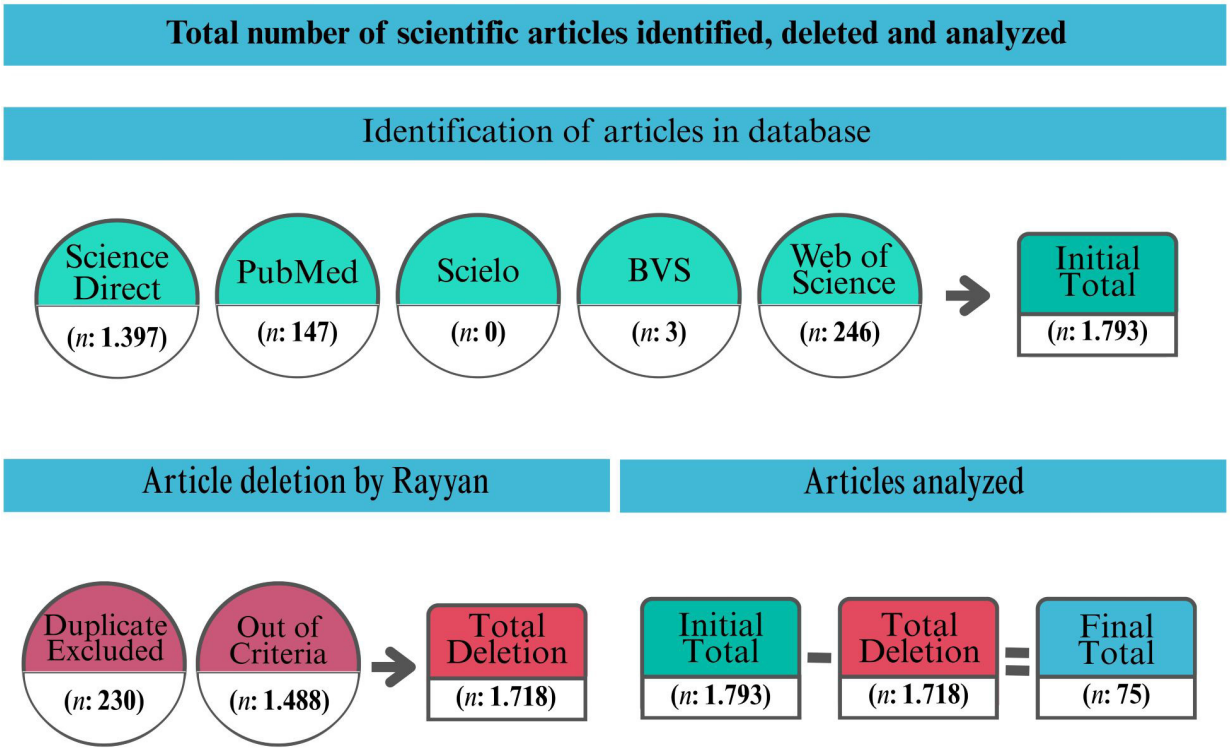


Figure 2. Diagram representing the methodology used in the review containing thiosemicarbazone hybrids aimed at antitumor activity.

in the study. However, this also represents a significant portion of the analyzed articles (14.66%) and the discussed hybrids (15.17%). In addition, it is worth noting the greater emphasis placed on studies using the MCF-7 cell line, observed in 36 studies (48.64%); MDA-MB-231 and A549 cell lines, both cited in 21 articles (28.37%); and the HepG-2 cell line, cited 20 times (27.02%). Furthermore, although a wide range of targets of interest for cancer was demonstrated, the most common targets in molecular docking studies were VEGFR-2 (Vascular Endothelial Growth Factor Receptor 2), present in 6.75% of the studies, and various types of topoisomerase, present in 4.05% of the articles.

Next, we will examine the classes of molecular fragments that undergo molecular hybridization with thiosemicarbazone.

Nitrogen-containing Heterocycles

Nitrogen heterocycles commonly have structures related to important pharmacophores, present in about 59% of low molecular weight drugs. The importance of these compounds is justified by their ability to bind to metals, mimic endogenous metabolites, and natural products. Among them are indole, isatin, quinoline, pyridine, pyrrolidine, pyrazole, piperazine, acridine, and others, which will be discussed below (Amin et al. 2022, Marshall et al. 2024).

Indole and related structures

Thiosemicarbazone hybrids containing the indole ring have been shown in the literature to exhibit biological activity that may be associated with their electronic properties and their ability to anchor to the active sites of their respective biological targets. The presence of structural modifications in the molecular frameworks — particularly at positions C-2 and N-1 of the indole ring and N-4 of the thiosemicarbazone ring — may be associated with the success of molecules such as compounds **6** and **8** and the failure of compound **7**, illustrating that simply filling hydrophobic pockets is insufficient to ensure the necessary activity without the support of targeted interactions (Figure 3).

In the study by Bakherad et al. (2019), compound **6** demonstrated that the introduction of specific groups (C-2: *p*-methoxyphenyl; N-4: methyl) allows for the occupation of hydrophobic pockets in targets such as tubulin and topoisomerase IIα (GoldScores of 52.70 and 59.61, respectively), in addition to establishing a crucial hydrogen bond with the Lys168 residue in TOPO IIα. This polar anchor stabilizes the complex, which may be associated with a promising cytotoxic profile in the A-549 cell line (IC_{50}= 12.50 ± 1.00 μM) and the induction of apoptosis in 27.5% of the cells. In contrast, compound **7** (N-4: phenyl), studied by Gomha et al. (2023), exemplifies this limitation by relying strictly on hydrophobic interactions with CDK2. Although it had a score of -9.20 kcal.mol^{-1}, the absence of multiple hydrogen bonds (only one observed with Gln131) resulted in a profile that prevented its advancement to biological evaluation stages (Bakherad et al. 2019) (Figure 3).

The importance of electronic modulation is supported by the studies by Batool et al. (2024) on tyrosinase inhibition. Compound **8** (N-1: benzyl; N-4: *p*-methylbenzyl), which exhibited greater inhibition than kojic acid (IC_{50}= 12.40 ± 0.26 μM versus 18.30 ± 0.41 μM for the control), demonstrated in SAR studies that substitutions at the *para* position of the aromatic ring enhance inhibitory activity and that, as the electronegativity of the substituents increases, the inhibitory potential decreases. With a Ki of 10.20 ± 0.006 μM and a docking energy of -5.157 kcal.mol^{-1}, compound **8** demonstrates that optimizing the electronic density at the *para* position of the aromatic ring is critical for

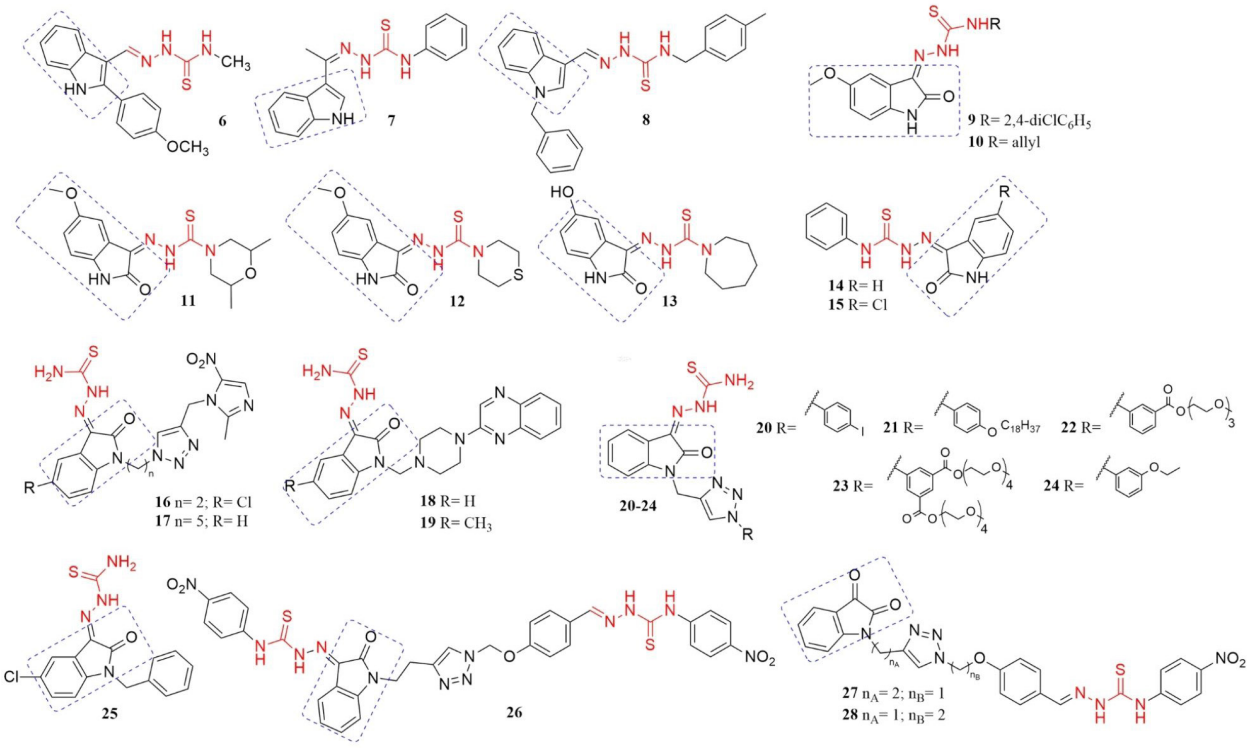


Figure 3. Thiosemicarbazone hybrids nitrogen-containing heterocycles — indoles and related structures (6-28).

competitive inhibition. In the *in silico* studies, ADMET predictions showed that the hybrid also exhibits favorable pharmacokinetic parameters. Thus, the success of compounds **6** and **8** lies in their ability to combine the lipophilicity of the hybrid with the presence of substituents that enable specific and favorable interactions within the protein environment (Figure 3) (Batool et al. 2024).

The synthesis of thiosemicarbazone-indolone hybrids — a carbonyl derivative of indole — has established itself as a prominent strategy in the search for antitumor agents, revealing that structural modulation, particularly at the C-5 position of the nitrogen-containing ring and the N-4 position of the thiosemicarbazone, can be crucial for the potency and selectivity of cytotoxic activity. A common feature among the different hybrids discussed in this review was the presence of electron-donating groups at the C-5 position of the indolone. The study proposed by Koçyigit et al. (2022), which yielded 15 thiosemicarbazone-isatin hybrids varying at the N-4 position of the thiosemicarbazone moiety, highlighted compound **9** (C-5= methoxy; R= 2,4-dichlorophenyl), which achieved an IC_{50} of 59.25 ± 0.40 µM in MCF-7 and 49.79 ± 1.01 µM in MDA-MB-231, exceeding the 117.28 ± 0.86 µM and 132.11 ± 1.26 µM values, respectively, of the cisplatin positive control. The influence of electronic substitutions at the C-5 position of isatin is confirmed by Yakan et al. (2023), who, upon comparing methoxy, fluorine, and chlorine groups, identified that the methoxy substituent in compound **10** (C-5= methoxy; R= allyl) exhibited superior activity (IC_{50}= 8.19 µM in MCF-7 and IC_{50}= 23.41 µM in MDA-MB-231) compared to the other halogens, reinforcing that the electronic density of the isatin core critically modulates the sensitivity of tumor cell lines (Figure 3) (Koçyiğit et al. 2022).

The efficacy of these structures is validated by mechanistic studies demonstrating robust interference with pro-proliferative signaling pathways. Chaudhary et al. (2023), building on the use of C-5 donor groups in the indolone core, proposed four 5-methoxyisatin thiosemicarbazone hybrids, distinguished by structural variations at N-4 of the Schiff base moiety. Compound **11** (N-4: 2,6-dimethylmorpholinyl) exhibited an IC_{50} of 4.80 μM in A549 and 2.52 μM in A431, while hybrid **12** (N-4: thiomorpholynil) proved to be more active against MCF-7 (IC_{50}= 2.93 μM). Molecular docking studies were performed only with hybrid **11**, which exhibited a binding energy of -6.3185 kcal.mol^{-1}. It was observed that the compound formed two hydrogen bonds with residues Ile1025 and Arg1027. Contrary, the co-crystallized ligand had a calculated binding energy of -9.0855 kcal.mol^{-1} and established five significant hydrogen bonds (Figure 3) (Chaudhary et al. 2023).

The effect on cell death in A431 cells was investigated, demonstrating that compound **11** was able to completely inhibit colony formation at concentrations of 3 μM and 10 μM. In addition, the compound promoted a concentration-dependent increase in the population of apoptotic cells and induced cell cycle arrest at the G0/G1 phase in cells treated with 0.3 μM and 1 μM, a phenomenon that may be associated with DNA damage. A431 cells treated with hybrid **11** exhibited concentration-dependent inhibition of the expression of β-catenin, C-Jun, and Akt — important signaling pathways related to cell proliferation, migration, and tumor apoptosis (Figure 3).

This ability to modulate cells can also be observed with compound **13** (Chaudhary et al. 2024), which follows a similar approach by replacing the methoxy group with a hydroxy group at C-5 of the nitrogen-containing ring. The authors synthesized ten indolone thiosemicarbazone hybrids, distinguished by substitutions at the N-4 position of the thiosemicarbazone moiety. Initially, the compounds were evaluated for their effect on the cell viability of the PC-3, MCF-7, A549, MDA-MB-231, NCI-H460, A431, and PNT-2 cell lines at a concentration of 10 μM. Compound **13** (N-4: azepane) stood out for promoting a significant reduction in cell proliferation, particularly in the A431 cell line, which exhibited cell viability of 20.62 ± 1.15%, and in the MCF-7 cell line, with viability of 22.51 ± 5.49%. Compound **13** exhibited high selectivity (SI > 526) against A431 cells (IC_{50}= 0.19 μM) when compared to the non-tumor PNT-2 cell line (IC_{50} > 100 μM). Its mechanism of action was also investigated, and Western blot analyses demonstrated that the hybrid was capable of reducing the expression of key components of the MAPK pathway, including ERK1/2, whose expression decreased from 0.57 to 0.23 when the concentration was increased from 1 to 3 μM, and c-Jun, whose expression decreased from 0.58 to 0.38 at the same concentrations. These proteins are directly related to cell proliferation, angiogenesis, and tumor survival (Chaudhary et al. 2024) (Figure 3).

In addition, a significant increase in the activity of the apoptotic protein caspase-3 was observed, rising from 0.075 ± 0.012 to 1.58 ± 0.12 at a concentration of 1 μM compared to the control. The compound also induced changes in the cell cycle profile of the A431 cell line, reducing the population of cells in the G0/G1 phase from 46.57 ± 3.40% to 31.26 ± 0.48% (1 μM) and 19.32 ± 3.48% (3 μM), while increasing the population of cells in the S phase from 38.53 ± 5.79% to 44.51 ± 2.82% (1 μM) and 78.79 ± 4.15% (3 μM). The ability to inhibit cell migration was also evaluated using a wound healing assay on A431 cell monolayers. Compound **13**, at a concentration of 3 μM, significantly reduced wound closure, leaving between 60 and 70% of

the injured area open even after 36 hours of incubation. Finally, molecular docking studies revealed that the hybrid exhibits a high affinity profile against multiple molecular targets. Against VEGFR-2 (PDB ID: 4ASD), the compound exhibited an interaction score of -11.10 kcal.mol^{-1}, forming interactions with the residues Lys868, Val899, Glu885, Leu889, Val848, Val916, Cys1045, and Phe1047. Against cyclin-dependent kinase 2 (CDK2; PDB ID: 2VTA), it exhibited a score of -10.40 kcal.mol^{-1} and interactions with Glu81, Leu83, Asp145, Ile10, Val18, Ala31, Phe82, Ala134, and Leu144. Against the kinase domain of VEGFR-2 (PDB ID: 3VHE), it had a score of -10.10 kcal.mol^{-1}, interacting with Leu840, Lys868, Val899, Cys1045, and Phe1047 (Figure 3) (Chaudhary et al. 2024).

Furthermore, there is a clear improvement in the antitumor activity of the compounds obtained by Chaudhary et al. (2024), particularly considering the submicromolar activity against the A431 cell line (IC_{50}= 0.19 μM) observed for compound **13**, as well as the high selectivity and multiple mechanisms of action associated with apoptosis, regulation of the MAPK pathway, and inhibition of cell migration. The replacement of the methoxy electron-donor group with a hydroxyl group at C-5 of the indolone ring may be associated with the maintenance and/or increase in biological activity, but a possible role for the structural substitutions at N-4 of the thiosemicarbazone moiety cannot be ruled out (Figure 3).

The impact of the C-5 donor group on the nitrogen-containing ring may be further supported by the study proposed by Freitas et al. (2024), who synthesized two N-phenylthiosemicarbazone hybrids containing an unsubstituted indolone (**14**) or a C-5-chloro group (**15**), which were used as intermediates for the preparation of thiazole-indolone derivatives. Both compounds **14** and **15** were found to be non-cytotoxic to human peripheral blood mononuclear cells (PBMCs) (>100% at 10 μM). Among the hybrids, compound **15** was the most cytotoxic, exhibiting cell proliferation rates of 42.9% for T-47D, 6.3% for MCF-7, and 8.0% for MDA-MB-231 at a concentration of 10 μM. In turn, compound **14** exhibited cell proliferation rates of 47.7% for T-47D, 18.0% for MCF-7, and 34.0% for MDA-MB-231. Furthermore, compound **15** exhibited a CC_{50} > 100 μM for PBMC, an IC_{50}= 11.42 ± 1.02 μM for MCF-7, and an IC_{50}= 15.60 ± 4.95 μM for MDA-MB-231, highlighting the importance of the presence of a substituent group at C-5, but it was considered less promising when compared to the other more active compounds evaluated in the study (Figure 3) (Freitas et al. 2024).

In addition to the structural modifications mentioned above, there has been an expansion of the molecular framework of indolone-thiosemicarbazone hybrids through the inclusion of complex heterocyclic moieties, such as 1,2,3-triazoles, quinoxalines, and piperazines, demonstrating a strategic evolution in the search for highly selective multi-target inhibitors. Unlike the hybrids discussed earlier, these compounds are not limited to modifications at the C-5 position of the nitrogen-containing ring; they also exploit the N-1 position of the indolone as a synthetically accessible site for functionalization, facilitating the incorporation of different pharmacophores with various aliphatic spacer groups, without necessarily altering the thiosemicarbazone moiety (Figure 3).

The influence of these structural modifications is evident in the studies by Kumar et al. (2018), who developed 11 thiosemicarbazone-indolone hybrids, taking advantage of the synthetic versatility of the N-1 position in the indolone for functionalization with other pharmacophore groups, such as 1,2,3-triazole and imidazole. The structural variations evaluated in the compounds consisted

of the number of carbon atoms in the spacer between the isatin and 1,2,3-triazole moieties (n= 2-5), as well as the presence of substituents at C-5 of the isatin ring (R= H, Cl, or F). Overall, the compounds exhibited only moderate activity against the cell lines; among them, compound **16** (n= 2; R= Cl) showed the greatest potential against MCF-7 (IC_{50} = 70.02 μM), while compound **17** (n= 5; R= H) showed the best results against MDA-MB-231 (IC_{50}= 70.40 μM), highlighting the influence of chlorine on the selectivity profile of the hybrids, favoring greater activity against the MDA-MB-231 line compared to MCF-7, indicating that small electronic modifications in the isatin core can modulate the biological response. Furthermore, compound **17** was evaluated against the non-tumor HEK-293 cell line, exhibiting an IC_{50} greater than 100 μM. In molecular docking studies against the IGF-1 receptor kinase (PDB ID: 1JQH), compound **17** exhibited a binding energy of -6.70 $kcal.mol^{-1}$, forming significant van der Waals interactions with residues Leu22, Val30, Ala48, and Met99, as well as hydrogen bonds with Ser26, Lys176, Lys50, Gly167, and Met99 (Figure 3) (Kumar et al. 2018).

The efficacy of modifications at the N-1 position of the nitrogen-containing ring is maximized when such hybrids are designed to act on kinases such as c-Kit. Esam et al. (2023) reported hybrids containing quinoxaline and piperazine (compounds **18** and **19**) that surpassed the activity of imatinib, with compound **18** (R= H) exhibiting an IC_{50} of 3.034 μM against HCT-116 and an IC_{50} of 3.384 μM against SCOV-3 and **19** (R= methyl) with an IC_{50} of 3.229 μM against HCT-116 and an IC_{50} of 3.464 μM against SCOV-3, in addition to exhibiting a satisfactory selectivity profile, 7.2 to 11.6 times higher (Figure 3) (Esam et al. 2023).

Furthermore, the study by El Malah et al. (2024) on triazole derivatives shows that cytotoxic potential may be related to the variations proposed in this heterocycle. Although compounds **20**, **21**, **22**, and **23** exhibited moderate activity in inhibiting cell growth, with IC_{50} values of 52.98 ± 3.17, 55.10 ± 3.40, 75.10 ± 4.40, and 52.68 ± 2.83 μM, respectively, against non-tumoral WI38 cell line. For the HCT116 cell line, compound **23** exhibited the highest cytotoxicity, with an IC_{50} of 15.42 ± 1.18 μM, as well as for MCF-7, for which an IC_{50} of 11.76 ± 0.82 μM was observed. In addition, compounds **22** and **24** showed promising activity against MCF-7 with IC_{50} values of 27.87 ± 2.11 μM and 56.89 ± 5.00 μM, respectively (Figure 3) (El Malah et al. 2024).

Contrary to the studies presented by Kumar et al. (2018), Esam et al. (2023), and El Malah et al. (2024), Mahmoud et al. (2020) synthesized a new indolone-thiosemicarbazone derivative, which differs from the previous ones due to the replacement of spaced heterocyclic moieties with the addition of a benzyl group at the N-1 position of the nitrogen-containing ring. Compound **25** was used in the synthesis of new 2-indolinone-thiazole hybrids and evaluated for its inhibitory activity against the VEGFR-2 enzyme, yielding an IC_{50} of 0.174 ± 0.005 μM, a result lower than that of the reference drug sunitinib (IC_{50}= 0.075 ± 0.002 μM). Consequently, the hybrid was not selected for subsequent stages of biological evaluation (Figure 3) (Mahmoud et al. 2020).

Other structural modification strategies for thiosemicarbazone-indolone hybrids involve the synthesis of compounds that preserve both carbonyl groups on the nitrogen-containing ring, given the previously described ability of the N-1 position of the indolone to serve as a synthetically accessible site for functionalization and/or the possibility of synthesizing bis-thiosemicarbazones.

In this regard, the work by Mushtaq et al. (2024)—which utilized quantum physicochemical criteria to guide the development of new compounds, selecting hybrids based on kinetic

stability defined by an FMO energy gap (HOMO-LUMO) of less than 2.2 eV — stands out. This precision enabled compound **26** to achieve a binding energy of -10.30 kcal.mol^{-1} against PI3K, reinforcing the idea that optimizing linkers and electronic substitutions can ensure stable anchoring at the active site via hydrogen bonds with critical residues such as His670 and Met811. In addition, compounds **27** (R= NO_2, ligand A n= 2, ligand B n= 1) and **28** (R= NO_2, ligand A n= 1, ligand B n= 2) also showed good results, with binding energies of -8.60 kcal.mol^{-1} and -8.90 kcal.mol^{-1}, respectively. Among the interactions observed, compound **27** interacts with the amino acids Gln630, Gln815, Lys271, Leu755, His670, Phe666, Leu814, Glu849, and Ser629, while **28** interacts with Lys548, Asn575, Cys361, Leu367, Cys368, Pro366, Asp454, and Pro458 (Figure 3) (Mushtaq et al. 2024).

The development of thiosemicarbazone hybrids based on isatin scaffolds has presented a constant challenge in balancing cytotoxic potency with biological selectivity. In the studies by Cardoso et al. (2015), thalidomide hybrids **29**, **30**, and **31** — distinguished by substitutions at the N-2 (R_1) and N-4 (R_2) positions of the thiosemicarbazone moiety — demonstrated a remarkable ability to inhibit tumor cell lines, exhibiting cell proliferation rates of 17.8 ± 4.1% (at 190.62 µM), 28.5 ± 10.2% (at 180.95 µM), and 22.0 ± 6.1% (at 180.95 µM) for the MDA/MB-435 line, respectively, and 30.1 ± 0.8% (at 190.62 µM), 21.8 ± 6.1% (at 180.95 µM), and 26.4 ± 0.2% (at 180.95 µM) for the HCT-8 line, respectively. The success of these compounds, however, was limited by

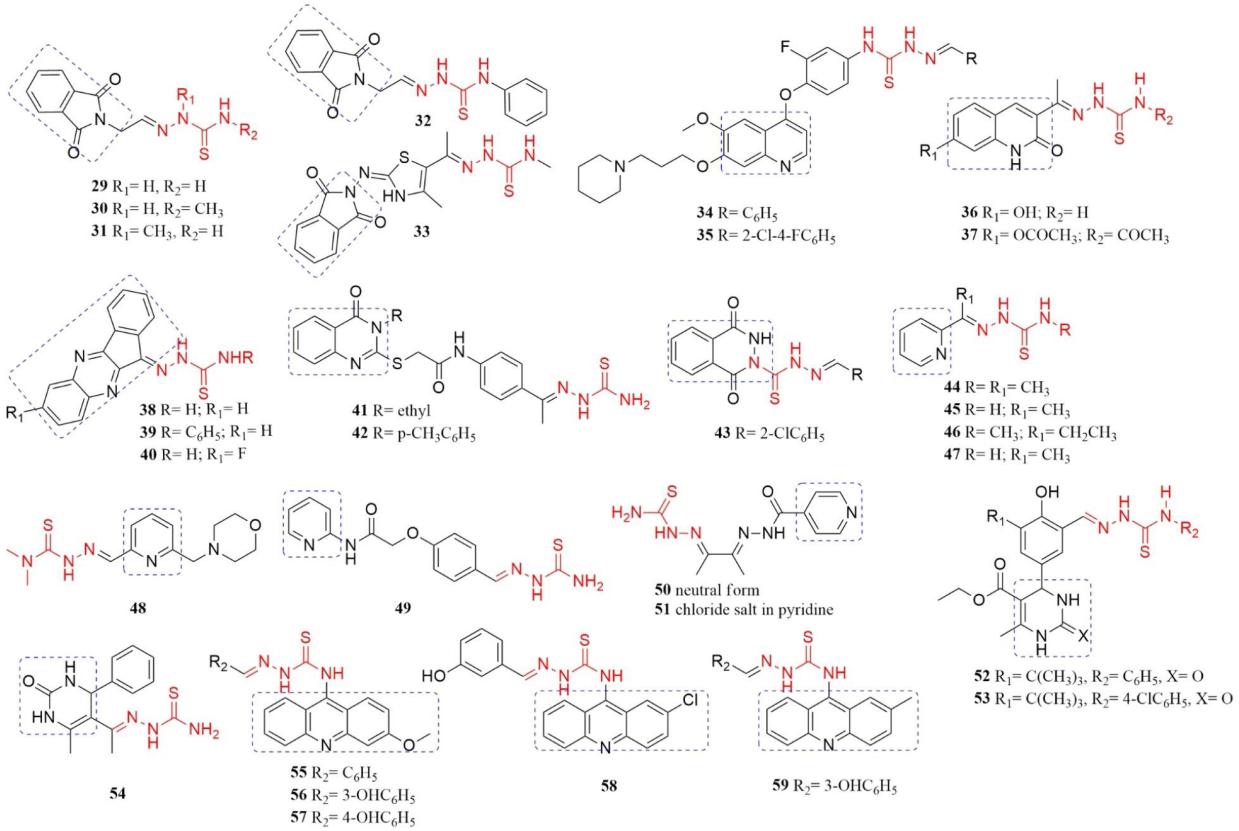


Figure 4. Thiosemicarbazone hybrids nitrogen-containing heterocycles — indoles and related structures (29-33), quinoline and related structures (34-43), pyridine and related structures (44-54), and acridine (55-59).

varying selectivity profiles, with the selectivity index ranging from 2.4 to 4.9, indicating that, although effective, the margin between tumor toxicity and cytotoxicity in normal lymphocytes is still narrow (Figure 4) (Cardoso et al. 2015).

The quest for greater precision advanced with Santos et al. (2016), who investigated phthalimide hybrids targeting the HT-29 cell line. Compound **32** (N-4= phenyl) stood out for having an IC_{50} value of 13.44 μM. However, critical analysis revealed structural deficiencies, as selectivity was compromised by an IC_{50} of 28.66 μM in J774A.1 macrophages. The most concerning finding of this study was the identification of necrosis as the predominant mechanism of cell death, which disqualified the compound for further stages (Figure 4) (Santos et al. 2016).

This "trial-and-error" approach reached a new level with Oliveira et al. (2021), whose efforts focused on phthalimide-thiazole hybrids. Compound **33** (N-4= methyl) stood out in the initial screening by reducing cell viability by more than 59% at a concentration of 10 μM, outperforming doxorubicin (IC_{50}= 6.4 μM) with an IC_{50} of 6.0 μM for the MOLT-4 cell line, in addition to exhibiting a significant SI greater than 16.6. Despite its superior performance, the derivative did not advance, demonstrating that, in drug development, the rigor of comparative screening often discards promising molecules in favor of even more optimized pharmacokinetic profiles (Figure 4) (Oliveira et al. 2021).

Quinoline and related structures

Thiosemicarbazone hybrids with quinolines and/or related structures generally aim to increase molecular planarity and extend the π-conjugated system, thereby enabling greater recognition and selectivity toward tumor targets. The inclusion of rigid nuclei — such as phenoxyquinoline, quinazolin-4(3H)-one, indenoquinoxaline, and phthalazinone — can electronically modulate hydrophobic and π-π interactions with target proteins.

First, we can highlight the work proposed by Zhai et al. (2016), who synthesized thiosemicarbazone hybrids containing the disubstituted phenoxyquinoline moiety, with structural variations at the carbon atom of the azomethine group (R) in the thiosemicarbazone portion. Among the derivatives, compound **34** (R= phenyl) stood out for having the best IC_{50} values: 0.33 ± 0.02 μM (A549), 0.21 ± 0.02 μM (HT-29), 0.71 ± 0.08 μM (MKN-45), 1.20 ± 0.17 μM (MDA-MB-231), and 78.36 ± 6.54 μM (PBL). Compound **35** (R= 2-chloro-4-fluorophenyl) also exhibited high activity, with IC_{50} values of 0.23 ± 0.02 μM (A549), 0.42 ± 0.09 μM (HT-29), 0.82 ± 0.21 μM (MKN-45), 1.40 ± 0.15 μM (MDA-MB-231), and 34.12 ± 2.72 μM (PBL). Furthermore, compound **34** proved to be more potent than Foretinib and PAC-1 against the HT-29 cell line (IC_{50}= 0.26 ± 0.03 and 0.83 ± 0.07 μM, respectively), while both hybrids were more active than PAC-1 against the MDA-MB-231 cell line (IC_{50}= 4.60 ± 0.33 μM) (Figure 4) (Zhai et al. 2016).

In contrast to the promising results observed for the thiosemicarbazone-phenoxyquinoline hybrids described by Zhai et al. (2016), replacing this ring with quinolin-2-one did not result in an increase in antitumor activity. Although the influence of differences in substituent groups and functionalization patterns between the studies cannot be ruled out, the quinolin-2-one derivatives exhibited a less pronounced biological profile, as can be seen in the study by Aldhahrani et al. (2025), who obtained two thiosemicarbazone hybrids containing quinolin-2-one, with substitutions at C-7 (R_1) of the quinoline and at N-4 (R_2) of the thiosemicarbazone. The results showed that compound **36** (R_1= hydroxy; R_2= H) exhibited moderate activity (IC_{50}= 160.77 ± 14.05 μM), while compound **37** (R_1= acetoxy; R_2= acetyl) exhibited

weak activity (IC_{50}= 615.80 ± 28.49 μM), when compared to doxorubicin (IC_{50}= 3.78 ± 0.06 μM) (Figure 4) (Aldhahrani et al. 2025).

In addition to the hybrids discussed earlier, several studies have explored the conjugation of thiosemicarbazone to the indenoquinoxaline ring. However, as evidenced for quinolin-2-one, this strategy yielded less promising results compared to quinoline hybrids, suggesting that the simple incorporation of this condensed aromatic system was not sufficient to confer high antitumor activity.

The study by Fayed et al. (2020) exemplifies this likely disadvantage. The authors synthesized and evaluated the antitumor activity of two new thiosemicarbazones conjugated to the indenoquinoxaline moiety, distinguished by substitutions at the N-4 (R) position of the thiosemicarbazone (**38**, R= H; **39**, R= phenyl), which were used as intermediates in the synthesis of new thiazole-indenoquinoxaline hybrids. The compounds were evaluated against the HCT-116 cell line (**38**: IC_{50}= 23.31 ± 1.40 μM; **39**: IC_{50}= 16.33 ± 1.05 μM; imatinib: IC_{50}= 4.70 ± 0.35 μM), HepG-2 (**38**: IC_{50}= 16.95 ± 1.09 μM; **39**: IC_{50}= 12.09 ± 0.93 μM; imatinib: IC_{50}= 5.80 ± 0.46 μM) and MCF-7 (**38**: IC_{50}= 26.55 ± 1.50 μM; **39**: IC_{50}= 17.90 ± 1.25 μM; imatinib: IC_{50}= 6.00 ± 0.53 μM). Since both exhibited lower activity than the reference drug, they were not selected for subsequent stages of biological evaluation (Figure 4) (Fayed et al. 2020).

Furthermore, Abdallah et al. (2023) described the evaluation of the antitumor potential of compound **38** through molecular docking studies against the estrogen receptor (ER) (PDB ID: 5FQP). Hybrid **38** did not exhibit any significant interaction with the receptor (docking score= -10.78 $kcal.mol^{-1}$), failing to outperform the co-crystallized ligand PTHIQ (a phenol derivative of tetrahydroisoquinoline), which had a docking score of -13.83 $kcal.mol^{-1}$. However, the compound established important interactions with Leu387, Leu384, and Met343 residues at the binding site (Figure 4) (Abdallah et al. 2023).

This same trend was evident in the study proposed by Abusaif et al. (2025), who proposed the synthesis of a thiosemicarbazone hybrid containing indenoquinoxaline (**40**). The hybrid was evaluated *in vitro* against the tumor cell lines HepG-2 and HuH-7 tumor cell lines, as well as the non-tumor THLE-2 cell line, with IC_{50} values of 27.75 ± 1.64 μM, 37.55 ± 0.50 μM, and 48.95 ± 2.57 μM, respectively. The hybrid exhibited a less cytotoxic profile than the other compounds evaluated in the study. In summary, both studies presented indicate that the indenoquinoxaline-thiosemicarbazone conjugate proved less effective in yielding significant gains in potency or selectivity when compared to the other related structures discussed thus far (Figure 4) (Abusaif et al. 2025).

In contrast to the results observed for compounds containing quinolin-2-one and indenoquinoxaline, the incorporation of the quinazolin-4(3H)-one ring proved to be a promising strategy for the development of antitumor agents hybridized with thiosemicarbazones. This nitrogen-containing ring appears to promote interactions with targets related to tumor activity, such as vascular endothelial growth factor receptor 2 (VEGFR-2).

In this context, Mahdy et al. (2020) synthesized and evaluated the antitumor activity of a new thiosemicarbazone hybrid containing quinazolin-4(3H)-one. Compound **41** was tested in an MTT assay using a panel of three human tumor cell lines — HepG-2, HCT-116, and MCF-7 — and exhibited IC_{50} values ranging from 14.12 ± 0.65 to 17.84 ± 1.53 μM, similar to those of the reference drugs doxorubicin (IC_{50}= 7.67 ± 0.36 to 9.62 ± 0.36 μM) and sorafenib (IC_{50}= 7.31 ± 0.43 to 11.40 ± 0.43 μM). The hybrid was also investigated for its *in vitro* inhibitory activity against the VEGFR-2

receptor, showing an IC_{50} value of 4.1 ± 0.06 μM, similar to that observed for sorafenib (IC_{50}= 2.4 ± 0.05 μM). Finally, molecular docking studies were performed using the crystallographic structure of VEGFR-2 (PDB ID: 2OH4). The hybrid exhibited a binding energy of -53.80 kJ.mol^{-1}, similar to that of the reference ligand (-52.20 kJ.mol^{-1}), corroborating the enzymatic inhibition potential observed in the *in vitro* assay (Figure 4) (Mahdy et al. 2020).

This trend was subsequently demonstrated by El-Adl et al. (2021), who synthesized and evaluated the antitumor activity of a new thiosemicarbazone hybrid containing quinazolin-4(3H)-one. Thus, compound **42** was initially tested in an MTT assay using three human tumor cell lines — HepG-2, HCT-116, and MCF-7 — and exhibited IC_{50} values ranging from 8.32 ± 0.33 to 9.89 ± 0.39 μM, similar to those of the reference drugs doxorubicin (IC_{50}= 7.67 ± 0.30 to 9.63 ± 0.38 μM) and sorafenib (IC_{50}= 7.21 ± 0.28 to 9.40 ± 0.37 μM). Similar to the previous study, the hybrid exhibited significant inhibitory activity against the VEGFR-2 receptor, with an IC_{50} value of 1.00 ± 0.13 μM, similar to that observed for sorafenib (IC_{50}= 1.26 ± 0.08 μM). Finally, molecular docking studies were performed using the crystallographic structure of VEGFR-2 (PDB ID: 2OH4), with sorafenib as the reference compound. The hybrid exhibited a binding energy of -47.72 kJ.mol^{-1}, close to that of the reference ligand (-52.20 kJ.mol^{-1}), corroborating the enzymatic inhibition potential demonstrated *in vitro* (Figure 4) (El-Adl et al. 2021).

The best antitumor activity results obtained for thiosemicarbazone hybrids with quinolines and/or related compounds were achieved through conjugation with the phthalazinone ring, as demonstrated in the study by Elkafoury et al. (2024), who synthesized 27 hybrids, distinguished by substitutions in the azomethine (R) moiety of the thiosemicarbazone. The incorporation of a rigid and electronically favorable aromatic heterocycle appears to enhance the recognition of multiple molecular targets involved in tumor progression, particularly the enzymes PARP-1 and TOPO-I, with compound **43** (R= 2-chlorophenyl) stood out with IC_{50} values of 32.2 ± 3.26 nM and 46.2 ± 3.3 nM, respectively, while maintaining high selectivity for PARP-1 over PARP-2 (IC_{50}= 2844 ± 111 nM; SI= 88.32). The structure-activity relationship revealed that halogenated derivatives were the most active, with satisfactory growth inhibition percentages (GI%), particularly compound **43**, against the HCT-116 (GI= 175%), U251 (GI= 155%), UACC-62 (GI= 164%), BT-549 (GI= 157%), and RXF393 (GI= 158%). Furthermore, compound **43** was evaluated against a panel of sixty cancer cell lines, against all of which exhibited significant inhibitory activity, particularly against the HL-60 (GI_{50}= 1.65 μM), K-562 (TGI= 1.06 μM), and SK-MEL-2 (LC_{50}= 9.48 μM). Compound **43** was also tested against metastatic triple-negative breast cancer cell lines, showing positive results for MDA-MB-436 (IC_{50}= 2.88 μM), MDA-MB-231 (IC_{50}= 2.99 μM), and MDA-MB-468 (IC_{50}= 1.83 μM). Furthermore, in the ER+/HER2− MCF-7 cell line, the results demonstrated sensitivity to compound **43**, with an IC_{50} of 2.4 μM (Figure 4) (Elkafoury et al. 2024).

In addition, it was found that the proliferation of BRCA2-deficient HCT-116 cells was significantly lower than that observed in wild-type cells proficient in this gene, indicating that compound **43** induces synthetic lethality. Compound **43** was also evaluated for cytotoxicity in non-tumor HEK-293 cells, demonstrating low cytotoxicity (IC_{50}= 66.25 μM). Furthermore, it was found that compound **43** interferes with the cell cycle and exerts a pro-apoptotic effect in MDA-MB-468 cells, reducing the percentage of cells in the G0/G1 and G2/M phases (from 61.07% to 49.33% and from 11.6% to 6.19%, respectively). In contrast, a 44.48% increase in the S phase was

observed compared to the control group. The compound also induced early apoptosis (7.37%) relative to control (0.36%) and late apoptosis (22.54%) compared to untreated cells (0.19%). The induction of apoptosis was accompanied by a five-fold and four-fold increase in the expression of active caspases 3 and 9, respectively, compared to the control group (Elkafoury et al. 2024).

In molecular docking studies, compound **43** was evaluated against the PARP-1 (PDB ID: 7AAD) and TOPO-I (PDB ID: 1T8I) proteins. The results demonstrated high affinity of the compound for PARP-1, with interactions involving the residues Ser904, Gly863, Ser864, Glu763, and Tyr907, and high affinity for TOPO-I, interacting with Asn722, Arg364, Lys532, and His632, with binding energies ranging from -44.5312 kcal.mol^{-1} to -42.4321 kcal.mol^{-1}. Hybrid **43** was also subjected to molecular dynamics simulations with the PARP-1 target, where the compound remained bound to the binding groove located within the protein's active site, exhibiting stable behavior and progressively moving into deeper regions of the binding pocket. This behavior may be related to the strong inhibitory activity observed in previous experimental assays (Figure 4) (Elkafoury et al. 2024).

Pyridine and related structures

In addition to thiosemicarbazone hybrids containing quinoline and/or related compounds, other studies are distinguished by the incorporation of a pyridine ring, which preserves the heteroaromatic nature of the ring but results in a shorter π-conjugated system. This structural difference appears to directly influence the recognition of hydrophobic molecular interactions with biomacromolecules, thereby affecting antitumor activity.

In this context, Santos et al. (2016) synthesized thiosemicarbazone hybrids containing the pyridine moiety, featuring modifications at the N-4 nitrogen (R) of the thiosemicarbazone and at the carbon of the azomethine portion (R_1). The compounds were tested for cytotoxic activity against Jurkat cells and J774A.1 macrophages. Among them, the compounds that exhibited the best activity against Jurkat cells were derivatives **44** (R=R_1= methyl) and **45** (R= H; R_1= methyl), with IC_{50} values of 14.91 μM and 32.80 μM, respectively. However, only compound **45** exhibited a good selectivity profile, with an IC_{50} of 182.57 μM against J774A.1 macrophages. Studies aimed at understanding the type of cell death induced by compound **45** indicated that the compound predominantly induces necrosis in Jurkat tumor cells (Figure 4) (Santos et al. 2016).

Similarly, in the study conducted by Kassem et al. (2024), two thiosemicarbazone hybrids containing a pyridine group were evaluated, with variations in the N-4 (R) position of the thiosemicarbazone; compound **46** (R= methyl; R_1= ethyl) and compound **47** (R= H; R_1= methyl). The authors highlighted compound **46**, which exhibited inhibition percentages of 69.85 ± 1.9% for HepG-2, 61.01 ± 1.2% for MCF-7, 69.46 ± 1.9% for Hep-2, and 63.63 ± 1.5% for Vero cell lines, respectively, at a concentration of 449.82 μM. Compound **47** exhibited inhibition percentages of 66.17 ± 0.9%, 57.62 ± 2.3%, 79.91 ± 0.7%, and 61.21 ± 1.8% for the HepG-2, MCF-7, Hep-2, and Vero cell lines, respectively, at a concentration of 515.30 μM. Subsequently, compound **47** was evaluated for its inhibitory activity against the enzymes CDK2 and GSK3β, demonstrating that it is a relatively weak inhibitor compared to the reference compounds. For the CDK2/cyclin A complex, it exhibited an IC_{50} of 16.73 μM, whereas roscovitin exhibited an IC_{50} of 2.48 μM. Regarding GSK3β, the compound exhibited an IC_{50} of 2.25 μM, while the reference inhibitor CHIR-99021 exhibited an IC_{50} of 0.36 μM. Regarding

pharmacodynamic properties, a molecular docking study was conducted against the CDK2 (PDB ID: 6GUH) and GSK3β (PDB ID: 4PTE) proteins. For CDK2, compound **47** exhibited a binding affinity of -6.40 kcal.mol^{-1}, forming three hydrogen bonds with residues Ile10 (2.74 Å), Asp86 (2.40 Å), and Gln131 (2.21 Å). For GSK3β, the compound exhibited a binding affinity of -5.50 kcal.mol^{-1}, establishing three hydrogen bonds, two of which were with residues Val135 and Pro136 (Figure 4) (Kassem et al. 2024).

In contrast to previous studies, the incorporation of heterocycles into the pyridine ring framework was investigated for its influence on antitumor activity. In this context, Bacher et al. (2015) synthesized thiosemicarbazone-pyridine hybrids, in which piperazine or morpholine groups can be attached to the structure, differing by the presence of substitutions on the N-4 nitrogen (R) of the thiosemicarbazone (R= hydrogen or methyl). Among the synthesized compounds, only derivative **48** exhibited cytotoxic activity, exclusively against the LS-174 cell line, with an IC_{50} of 15.9 ± 0.6 μM, and demonstrated a good selectivity profile, as it had an IC_{50} of 63.2 ± 4.2 μM for the non-tumor MRC-5 cells. Regarding the structure-activity relationship, a significant correlation was observed between the presence of the dimethyl group at the N-4 position of the thiosemicarbazone and the antitumor activity of the compounds. Taken together, the results suggest that the incorporation of heterocycles (morpholine or piperazine) into the pyridine ring did not lead to a consistent increase in antitumor potency compared to structurally simpler pyridine hybrids. However, the possible influence of substitutions on the azomethine moiety cannot be ruled out (Figure 4) (Bacher et al. 2015).

Another strategy explored for thiosemicarbazone-pyridine hybrids involved the insertion of spacer groups between the thiosemicarbazone moiety and the nitrogen-containing ring. This structural modification does not appear to increase the antitumor activity of the hybrids, as demonstrated by Alqahtani & Bayazeed (2020), who synthesized a hybrid containing thiosemicarbazone and pyridine moieties using a phenoxyacetamide spacer. Compound **49** exhibited the best activity against the HepG-2 and MCF-7 cell lines, with IC_{50} values of 34.04 ± 0.46 μM and 33.21 ± 0.11 μM, respectively. However, the compound was not considered one of the most promising when compared to the other derivatives synthesized in the study. Furthermore, it exhibited low selectivity, as it showed an IC_{50} of 10.35 ± 0.88 μM against the non-tumor cell line WI38. Regarding molecular docking studies using the ROCK-1 protein (Rho-associated protein kinase 1; PDB ID: 3TWJ), compound **49** exhibited a binding energy of -6.7686 kcal.mol^{-1}, where the thiosemicarbazone moiety established interactions with residues Asp374 and Arg84 via three hydrogen bonds (Figure 4) (Alqahtani & Bayazeed 2020).

Contrary, replacing the inert spacer group with a pharmacophore appears to increase biological activity, as described by Blázquez-Tapias et al. (2024), who proposed the synthesis of a thiosemicarbazone hybrid conjugated with an isonicotinic hydrazone moiety, both in the neutral form (**50**) and as a chloride salt (**51**). For compound **50**, the following IC_{50} values were obtained: MDA-MB-231 (2.42 ± 0.33 μM), HeLa (1.06 ± 0.21 μM), PC-3 (4.86 ± 0.75 μM), HepG-2 (5.14 ± 0.52 μM), and WI38 (10.78 ± 0.96 μM). For compound **51**, the observed values were: MDA-MB-231 (2.48 ± 0.47 μM), HeLa (1.49 ± 0.46 μM), PC-3 (3.49 ± 0.73 μM), HepG-2 (6.27 ± 0.98 μM), and WI38 (14.09 ± 0.48 μM). The results demonstrated that both ligands exhibited greater antiproliferative activity compared to cisplatin. Overall, compound **50** proved to be more potent than compound **51** in all cell lines

evaluated, except for the PC-3 cell line. Regarding activity against the non-tumor WI38 cell line (**50**: IC_{50}= 10.78 ± 0.96 μM; **51**: IC_{50}= 14.09 ± 0.48 μM), the authors highlighted the selectivity profile of the compounds compared to the standard used. However, no further studies were conducted to investigate the antitumor mechanism of action in detail, due to the lower activity of these compounds compared to the other derivatives synthesized in the study (Figure 4) (Blázquez-Tapias et al. 2024).

Although hybridization with pyridine cores has yielded some compounds with promising antitumor activity — particularly those based on conjugation with an isonicotinic hydrazone moiety — the results vary widely and are influenced by substitutions, especially in the thiosemicarbazone moiety, indicating that this moiety does not make a significant contribution to increased antitumor activity. Other alternatives have been explored in more recent studies, utilizing hybridization with the related dihydropyrimidinone (DHPM) structure, a bioactive core containing a greater number of sites capable of interacting with macromolecules. In this context, Sashidhara et al. (2016) proposed the synthesis and *in vitro* evaluation of the antitumor activity of nine dihydropyrimidinone-thiosemicarbazone hybrids, which differed in the substituents at the C-5 position (R_1) of the phenolic ring — which acts as a spacer between the dihydropyrimidinone and the thiosemicarbazone — at the N-4 position (R_2) of the thiosemicarbazone, and at the C-2 position (X) of the dihydropyrimidinone. Initially, all compounds were evaluated for their inhibitory activity against DNA ligase-1 (hLig1) at a single concentration of 100 μM. Compounds **52** (R_1= *tert*-butyl, R_2= phenyl, and X = O) and **53** (R_1= *tert*-butyl, R_2= 4-chlorophenyl, and X = O), which exhibited the highest inhibition percentages (88.1% and 80.9%, respectively). In addition, the compounds were also evaluated for cytotoxicity against the tumor cell lines HepG-2, A549, HCT-116, DLD-1, and MDA-MB-231, as well as against the non-tumor cell line HEK-293, at a concentration of 10 μM, showing that compounds **52** (43.0%; 48.7%; 43.2%; 30.0%; 50.4%; 48.3%, respectively) and **53** (78.9%; 53.3%; 82.5%; 43.0%; 83.6%; 53.1%, respectively) exhibited high percentages of cell death in the evaluated cell lines (Figure 4) (Sashidhara et al. 2016).

Furthermore, this trend observed for thiosemicarbazone-hydropyrimidin-2(1H)-one hybrids — as well as that observed for pyridine-conjugated compounds — may be associated with the molecule's greater structural complexity, resulting from substitutions on the nitrogen-containing ring and the thiosemicarbazone moiety. This parallel can be drawn when comparing with a simpler structural framework, as illustrated in the study conducted by Abolibda et al. (2025), who synthesized and evaluated the antitumor activity of a new thiosemicarbazone derivative conjugated to hydropyrimidine-2(1H)-one. The hybrid in question, compound **54**, exhibited moderate antitumor activity, with an IC_{50} of 21.29 ± 2.47 μM against the HepG-2 cell line, compared to doxorubicin (IC_{50}= 6.18 ± 0.29 μM). Furthermore, molecular docking studies were performed using the CK2α protein kinase (PDB ID: 6TGU), with doxorubicin serving as a positive control. Compound **54** exhibited a binding energy of -5.17 $kcal.mol^{-1}$, a value similar to that observed for doxorubicin (-6.53 $kcal.mol^{-1}$), and was characterized by hydrogen-bonding interactions with the amino acid residue His161 (Figure 4) (Abolibda et al. 2025).

Acridine

Acridines differ from the pyridine core in terms of the extent of the pi-conjugated system due to the insertion of aromatic rings, making them an interesting core for modulating

potential new hydrophobic interactions with the macromolecular site. In general, thiosemicarbazone-acridine hybrids exhibited antitumor activity similar to that of pyridine-hybridized compounds and their analogs, differing in their application against multidrug-resistant leukemia cell lines. This fact is described in the study proposed by Sousa et al. (2024), who detailed the design, synthesis, and evaluation of the antitumor activity of 18 new acridine-thiosemicarbazone hybrids. In this evaluation, all compounds exhibited IC_{50} values higher than those observed for DOX and 5-FU in the three cell lines, indicating lower potency compared to the reference drugs. Subsequently, assays were conducted using multidrug-resistant leukemia cell lines. Derivatives **55** (R_1= methoxy; R_2= phenyl; IC_{50}= 8.83 μM) and **56** (R_1= methoxy; R_2= 3-hydroxyphenyl; IC_{50}= 10.69 μM) showed promising results against the Lucena-1 line, while doxorubicin had an IC_{50} of 40.78 μM. Furthermore, against the FEPS cell line, compound **57** (R_1= methoxy; R_2= 4-hydroxyphenyl) stood out, with an IC_{50} of 26.61 μM, making it the most potent derivative for this cell line (Figure 4) (Sousa et al. 2024).

The authors also calculated the relative resistance index (RR), defined as the ratio of the biological activity observed in the resistant strain to that observed in the parental strain (K-562). In this context, compounds **55** (RR= 0.11) and **56** (RR= 0.10) exhibited the lowest resistance indices for the Lucena-1 line, while compound **57** stood out against the FEPS line, with an RR of 0.33. Next, a human TOPO IIα inhibition assay was conducted, in which all evaluated hybrids demonstrated the ability to inhibit the enzymatic activity of topoisomerase IIα at a concentration of 100 μM. The highest inhibition percentages were observed for compounds **58** (97%), **56** (95%), **55** (94%), and **59** (90%). Finally, molecular docking and molecular dynamics studies using the crystallographic structure of TOPO IIα (PDB ID: 5GWK) indicated that all hybrids containing R_2= 3-hydroxyphenyl interacted with residues Arg487 and Asp463, which are considered essential for enzyme inhibition. Among them, compound **56** exhibited the best interaction profile (score= 95.33), slightly outperforming the reference compound *m*-AMSA (score = 95.21) (Figure 4) (Sousa et al. 2024).

Pyrazole, Triazole, and related Structures

Unlike previous studies, which addressed molecular hybridization with 6-membered aromatic nitrogen-containing rings — whether complex or not — other studies have focused on conjugation with smaller rings, particularly pyrazoles and triazoles. Regarding pyrazoles, we first highlight the study by Afifi et al. (2019), which aimed to develop thiosemicarbazone-substituted purine-pyrazole hybrids, featuring structural variations at the N-4 position (R_1) of the thiosemicarbazone and at the C-3 position (R) of the pyrazole group. When evaluating antitumor potential against different cell lines, compound **60** (R_1= phenyl; R= phenyl) stood out, exhibiting activity against the MCF-7 and HepG-2 cell lines, with IC_{50} values of 235.97 μM and 276.54 μM, respectively, as did compound **61** (R_1= phenyl; R= *p*-methoxyphenyl), which demonstrated activity against the A549 and HepG-2 cell lines, with IC_{50} values of 369.24 μM and 469.85 μM, respectively (Figure 5) (Afifi et al. 2019).

The antitumor activity observed for the hybrids was not significant; a possible contributing factor is thought to be the presence of bulky groups at the N-1 position of the pyrazole ring and the N-4 position of the thiosemicarbazone moiety, which likely lead to a high degree of steric hindrance, conformational rigidity, and probable insolubility in water. This parallel can be drawn when comparing the results with the study by Azimi et al. (2024), who

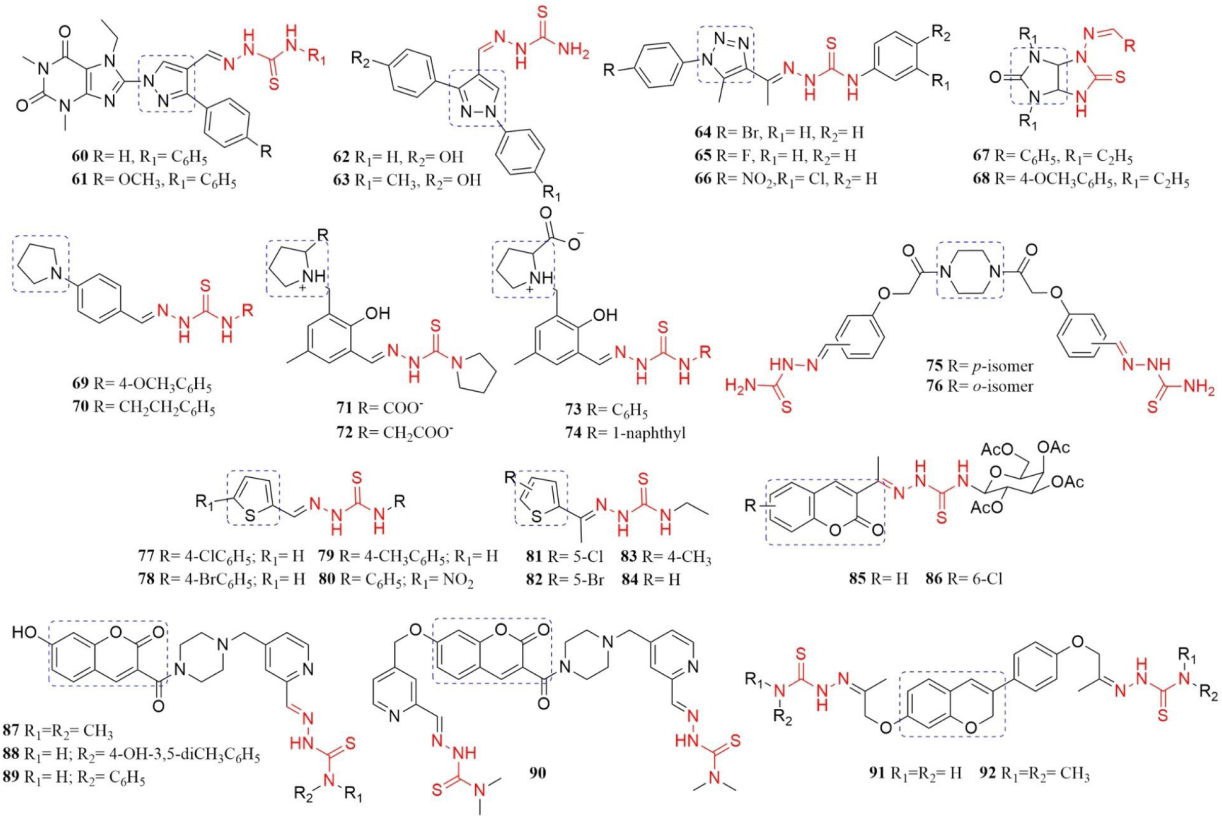


Figure 5. Thiosemicarbazone hybrids containing nitrogen-containing heterocycles — pyrazole and related structures (60-68), pyrrolidine and related structures (69-74), piperazine (75,76) and thiosemicarbazone hybrids containing oxygen-containing heterocycles — coumarin and related structures (85-92).

synthesized 14 thiosemicarbazone-pyrazole hybrids; their work differed from the previous study mainly in the replacement of purine with *p*-substituted phenyl groups, as well as the absence of bulky groups at the N-4 position of the thiosemicarbazone moiety.

In general, the derivatives reported by Azimi et al. (2024) differ from one another due to substitutions at the *para* position of the phenyl ring linked to positions N-1 (R_1) and C-3 (R_2) of the pyrazole ring. The hybrids were initially evaluated for their ability to inhibit the enzyme tyrosinase, with compounds **62** (R_1= H; R_2= OH) and **63** (R_1= CH_3; R_2= OH), which exhibited IC_{50} values of 2.09 ± 0.32 µM and 3.18 ± 0.19 µM, respectively, and were significantly more potent than kojic acid (IC_{50}= 16.38 ± 1.66 µM). Furthermore, enzyme kinetic assays revealed that compounds **62** and **63** act predominantly as noncompetitive inhibitors of tyrosinase. Compounds **62** and **63** also reduced melanogenesis by 68.99% and 75.05%, respectively, at a concentration of 8 µM. Cell viability was investigated in the B16F10 cell line, with values of 77.18 ± 5.12% for compound **62** and 72.44 ± 9.85% for compound **63**, both at a concentration of 8 µM. Finally, molecular docking studies were performed using tyrosinase (PDB ID: 2Y9X) as the target. The results obtained for compound **62** demonstrated that the sulfur atom of the thiosemicarbazone was able to interact with the Cu^{2+} ion present in the enzyme's active site, in addition to establishing π-sulfur interactions with residues His61, His259, and His296, contributing to an increase in the hybrid's chelating effect. Additionally, the compound formed important hydrogen bonds

with the Cys83 and Asn81 residues. Overall, compound **62** was considered the most potent tyrosinase inhibitor and the derivative with the greatest antimelanogenic potential among the hybrids evaluated (Figure 5) (Azimi et al. 2024).

In line with the trend toward hybridization of thiosemicarbazone with 5-membered nitrogen-containing rings, the study proposed by Othman et al. (2022) aimed to synthesize five thiosemicarbazone-triazole hybrids, which differed from one another in terms of substitutions at the N-4 position of the thiosemicarbazone and at the *para* position of the phenyl group attached to N-1 of the triazole ring. The compounds exhibited promising antitumor activity, which appears to be related to the presence of the triazole heterocycle, an important pharmacophore that is bioisosteric to pyrazole. The synthesized compounds were evaluated against a panel of sixty human tumor cell lines, with hybrids **64**, **65**, and **66** standing out. These compounds bear, respectively, *p*-bromophenyl, *p*-fluorophenyl, and *p*-nitrophenyl substituents on the triazole ring. At the N-4 position of the thiosemicarbazone, compounds **64** and **65** possess a phenyl group, while compound **66** bears a 3-chlorophenyl group (Figure 5) (Othman et al. 2022).

The highlighted compounds showed good results against different cell lines, but demonstrated greater activity against leukemia cells, including the CCRF-CEM, HL-60 (TB), K-562, MOLT-4, RPMI-8226, and SR cell lines, with average growth inhibition rates of 54.14%, 51.91%, and 66.56%, respectively. The best results were observed for the HL-60 line, with 72.19% inhibition for compound **64** and 84.47% for compound **66**, and for the SR cell line, with 64.98%, 68.25%, and 74.44% inhibition for compounds **64**, **65**, and **66**, respectively. Subsequently, compounds **64** and **66** were evaluated against the HL-60 cell line, yielding IC_{50} values of 0.47 ± 0.03 μM and 1.09 ± 0.01 μM, respectively. Compound **65**, on the other hand, was tested against the SR cell line, exhibiting an IC_{50} of 0.16 ± 0.02 μM. All compounds were also evaluated for cytotoxicity against the non-tumor WI-38, yielding IC_{50} values of 29.47 ± 1.6 μM, 69.81 ± 3.8 μM, and 56.55 ± 3.08 μM for compounds **64**, **65**, and **66**, respectively. The three derivatives were also evaluated for their inhibitory activity against the VEGFR-2 receptor, yielding IC_{50} values of 0.128 ± 0.005 μM, 0.413 ± 0.003 μM, and 0.067 ± 0.028 μM, respectively (Figure 5) (Othman et al. 2022).

To investigate the mechanism of cell death, only compound **66**, at a concentration of 10 μM, was evaluated in the HL-60 cell line. The results showed a significant increase in early apoptosis, from 0.46% to 4.36%. The percentage of cells in late apoptosis increased from 0.27% to 33.62%, while necrosis increased from 1.44% to 19.51%. The expression levels of apoptosis-related genes were also evaluated following treatment with compound **66**. Overexpression of the pro-apoptotic BAX gene (8.13-fold) was observed, as well as of the Caspase-3 (4.64-fold) and Caspase-9 (5.26-fold) genes. In contrast, a reduction in the expression of the anti-apoptotic Bcl-2 gene (0.30-fold) was observed in treated cells compared to the untreated control. Analysis of the effect of compound **66** on the cell cycle of the HL-60 cell line revealed a reduction in the cell population in the G2/M phase, from 9.09% to 4.92%, and in the G0/G1 phase, from 61.36% to 50.02%. An increase in the cell population in the Pre-G1 and S phases was observed, indicating that compound **66** can induce apoptosis and promote cell cycle arrest in the G2/M and G0/G1 phases. Finally, molecular docking studies demonstrated that compound **66** exhibited the best interaction score (-7.33 $kcal.mol^{-1}$) against VEGFR-2 (PDB ID: 3WZE), establishing interactions with the amino acid residues Cys919, Cys1045,

Glu885, and Val899 (Figure 5) (Othman et al. 2022).

Contrary to the previous 5-membered aromatic heterocycles, the study by Gazieva et al. (2016) proposed the synthesis of thiosemicarbazone-imidazolidinone hybrids, conjugated at the N-1 and N-3 positions of the thiosemicarbazone, giving rise to a bicyclic compound called thioglycoluril, a thioxoimidazo-imidazole system. In this study, the increase in conformational rigidity, coupled with the loss of the aromatic system present in the pyrazole and triazole hybrids, was proposed for the evaluation of antitumor activity, in which the bicyclic hybrids exhibited lower potency. Thus, 20 compounds were synthesized with structural variations in the azomethine group (R) of the thiosemicarbazone and in the nitrogen atoms of the imidazolidinone moiety (R_1). Regarding antitumor activity, the compounds were evaluated against the RD, A549, and MS cell lines, with compounds **67** (R= phenyl; R_1= ethyl) and **68** (R= *p*-methoxyphenyl; R_1= ethyl) standing out. Compound **67** exhibited IC_{50} values of 20.56 ± 5.23 μM, 23.67 ± 3.14 μM, and 6.44 ± 0.58 μM against the RD, A549, and MS cell lines, respectively. Compound **68**, on the other hand, exhibited IC_{50} values of 20.00 ± 3.17 μM, >100 μM, and 20.98 ± 4.03 μM against the same cell lines, respectively. In the cytotoxicity assay against non-tumor HEK-293 cells, only compound **67** exhibited a satisfactory selectivity profile, with an IC_{50} of 72.49 ± 0.27 μM. Furthermore, in cell death assays, it was found that treatment with compound **67** had no significant effect on the induction of apoptosis in K-562 cells, with only a slight reduction in the percentage of viable cells observed compared to the control group. Based on these results, the authors suggest that the mechanism responsible for the suppression of cell proliferation induced by compound **67** requires further investigation (Figure 5) (Gazieva et al. 2016).

Pyrrolidine

Following the strategy of conjugating thiosemicarbazone with 5-membered nitrogen-containing heterocycles, the introduction of a pyrrolidine ring was proposed in the study by Aftab et al. (2024), which yielded 18 compounds through substitutions at the N-4 position of the thiosemicarbazone. Similar to what was observed for thiosemicarbazone-imidazolidinone hybrids, the compounds did not show superior results compared to derivatives containing aromatic groups in their molecular framework, suggesting that the loss of the pi-conjugated system directly impacted the compounds' success in the evaluation of their antitumor activity. Thus, the molecules were evaluated for their inhibitory activity against the enzyme DHFR (dihydrofolate reductase), an enzyme essential for DNA synthesis and cell proliferation. In this study, the hybrids containing the *p*-methoxyphenyl (**69**) and β-phenethyl (**70**) groups at the N-4 position, which exhibited IC_{50} values of 12.37 ± 0.48 μM and 12.38 ± 0.25 μM, respectively, compared to methotrexate (IC_{50}= 0.086 ± 0.07 μM) against DHFR (Dihydrofolate Reductase). Regarding the structure-activity relationship, it was demonstrated that the hybrids containing the phenyl group substituted with electron-donating groups exhibited greater inhibitory activity. This behavior was attributed to the possible enhancement of interactions with the enzyme's active site, resulting from the increased electron density of the aromatic ring. In molecular docking studies using DHFR (PDB ID: 1KSM), compound **69** yielded the best results, forming significant interactions with the amino acid residues Ser59, Val115, Ile7, Phe34, and Leu22, as well as interacting with the cofactor NADP (Figure 5) (Aftab et al. 2024).

An extension of the findings in this study can be seen in the work of Dobrova et al. (2016) and Milunović et al. (2017), who proposed the synthesis of thiosemicarbazone hybrids with amino acid fragments (proline and homoproline) to evaluate the antitumor activity of the compounds. In the study by Dobrova et al. (2016), the synthesis of two thiosemicarbazone hybrids — thiosemicarbazone-proline (**71**) and thiosemicarbazone-homoproline (**72**) — was reported. Compounds **71** and **72** demonstrated greater efficacy against the CH1 cell line, with IC_{50} values of 2.7 ± 0.2 μM and 6.7 ± 0.1 μM, respectively. An assessment of cytotoxicity against the non-tumor NIH/3T3 cell line revealed IC_{50} values of 21.0 ± 1.0 μM for compound **71** and 34.7 ± 0.2 μM for compound **72**, demonstrating the greater selectivity of these derivatives toward tumor cell lines. Furthermore, analysis of cell death showed an increase in the population of cells undergoing late apoptosis and necrosis in A549 cells treated with 20 μM of the compounds, corresponding to 51.9% for derivative **71** and 68.7% for derivative **72**. In comparison, cisplatin, used as a positive control, showed 48.4% of cells in late apoptosis and necrosis (Figure 5) (Dobrova et al. 2016).

Similar to the presence of the additional pyrrolidine ring at the N-1 position of the thiosemicarbazone, as observed in compounds **73** and **74**, it appears that the introduction of other bulky groups in this region may be associated with increased selectivity for tumor cell lines, while still impairing the biological activity of thiosemicarbazone-proline hybrids. This is demonstrated in the work of Milunović et al. (2017), who proposed the synthesis of four thiosemicarbazone-proline hybrids with structural variations at the N-4 (R) position of the thiosemicarbazone; the most promising compounds featured phenyl (**73**) and 1-naphthyl (**74**) groups as substituents. Compound **73** exhibited promising activity against the LS-174 and FemX cell lines, with IC_{50} values of 48 ± 3 μM and 31 ± 2 μM, respectively. Compound **74**, on the other hand, demonstrated significant activity only against the FemX cell line, with an IC_{50} of 15 ± 2 μM. However, both compounds exhibited high selectivity for tumor cells, as indicated by the IC_{50} values obtained against the non-tumor MRC-5 cell line: 211 ± 9 μM for compound **73** and 204 ± 10 μM for compound **74**. The authors suggested that the activity of the hybrids may be related to the introduction of aromatic groups into the structure, which increases the lipophilicity of the compounds, facilitating their passage through the cell membrane and, consequently, increasing cytotoxicity. However, the hybrids showed lower potency compared to cisplatin, which exhibited IC_{50} values ranging from 8 ± 2 μM to 22 ± 7 μM in the tumor cell lines evaluated (Figure 5) (Milunović et al. 2017).

Piperazine

Expanding the scope of thiosemicarbazone hybrids with nitrogen-containing groups, Mohamed et al. (2024) describes the synthesis of two novel hybrids, distinguishing themselves from other studies by exploring the use of bis-thiosemicarbazones. In this context, the study describes two isomers of bis-thiosemicarbazones, in which the 1,4-bis(phenoxyacetamido)piperazine moiety acts as a spacer for the insertion of the thiosemicarbazone fragment. In compound **75**, this fragment is attached to the *para* position of the phenoxy group, whereas in compound **76** it is attached to the *ortho* position. Regarding antitumor activity, compound **75** stood out, exhibiting a good profile of cell growth inhibition at a single concentration of 100 μM, with inhibition percentages of 89.13 ± 2.22% for HepG-2, 90.07 ± 3.41% for HCT-116, and 88.90 ± 5.46% for MCF-7. However, the compound showed low selectivity toward tumor cells, as

it also significantly inhibited the growth of the non-tumor HDF cell line, with an inhibition rate of 66.45 ± 11.4%. Hybrid **75** exhibited IC_{50} values of 20.66 ± 1.5 μM, 41.3 ± 3.9 μM, and 48.5 ± 4.8 μM against the HCT-116, HepG-2, and MCF-7 cell lines, respectively. Finally, compound **75** was investigated for its inhibitory activity against EGFR kinase. The derivative exhibited 89.7 ± 2.8% enzyme inhibition and an IC_{50} of 3.5 ± 0.1 nM, compared to erlotinib, used as a standard, which exhibited an IC_{50} of 1.3 nM and 97.8% enzyme inhibition (Figure 5) (Mohamed et al. 2024).

In this context, there is a considerable discrepancy between the values obtained for both bis-thiosemicarbazones, suggesting that conformational aspects may be related to the modulation of the antitumor effect against the tested cell lines.

Sulfur-containing Heterocycles

Sulfur heterocycles are cyclic compounds that contain sulfur as a heteroatom, notably thiophene, thiopyran, benzothiophene, among others. The insertion of sulfur into a cycle promotes changes in the physical-chemical and electronic properties of the molecule, increasing lipophilicity and influencing typical pharmacokinetic parameters such as permeability and bioavailability. In addition, they can provide new intermolecular interactions with different biological targets and metal ions. The pharmacological action of these compounds and their derivatives at the anticancer level aims to inhibit enzymes involved in the cell cycle, modulating the growth and survival of cancer cells (Pathania et al. 2019, Hamad 2025).

Thiophene

An integrated analysis of the studies by Oliveira et al. (2015, 2025) and Marques et al. (2019) confirms the thiophene core as a relevant subunit for the design of chemotherapeutic agents, while also demonstrating how small bioisosteric modifications determine the threshold between biological inactivity and pharmacodynamic success at the nanomolar or micromolar scale. Furthermore, the importance of electronic balance becomes evident when contrasting the 2-thiophene-thiosemicarbazone series developed by Oliveira et al. (2015) with the inactive derivatives of Oliveira et al. (2025). In the series obtained by Oliveira et al., modifications at the N-4 position (R) revealed that the introduction of halogens that act as electron-withdrawing groups via inductive effects yielded the most potent compounds. Notably, compound **77** (*p*-chlorophenyl) was active against U251, UACC-62, NCI-ADR/RES, 786-0, and K-562 (GI_{50}= 8.3, 15.8, 2.8, 7.4, and 2.0 μM, respectively), and compound **78** (*p*-bromophenyl) against U251, MCF-7, NCI-ADR/RES, 786-0, NCI-H460, PC-3, and HT-29 (IC_{50}= 4.2, 0.74, 1.7, 4.5, 4.7, 79.4, 17. 7 μM, respectively) and **79** (*p*-methylphenyl) against UACC-62 and K-562 (GI_{50}= 16.8 and 1.7 μM, respectively). Despite their antiproliferative activity, the hybrids also exhibited cytotoxicity against the HaCaT cell line. Subsequent studies with compound **78** in the 786-0 cell line determined a TGI of 28 μM and an LC_{50} of 91.8 μM. In addition, the compound induced cell death via apoptosis, as evidenced by the externalization of phosphatidylserine, without altering cell cycle distribution. In the *in vivo* Ehrlich solid tumor model, at a dose of 30 $mg.kg^{-1}$, treatment reduced tumor growth by 30% starting on day 6, reaching 71.1% inhibition between days 12 and 15 compared to the negative control (Figure 5) (Oliveira et al. 2015).

Marques et al. (2019) are notable for introducing a strongly electron-withdrawing group that induces oxidative stress at the C-5 position of the heterocycle, yielding the 2-(5-nitro-thiophene)-thiosemicarbazone series. Thus, compound **80** (N-4: phenyl)

demonstrated exceptional cytotoxic potency and exhibited the best antitumor profile, with good IC_{50} values against Hep-2 (6.20 μM), HL-60 (1.63 μM), HT-29 (6.20 μM), K-562 (4.57 μM), MCF-7 (3.26 μM), MOLT-4 (2.28 μM), and NCIH-292 (2.61 μM). When evaluating the transmembrane potential of compound **80** in K-562 cells, a significant increase in mitochondrial depolarization was observed at a concentration of 9.13 μM (64.2 ± 2.5%), indicating the induction of apoptosis. Furthermore, upon investigating the cell cycle, reductions in the G2/M phase were observed in cells treated with concentrations of 2.28, 4.56, and 9.13 μM, as well as an increase in the proportion of cells in the G1 phase (66.0 ± 2.3%; 86.1 ± 0.3%; and 70.3 ± 7.0%). Furthermore, the compound showed no inhibitory activity against topoisomerase II. Next, the ability of compound **80** to interact with ctDNA was evaluated using UV-vis spectroscopy; it was found to be capable of inserting itself between the nitrogenous base pairs of ctDNA, interacting via intercalation (Figure 5) (Marques et al. 2019).

On the other hand, the absence of an aromatic group at the N-4 position of the thiosemicarbazone resulted in a decrease in the activity pattern, as reported by Oliveira et al. (2025), who synthesized compounds **81**, **82**, **83**, and **84**, which possess only an ethyl group at N-4 (R) and a thiophene ring distinguished by the presence or absence of substituents. The compounds were tested against the A549, MDA-MB-231, DU-145, A2780cis, and MRC-5 cell lines but were not effective, exhibiting IC_{50} values > 100 μM (Figure 5) (Oliveira et al. 2025).

Oxygen-containing Heterocycles

Oxygenated heterocycles are widely explored in medicinal chemistry because they constitute an important class of bioactive molecules, exhibiting favorable activity for numerous pathophysiological conditions. *O*-heterocycles stand out in cancer treatment, where they can provide sufficiently potent molecular frameworks with lower toxicity risk and significant specificity. In addition, it is possible to mention some structures that are extracted from natural sources and subsequently used as lead compounds in the development of new drugs, as in the case of coumarin (Singh & Silakari 2018).

Coumarin and related structures

Among the oxygenated nuclei, coumarin was identified in the studies presented by Toan & Thanh (2021), Stepanenko et al. (2021), and Yee et al. (2017) as an important compound for hybridization with thiosemicarbazone. The work by Toan & Thanh (2021) introduces remarkable refinement in molecular design by fusing the coumarin ring and *D*-galactose to thiosemicarbazone. In medicinal chemistry, the glycosylation of pharmacophores is an elegant strategy that exploits the overexpression of glucose transporters (GLUT) in tumor cells with high metabolic demand to maximize intracellular accumulation of the compound. This rationale can be applied to hybrid **85** (unsubstituted coumarin), which was the most active against the MCF-7 (IC_{50}= 1.28 μM) and HepG-2 (IC_{50}= 1.53 μM) cell lines, and compound **86** (6-chloro-coumarin), which also showed low IC_{50} values against the MCF-7 (IC_{50}= 1.81 μM) and HepG-2 (IC_{50}= 1.75 μM) cell lines (Figure 5) (Toan & Thanh 2021).

Furthermore, both were evaluated for EGFR inhibition and showed high efficacy, with an IC_{50} of 0.512 μM for **85** and an IC_{50} of 0.258 μM for **86**. Subsequently, these two hybrids were tested for activity against two other types of EGFR tyrosine kinase, EGFR T790M-TK and EGFR L858R-TK. Thus, **86** exhibited lower IC_{50} values for both forms of EGFR, EGFR-L858R-TK (IC_{50}= 85.92 ± 0.32 μM) and EGFR-T790M-TK (IC_{50}= 432.65 ± 2.91 μM), while

also exhibiting greater inhibitory activity than erlotinib in the assay against EGFR-L858R-TK (IC_{50}= 91.23 ± 0.41 μM). In the cell death assay, compounds **85** and **86** demonstrated the ability to induce apoptosis (in both early and late stages) and necrosis in HepG-2 cells. Molecular docking studies with EGFR (PDB ID: 4HJO) revealed that compounds **85** and **86** exhibited favorable binding energy values (-6.847 and -6.804 kcal.mol^{-1}, respectively) compared to the binding energy of erlotinib (-8.984 kcal.mol^{-1}). Compound **85** interacted with Asp831, Thr830, Thr766, Cys773, and Gly772, while compound **86** interacted with Asp831, Thr830, Cys773, Arg817, and Gly772. Furthermore, the *D*-galactose and coumarin moieties of compounds **85** and **86** inserted more effectively into the adenine binding pocket of the EGFR receptor, which may be related to the greater EGFR inhibitory activity of these compounds (Figure 5) (Toan & Thanh 2021).

Furthermore, Stepanenko et al. (2021), who investigated substitutions at the N-4 terminal portion of the thiosemicarbazone while preserving a hydroxy group at the C-7 position of the coumarin, established a clear structure-activity relationship (SAR) based on steric effects. Unlike previous studies in which bulky aromatic substituents at N-4 increased activity, in this specific coumarin series, the introduction of bulky and hydrophobic groups abolished the potency. The highlight was analog **87** (R_1=R_2= methyl), which showed good results against different cell lines (MDA-MB-231 IC_{50}= 4.8 ± 1.3 μM; COLO-205 IC_{50}= 9.2 ± 0.1 μM; COLO-320 IC_{50}= 6. 7 ± 0.9 μM), similar to that of 3-AP (MDA-MB-231 IC_{50}= 1.5 ± 1.1 μM) and doxorubicin (COLO-205 IC_{50}= 3.3 ± 0.2 μM and COLO-320 IC_{50}= 3.1 ± 0.3 μM). While derivatives **88** (R_1= H; R_2= 4-OH-3,5-di$CH_3C_6H_5$) and **89** (R_1= H; R_2= phenyl) exhibited lower activity, and **90** (disubstituted coumarin) also exhibited adequate efficacy against the cell lines (MDA-MB-231 IC_{50}= 3.0 ± 0.3 μM; COLO-205 IC_{50}= 4.4 ± 0.7 μM; COLO-320 IC_{50}= 4.6 ± 0.3 μM). Regarding the cytotoxicity trend for the evaluated cell lines, it is observed that 100 ≈ 98 < 97 ≤ 99, indicating that aromatic substituents in the thioamide group have a detrimental effect on the compounds' efficacy. However, although compound **90** outperformed compound **87**, compound **87** exhibited lower cytotoxicity against the MRC-5 cell line compared to compound **90** (41 ± 1 μM vs. 4.0 ± 0.3 μM). Subsequently, compound **87** was tested for its ability to reduce the tyrosyl radical in the R_2 subunit of mouse ribonucleotide reductase. The results show that compound **87** reduced the tyrosyl radical by approximately 25%. When compared to triapine, which reduces 100% of the tyrosyl radical in 3 minutes, compound **87** proved to be an inefficient inhibitor of mR2 (Figure 5) (Stepanenko et al. 2021).

In turn, Yee et al. (2017) proposed the synthesis of new phenoxodiol hybrids condensed with one or two thiosemicarbazones, following a structural pattern similar to that of compound **90** and preserving variations at the N-4 position. Based on the evaluation of *in vitro* results against the SKN-BE(2)C, MDA-MB-231, and U87 cell lines, it was found that applying this strategy — which differs from that reported by Stepanenko et al. (2021) — yields less effective results, with IC_{50} values exceeding 100 μM for these cell lines, with the exception of compound **91** (R_1=R_2= hydrogen), which stood out against MDA-MB-231 (GI_{50} = 25 ± 4.4 μM), and **92** (R_1=R_2= methyl), which stood out against SKN-BE (2)C (GI_{50}= 45.4 ± 7.4 μM); both exhibited values lower than those of phenoxodiol (MDA-MB-231: GI_{50}= 33.3 ± 4.0 μM; SKN-BE(2)C: GI_{50}= 4.5 ± 0.3 μM). Furthermore, regarding the monosubstituted compounds at the C-8 position of phenoxodiol, most compounds exhibited potent antiproliferative properties against the three tumor lines, with

compound **93** (N-4= *p*-chlorophenyl) standing out against the SKN-BE (2)C (IC_{50}= 1.9 ± 0.1 μM), MDA-MB-231 (IC_{50}= 4.7 ± 0.1 μM), and U87 (IC_{50}= 8.3 ± 1.9 μM). In addition, the specificity of the compounds was calculated, with compound **93** exhibiting the highest specificity (2.6) against the SKN-BE(2)C cell line. The author also points out a correlation between the lipophilicity of the hybrids and their antiproliferative activity for all three cell lines, since as lipophilicity increased, so did antiproliferative activity. Therefore, the authors observed that lipophilicity plays a significant role related to permeability through the cytoplasmic membrane of tumor cells (Figure 5) (Yee et al. 2017).

Benzofuran

An analysis of the study by Babahan-Bircan et al. (2022) reveals a clear structural and pharmacophore similarity to the coumarin hybrids discussed earlier, as in both cases, oxygenated, electron-dense heterocyclic rings are incorporated with thiosemicarbazone. In this work, the authors explored the egonol skeleton — a bioactive natural benzofuran structurally analogous to coumarins — to design hybrids **94** (thiosemicarbazone-egonol) and **95** (thiosemicarbazone-egonol-dioxime). When evaluated *in vitro* against MCF-7 and PC-3 cell lines, the compounds exhibited a moderate cytotoxic profile, revealing subtle positional selectivity depending on the tumor cell line, with hybrid **94** showing slightly greater activity against MCF-7 cells (IC_{50}= 47. 7 μM) than **95** (IC_{50}=

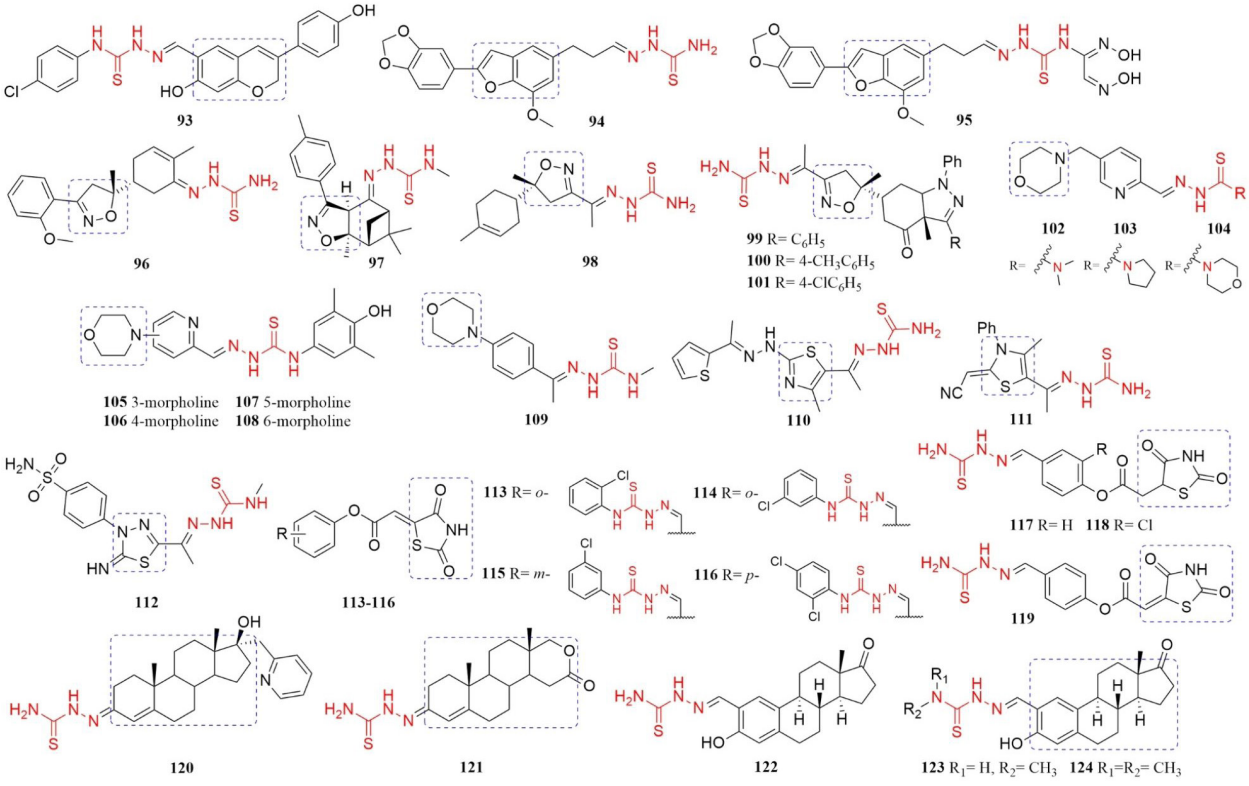


Figure 6. Thiosemicarbazone hybrids oxygen-containing heterocycles — coumarin and related structures (93), benzofuran (94,95), thiosemicarbazone hybrids containing various heterocycles — isoxazole (96-101), morpholine (102-109), thiazole (110,111), thiadiazole (112), and thiazolidinedione (113-119) and thiosemicarbazone hybrids containing steroid analogues (120-124).

64.74 μM), while the dioxime-modified analog **95** was more effective against the PC-3 line (IC_{50}= 44.48 μM) compared to its precursor (IC_{50}= 50.76 μM) (Figure 6) (Babahan-Bircan et al. 2022).

Although both derivatives demonstrated lower overall antiproliferative potency and significantly higher IC_{50} values than the control drug paclitaxel (which had IC_{50} values ranging from 9.99 μM to 10.47 μM) and the previously reported coumarin derivatives. However, the major pharmacodynamic distinction of this series lay in the massive activation of programmed cell death pathways. Hybrid **95** drastically outperformed analog **94** and Paclitaxel itself in terms of pro-apoptotic efficacy, inducing remarkable apoptosis rates of 78.22% in MCF-7 cells and 66.33% in PC-3 cells, compared to the modest 9.99% and 10.47% observed in the positive control, respectively. These findings suggest that egonol derivatives may act as an excellent platform for inducing apoptosis, demonstrating that the peripheral insertion of nitrogen-containing moieties such as dioxime functions as a crucial electronic trigger to redirect the cellular fate from nonspecific inflammatory necrosis toward programmed and clean cell death (Figure 6) (Babahan-Bircan et al. 2022).

Various Heterocycles

Among compounds that exhibit biological activity, more than 85% contain at least one heterocyclic ring in their structure. This data highlights the central importance of heterocycles in the modern development of antitumor drugs, since the use of these structures has proven to be an effective strategy for adjusting crucial physicochemical characteristics in drugs and/or molecules under development, such as solubility, lipophilicity, polarity, and the ability to form hydrogen bonds, resulting in improved pharmacokinetic and toxicological profiles of these structures (Jampilek 2019).

Isoxazole

The 5-membered isoxazole heterocycle was also targeted in molecular hybridization strategies with thiosemicarbazone, capable of producing hybrids with moderate antitumor activity when compared to the compounds already discussed in the study, with no derivative exhibiting notable biological activity. Overall, the IC_{50} values ranged in the micromolar range of 13-35 μM, suggesting that the isoxazole moiety may contribute to maintaining interactions with macromolecules and pharmacokinetic properties, but without sufficiently impacting the cytotoxic potency of the hybrids.

In this regard, Oubella et al. (2022) synthesized and evaluated four isoxazole-thiosemicarbazone hybrids as potential anticancer agents, which featured variations at the C-3 position of the isoxazoline group. The hybridization was carried out using (*R*)-carvone, and the compounds were evaluated against the HT-1080, A549, MCF-7, and MDA-MB-231 tumor cell lines. Compound **96** (2-methoxyphenyl at isoxazole) exhibited the best IC_{50} values among the four hybrids (16.93 ± 2.41 μM for HT-1080; 20.13 ± 0.39 μM for A549; 15.56 ± 3.84 μM for MCF-7; and 22.02 ± 1.40 μM for MDA-MB-231). However, although it exhibited moderate activity, the compound was not selected for further evaluation because it is an intermediate in the main synthetic route proposed in the study (Figure 6) (Oubella et al. 2022).

Moderate antitumor activity has also been observed in other studies, such as the one conducted by Laamari et al. (2025a), who synthesized a thiosemicarbazone hybrid containing an isoxazole ring and evaluated its antitumor activity using the human cell lines MDA-MB-231 and A549. Compound **97** exhibited

IC_{50} values of 29.47 ± 1.21 μM and 35.12 ± 2.63 μM, respectively. In molecular docking studies, the interaction of the ligand with the cIAP, bTNAP, and bCAII proteins was investigated. The binding energies obtained were -30.66 $kJ.mol^{-1}$ for cIAP (L-phenylalanine control: -22.68 $kJ.mol^{-1}$), -29.82 $kJ.mol^{-1}$ for bTNAP (levamisole control: -23.10 $kJ.mol^{-1}$) and -23.94 $kJ.mol^{-1}$for bCAII (acetazolamide control: -19.74 $kJ.mol^{-1}$). It was observed that the ligand interacted with residues Ser130, Val108, and Phe109 of cIAP; His434, Glu435, His321, and His324 of bTNAP; and Asp163, Leu222, and Lys223 of bCAII. The compound exhibited high gastrointestinal absorption and a logP of 3.22, indicating good lipophilicity and moderate bioavailability (0.55). Its structure contains three hydrogen-bond acceptors and two hydrogen-bond donors, characteristics that influence their molecular interactions. Although it exhibits good absorption, the compound does not cross the blood-brain barrier and is a substrate of P-glycoprotein, which may reduce its intracellular efficacy. Furthermore, it inhibits the enzymes CYP1A2, CYP2C19, CYP2C9, and CYP3A4, suggesting potential for drug interactions, without affecting CYP2D6 (Figure 6) (Laamari et al. 2025a).

The same group, Laamari et al. (2025b), also reported the synthesis and characterization of a new thiosemicarbazone conjugated to a monoacetyl-dihydroisoxazole system, used as an intermediate for the preparation of isoxazole hybrids linked to the 1,3,4-thiadiazole ring. The thiosemicarbazone hybrid **98** was evaluated for antitumor activity against the human tumor cell lines HT-1080 (IC_{50}= 31.74 ± 2.13 μM), A549 (IC_{50}= 51.92 ± 1.72 μM), MCF-7 (IC_{50}= 29.11 ± 0.97 μM), and MDA-MB-231 (IC_{50}= 41.98 ± 1.53 μM). These results were lower than those obtained for doxorubicin, which was used as a positive control (HT-1080: IC_{50}= 6.36 ± 1.38 μM; A549: IC_{50}= 6.05 ± 1.57 μM; MCF-7: IC_{50}= 6.83 ± 1.82 μM; MDA-MB-231: IC_{50}= 5.77 ± 2.02 μM). Consequently, the compound was not considered for subsequent stages of biological evaluation (Figure 6) (Laamari et al. 2025b).

Furthermore, it is important to note that structural modifications — generally at the C-3 and C-5 positions of the isoxazole ring — resulting from the insertion of other pharmacophores appear to influence the anticancer biological activity of the hybrids. The study proposed by Bimoussa et al. (2024) employed a molecular hybridization strategy to obtain three thiosemicarbazone hybrids containing both isoxazole and pyrazole rings, with variations at the C-3 position of the pyrazole ring, with the aim of evaluating their antitumor potential. The thiosemicarbazone hybrids **99**-**101** exhibited significant cytotoxic effects compared to doxorubicin with IC_{50} values ranging from 13.41 ± 0.44 to 47.58 ± 1.98 μM for all evaluated cell lines. The antiproliferative activity of compound **100** (R= *p*-methylphenyl) against HT-1080 cells was the most pronounced (IC_{50}= 13.41 ± 0.44 μM), while compounds **99** (R= phenyl) and **101** (R= *p*-chlorophenyl) exhibited IC_{50} values of 16.02 ± 1.42 μM and 29.31 ± 1.40 μM, respectively (Figure 6) (Bimoussa et al. 2024).

To complement the results obtained, assays were conducted to assess annexin V-induced apoptosis and caspase-3/7 activity using compound **99**, which resulted in a 25.86% increase in apoptosis in HT-1080 cells. In addition, a 19-fold increase in the rate of late apoptosis was observed compared to the control (DMSO). The results also indicated a 19.1% increase in caspase-3/7 activity. In the investigation of cell cycle distribution, it was found that compound **99** induced cell cycle arrest at the G0/G1 phase, resulting in a 1.29-fold increase in the cell population, with 51.8% of HT-1080 cells arrested in this phase, compared to untreated cells. In the *in silico* analysis, the affinity of hybrid **99** for the caspase-3 enzyme (PDB ID: 3GJQ) was evaluated, showing the

lowest Schrodinger score (-4.966 kcal.mol^{-1}). Additionally, its pharmacokinetic (ADMET) profile was investigated, demonstrating an estimated oral absorption of 95%, as well as being a substrate of the CYP3A4 enzyme and an inhibitor of the CYP2C19, CYP2C9, and CYP3A4 isoforms. The clearance rate was 0.0016 log mL/min/kg. Finally, compound **99** showed satisfactory results in the AMES tests for mutagenicity and carcinogenicity and was classified as negative for both (Figure 6) (Bimoussa et al. 2024).

Morpholine

Regarding thiosemicarbazone-morpholine hybrids, the presence of the heterocycle stands out as a strategy that appears to modulate the pharmacokinetic and pharmacodynamic properties of the compounds, such as the ability to optimize interactions with macromolecular targets and modulate their solubility. Overall, the studies are characterized by similar structural frameworks, which differ at the N-4 position of the thiosemicarbazone, as well as in the aromatic intermediate moiety between the azomethine and the morpholine. Unlike the isoxazole hybrids, which exhibited moderate antitumor activity, the morpholine-hybridized compounds displayed variable biological activity, depending on the structural context and the optimization of the substituent groups.

This structural relationship is clearly demonstrated by the work of Ohui et al. (2019), who obtained five morpholine-thiosemicarbazone hybrids linked to pyridine, with variations in the N-4 position of the thiosemicarbazone. Compounds **102** (N,N-dimethyl), **103** (pyrrolidinyl), and **104** (morpholinyl) stood out for exhibiting results superior to those of the positive control, Triapine. Against the A2780 cell line, the compounds exhibited IC_{50} values of 0.010 ± 0.001 μM, 0.008 ± 0.002 μM, and 0.07 ± 0.01 μM, respectively, while for the A2780cisR line, the IC_{50} values were 0.035 ± 0.006 μM, 0.028 ± 0.006 μM, and 0.76 ± 0.06 μM, respectively. Regarding the selectivity index, all hybrids evaluated showed greater selectivity for the tumor cell lines compared to the HEK-293 cell line (IC_{50}= 0.39 ± 0.05 μM). Furthermore, the authors highlight a correlation between antitumor activity and the hydrophobicity of the hybrids (**103** > **102** > **104**), suggesting that increased hydrophobicity promotes the intracellular accumulation of the compounds (Figure 6) (Ohui et al. 2019).

Similarly, by proposing prototypes with an intermediate pyridine moiety, Milunovic et al. (2024) synthesized four morpholine-thiosemicarbazone hybrids, which share a redox-active *p*-aminodimethylphenol unit at N-4 as a common feature, differing only in the insertion of morpholine into the pyridine ring at the azomethine moiety. In the study, it became evident that the position of insertion of the morpholine heterocycle into the nitrogen-containing core was able to influence the antitumor activity observed for the compounds. The evaluated hybrids were found to be five to nine times less toxic to the parent MES-SA cells, with IC_{50} values of 2.9 ± 0.4 μM, 5.2 ± 0.8 μM, and 4.0 ± 0.7 μM for compounds **105** (R= 3-morpholine), **106** (R= 4-morpholine), and **107** (R= 5-morpholine), respectively. Furthermore, these hybrids exhibited even lower activity against the resistant MES-SA/Dx5 cells, with IC_{50} values of 13.1 ± 3.2 μM, 9.9 ± 0.4 μM, and 8.6 ± 0.9 μM, respectively. Contrary, hybrid **108** (R= 6-morpholine) exhibited greater cytotoxicity against both MES-SA cells (IC_{50} = 0.25 ± 0.05 μM) and MES-SA/Dx5 cells (IC_{50}= 4.2 ± 0.8 μM), when compared to the reference drug (Figure 6) (Milunovic et al. 2024).

Molecular docking studies revealed similar binding results for all active pro-ligands, suggesting a plausible interaction with the mR2

protein of ribonucleotide reductase (RNR) (PDB ID: 1W68). All compounds fell within the chemical space characteristic of drug-like molecules, indicating good biocompatibility. Among the scoring functions evaluated, ChemPLP yielded the best RMSD value (1.0908). In this function, the co-crystallized ligand (DAMA-colchicine) had a fitscore of 60.1, while the tested ligands exhibited higher values, indicating greater predicted affinity: **105**= 66.8; **106**= 64.3; **107**= 63.1; and **108**= 65.1. Specifically for compound **108**, hydrogen bonds were observed with the amino acid residues Trp324, Glu335, and Asp272, in addition to lipophilic interactions with Phe241, Val328, and Phe237 (Figure 6) (Milunovic et al. 2024).

In contrast, the simple introduction of morpholine — or, more precisely, the replacement of the pyridine intermediate moiety with a phenyl group — even while maintaining a bioisosteric relationship between them, appears to negatively affect the antitumor activity of the hybrids. This fact can be observed when comparing our results with the study proposed by Farghaly et al. (2020), who obtained thiosemicarbazone hybrids containing N-phenylmorpholine, which differed from one another at the N-4 (R) position of the thiosemicarbazone. The main difference from the previously described prototypes is the replacement of the pyridine moiety with a phenyl group, which significantly influences antitumor activity. Initially, regarding interaction with single-stranded DNA (ss-DNA), compound **109** (N-4= methyl) was shown to exhibit moderate to high binding capacity, as it displayed a binding constant (Kb) of 2.05 ± 0.3 x 10^4. In addition, the compound caused a slight increase in DNA viscosity, suggesting an electrostatic binding mode to the groove of the DNA molecule. With regard to antitumor activity, compound **109** exhibited an IC_{50} of 206.90 µM against the HepG-2 cell line and an IC_{50} of 345.41 µM against the MCF-7 cell line, results lower than those observed for cisplatin (IC_{50}= 12.23 µM and 17.33 µM, respectively) (Figure 6) (Farghaly et al. 2020).

Thiazole

The hybridization of thiosemicarbazone with the thiazole ring was also investigated, considering the role of the heterocycle as an important pharmacophore described in the literature, primarily due to its ability to promote hydrophobic interactions and hydrogen bonds with various macromolecular targets. However, the few prototypes developed appear to have limited antitumor activity when compared to the hybrids discussed so far, with low or moderate cytotoxicity. This was demonstrated in the study by Mahmoud et al. (2022), in which an arylazothiazole hybrid containing the thiosemicarbazone moiety was obtained. Compound **110** exhibited an IC_{50} of 78.29 ± 3.40 µM, and was considered five to six times less potent than the positive controls, cisplatin and vinblastine, which exhibited IC_{50} values of 17.26 ± 3.13 µM and 4.88 ± 0.76 µM, respectively (Figure 6) (Mahmoud et al. 2022).

Along the same lines, Bayazeed et al. (2023) synthesized a hybrid containing thiosemicarbazone and thiazole moieties. In the cytotoxicity assay, compound **111** yielded the following results against the following tumor cell lines: HepG-2 (IC_{50}= 51.26 ± 0.11 µM), HCT-116 (IC_{50}= 49.62 ± 0.26 µM), and MCF-7 (IC_{50}= 48.17 ± 0.47 µM). In addition, the hybrid was also evaluated against the non-tumor cell line WI38, yielding an IC_{50} of 52.29 ± 0.09 µM. The results were compared to those of doxorubicin, used as a positive control, which exhibited IC_{50} values of 31.17 ± 0.37 µM, 12.09 ± 0.33 µM, 24.19 ± 0.29 µM, and 69.47 ± 0.56 µM for the HepG-2, HCT-116, MCF-7, and WI38 cell lines, respectively. Overall, compound **111** was considered a hybrid with low

antitumor potency (Figure 6) (Bayazeed et al. 2023).

Thiadiazole

Contrary to what has been observed for thiosemicarbazone-thiazole hybrids, conjugation with the 1,3,4-thiadiazole ring has proven to be a promising strategy for increasing antitumor activity, potency, and selectivity, yielding hybrids in the submicromolar range against different tumor lines. This relationship is demonstrated in the study by Bondock et al. (2023), who synthesized a series of thiosemicarbazone-thiadiazole hybrids with variations at the N-4 position of the thiosemicarbazone (R= methyl, allyl, phenyl, or *p*-chlorophenyl). Compound **112** (N-4= methyl) stood out for its promising results against the HepG-2 (IC_{50}= 0.53 ± 0.01 µM), Caco-2 (IC_{50}= 1.01 ± 0.10 µM), and MCF-7 (IC_{50}= 1.12 ± 0.10 µM) tumor cell lines. In addition, it demonstrated greater potency in inhibiting cell growth when compared to staurosporine, used as a positive control (HepG-2: IC_{50}= 13.60 ± 0.80 µM; Caco-2: IC_{50}= 8.18 ± 0.70 µM; MCF-7: IC_{50}= 6.19 ± 0.30 µM). Additionally, compound **112** exhibited moderate inhibition of the normal WI38 cell line, with an IC_{50} of 18.40 ± 1.70 µM. In the molecular docking study targeting hCA IX (human carbonic anhydrase IX; PDB ID: 3IAI), compound **112** exhibited a binding energy of -11.47 kcal.mol^{-1} and favorable interactions within the enzyme's active site, forming hydrogen bonds with residues His94, Gln92, Leu198, and Thr199, with an average distance of 3.20 Å (Figure 6) (Bondock et al. 2023).

Thiazolidinedione

Another heterocycle of interest in the design of thiosemicarbazone hybrids is thiazolidine-2,4-dione (TZD), which has shown compounds with promising antitumor activity, improved selectivity, and consistent mechanistic evidence. The biological activity of these derivatives is strongly related to the nature of the substituent groups in the compounds' structural framework, indicating that the single presence of the heterocycle does not guarantee full antitumor activity. In general, studies on thiosemicarbazone-TZD hybrids feature a similar structural framework, containing a phenyl ester spacer group interposed between the azomethine moiety and the heterocycle, differing primarily in the N-4 substitutions of the thiosemicarbazone, a factor that appears to be linked to biological activity.

This modification is extensively explored in the study proposed by Paneth et al. (2023), who conducted *in silico* and *in vitro* assays to analyze the antitumor potential of thiazolidinedione-thiosemicarbazone hybrids, demonstrating that minor modifications to the phenyl group attached to the N-4 (R) position of the thiosemicarbazone, as well as its insertion into the spacer group, can affect biological activity. Compounds **113** and **114** were considered the most cytotoxic, exhibiting activity against the HepG -2 (IC_{50}= 10.39 and 2.97 µM, respectively), T98G (IC_{50}= 26.82 and 28.34 µM, respectively), and HT-29 (IC_{50}= 43.91 and 78.32 µM, respectively). In addition, hybrids **115** (IC_{50}= 42.37 µM) and **116** (IC_{50}= 13.87 µM) also showed superior results compared to the positive control (etoposide) against the T98G cell line. Compound **114** exhibited the best selectivity indices for HepG-2 (SI= 33.80), T98G (SI= 3.54), and HT-29 (SI= 1.28), and showed no significant hemolytic activity (Figure 6) (Paneth et al. 2023).

In addition, this compound was able to induce antitumor activity by promoting apoptosis, causing significant morphological changes and inhibiting the cells' ability to migrate. In molecular docking studies, compounds **113**, **114**, and **115** demonstrated efficient binding to the proteins HDAC4 (PDB ID:

2VQJ), HDAC4c (PDB ID: 4CBY), HDAC8 (PDB ID: 3SFF), and the ligand-binding domain of PPARγ (PDB ID: 6DGR), exhibiting calculated binding free energies comparable to or greater than those of native ligands. The binding energies obtained for compounds **113**, **114**, and **115** were, respectively, for HDAC4: -25.40, -27.00, and -27.80 kcal.mol^{-1}; for HDAC4c: -18.50, -18.50, and -18.00 kcal.mol^{-1}; for HDAC8: -21.90, -20.10, and -21.10 kcal.mol^{-1}; and for PPARγ LBD: -25.80, -25.50, and -28.50 kcal.mol^{-1}. The compounds interacted with key amino acid residues of the HDAC8 target, including hydrogen bonding with Tyr306, as well as several hydrophobic interactions with the side chains of residues located both in the acetyl-lysine substrate-binding tunnel (His143, Gly151, Phe152, His180, and Phe208) and in the acetate product release channel (Ile34, Trp141, Gly303, Gly304, and Tyr306) (Figure 6) (Paneth et al. 2023).

For the PPARγ LBD target, a hydrogen-bond interaction was observed between compounds **113** and **114** and the Tyr473 residue, which is essential for enzyme activation. Stabilizing interactions were also observed with residues Phe282, Gln286, Ser289, His323, His449, and Leu469. For compound **113**, interactions with Tyr327, Met364, and Lys367 were predicted, in addition to hydrogen bonds with Leu340 and hydrophobic contacts with Ile341 and Phe264. Finally, given the most promising results obtained for the open conformation of HDAC4, this protein was investigated in greater detail. Compounds **113**-**115** formed hydrogen bonds with the residues His158, His159, and Gly331, contributing to the stabilization of the complex, in addition to other interactions involving the residues Pro156, His159, Phe168, and Gly330 (Figure 6) (Paneth et al. 2023).

This structural relationship can be observed when comparing the results with the study proposed by Dzitko et al. (2023), who investigated the antitumor potential of thiosemicarbazone hybrids based on thiazolidine-2,4-dione; these differ from the previous compounds mainly due to the absence of N-4 substituents on the thiosemicarbazone moiety. Regarding cytotoxic activity against the non-tumor Hs27 cell line none of the hybrids exhibited significant cytotoxicity. Antiproliferative activity was investigated for the compounds considered most promising (**117**, **118**, and **119**), by evaluating their cytotoxic effect against the T98G tumor cell line. Compounds **117**, **118**, and **119** presented IC_{50} values of 258.51, 283.77, and 269.91 μM, respectively. The results obtained, even though superior to the reference drug, demonstrate that the combination of thiazolidine-2,4-dione with thiosemicarbazone does not guarantee high antitumor activity, reinforcing that efficacy depends on the nature of the substituent groups involved. These same compounds also demonstrated the ability to cross the blood-brain barrier, as evidenced by permeability coefficients (Pe) of 23.05 ± 0.71, 26.11 ± 1.30, and 24.37 ± 0.93 x 10^{-6} cm.s^{-1} for compounds **117**, **118**, and **119**, respectively (Figure 6) (Dzitko et al. 2023).

Steroid Analogues

Steroid nuclei consist of interesting hybridization frameworks against cancer, as they can act on nuclear steroid receptors, which become overexpressed in malignant conditions. Thus, the incorporation of steroid groups makes it possible to obtain compounds that can act effectively in the treatment of hormone-dependent cancers, mainly of reproductive tissues such as breast and prostate cancer (Šestić et al. 2025).

Similar to the heterocycles described above, steroid analogs were also evaluated for their ability to exert antitumor activity when hybridized with thiosemicarbazones. In addition to variations in substituent groups, the position of the thiosemicarbazone group's attachment to

the steroid ring was extensively evaluated for its ability to modulate the biological effect.

In the study by Janković et al. (2024), the synthesis of new androstane-thiosemicarbazone derivatives linked to 17α-homolactone or 17α-(pyridin-2-ylmethyl) structures were proposed, containing different substituents at the N-4 (R) position of the thiosemicarbazone. The antitumor activity of the compounds was evaluated *in vitro* against the HCT-116, HuH-7, MCF-7, MDA-MB-231, and PC-3 cell lines. Compound **120** (17α-homolactone hybrid, R= hydrogen) stood out for its significant cytotoxic activity with IC_{50} values of 17.3 μM for HCT-116, 8.6 μM for HuH-7, 10.1 μM for MCF-7, 18.0 μM for MDA-MB-231, and 15.6 μM for PC-3. In addition, the compound was evaluated for cytotoxicity against the non-tumor cell line BJ-5ta, in which hybrid **120** exhibited a significantly lower cytotoxic effect compared to the tumor cell lines, indicating a favorable selectivity profile. Next, the derivatives were evaluated for their affinity for the ligand-binding domain (LBD) of the hormone receptors ERα, ERβ, AR, and GR using fluorescence assays. Compound **121** [hybrid 17α-(pyridin-2-ylmethyl), R= hydrogen] exhibited specificity for the ligand-binding domain of the estrogen receptor alpha (ERα-LBD), with no detectable affinity for the ERβ isoform. In addition, this derivative exhibited moderate affinity for the ligand-binding domain of the glucocorticoid receptor (GR-LBD) (Figure 6) (Janković et al. 2024).

The ability of the compounds to inhibit the AKR1C3 and AKR1C4 enzymes was also evaluated. Compounds **120** and **121** were identified as potent inhibitors of AKR1C3, inducing 79.85% and 76.48% inhibition of the target enzyme, respectively — values higher than those observed for the ibuprofen control (64.68%). In contrast, both compounds exhibited less than 20% inhibition of the AKR1C4 enzyme, demonstrating high selectivity for AKR1C3. Finally, derivatives **120** and **121** were also subjected to molecular docking studies using the crystallographic structure of AKR1C3 (PDB ID: 1ZQ5). Compound **120** exhibited a binding energy of -9.90 $kcal.mol^{-1}$, attributed to interactions with the residues Trp227, Arg226, Tyr24, Ser118, and Asn167 present in the macromolecule's pocket, corroborating the inhibitory potential of hybrid **120** against the enzyme. Hybrid **121**, on the other hand, exhibited a binding energy of -10.04 $kcal.mol^{-1}$, suggesting an even more favorable ligand-protein interaction. Furthermore, it formed important interactions with residues Asn167, Tyr319, Tyr219, Tyr24, and Arg226 (Figure 6) (Janković et al. 2024).

As noted, the androstane-thiosemicarbazone hybrids associated with the 17α-homolactone and 17α-(pyridin-2-ylmethyl) structures were found to exhibit moderate antitumor activity. Contrary, Petrasheuskaya and colleagues adopted a different strategy by exploring a distinct molecular framework, featuring an aromatic ring in the estrone (**122**, **123**, and **124**) (Figure 6) and estradiol (**125**) (Figure 7) steroidal cores, as well as minor variations (H or CH_3) at N-4 of the thiosemicarbazone.

Petrasheuskaya et al. (2020) evaluated the antitumor effect of the hybrid 2-((3-hydroxyestra-1,3,5(10)-trien-2-yl) methylene)hydrazine-1-carbotioamide (**122**). Hybrid **122** was evaluated for its cytotoxicity against different tumor lines, showing, after 72 hours of exposure, IC_{50} values of 20.3 ± 1.4 μM for COLO-205, 9.85 ± 0.66 μM for COLO-320, and 6.42 ± 0.40 μM for MCF-7. After 24 hours of exposure, the values obtained were 31.4 ± 0.4 μM for MCF-7, 19.3 ± 0.6 μM for SK-BR-3, 54.8 ± 2.6 μM for SUM159, and IC_{50} > 50 μM for HepG-2. In addition, compound **122** was evaluated for cytotoxicity against the non-tumor cell line MRC-5, showing an IC_{50} of 22.6 ± 3.5 μM. Finally, the hybrid compound induced low production of reactive oxygen species (ROS) in SUM159 cells, as well

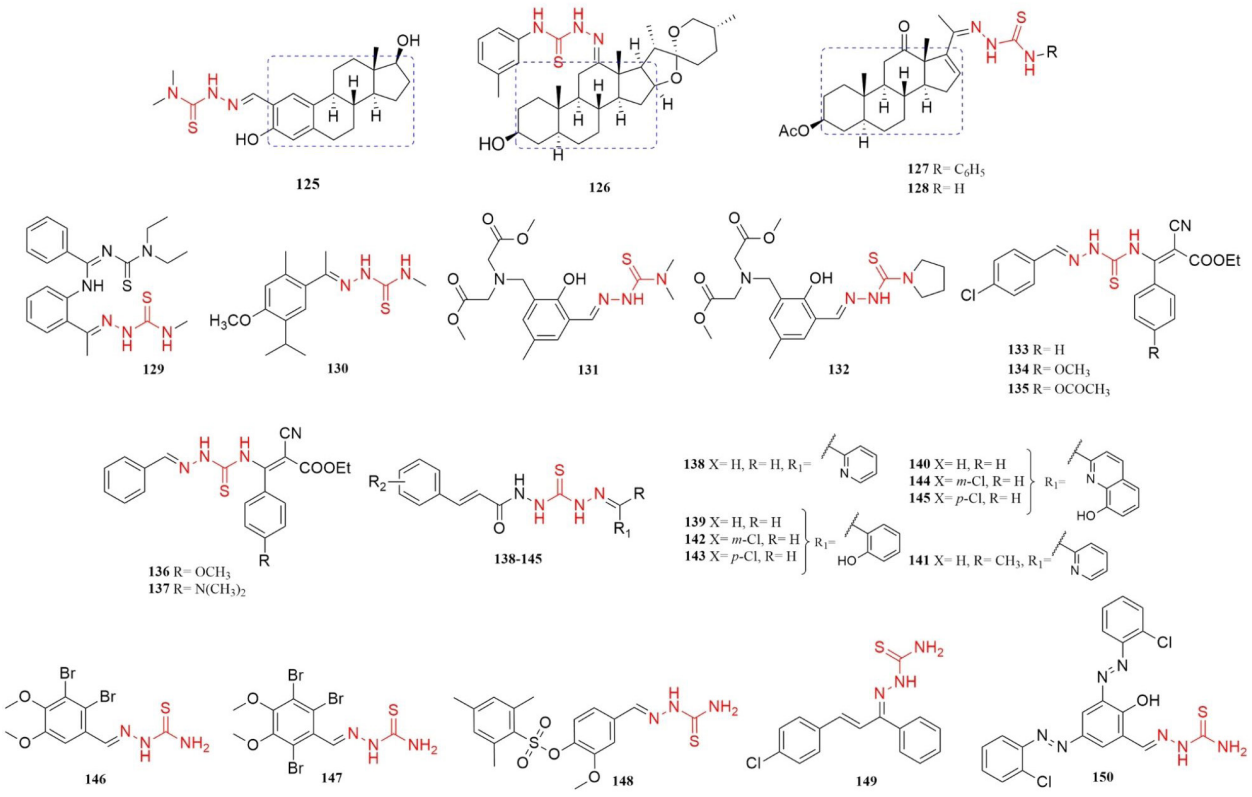


Figure 7. Thiosemicarbazone hybrids containing steroid analogues (125-128) and thiosemicarbazone hybrids containing various aromatics (129-150).

as low levels of reduced glutathione (GSH) and low catalase activity (Figure 6) (Petrasheuskaya et al. 2020).

Similarly, Petrasheuskaya et al. (2021) also proposed the synthesis of thiosemicarbazone hybrids containing other steroidal moieties, such as N-monosubstituted and N,N-dimethylated estrone-thiosemicarbazone derivatives at the terminal position. In this study, the compounds were evaluated *in vitro* against the HCT-116 cell line, yielding high IC_{50} values (**123**: IC_{50}= 20.81 ± 0.61 μM; **124**: IC_{50} > 25 μM). Due to the low activity observed, the authors did not conduct further studies with these derivatives (Figure 6) (Petrasheuskaya et al. 2021).

Similarly, Petrasheuskaya et al. (2022) also proposed the synthesis of thiosemicarbazone-estradiol hybrids containing a hydroxyl group at the C-17 position, with the aim of increasing the structure's hydrophilicity. The estradiol-thiosemicarbazone hybrids were evaluated for their antitumor properties against the MCF-7, MCF-7/KCR, DU-145, and A549 cell lines. Among the synthesized compounds, only hybrid **125** showed significant results, exhibiting an IC_{50} of 15.79 ± 1.03 μM against the A549 cell line. Other assays, such as the LDH (lactate dehydrogenase) assay to assess the loss of plasma membrane integrity in A549 and MCF-7 cells, as well as the reactive oxygen species (ROS) production assay to investigate DNA damage, were performed. However, none of the compounds yielded results considered satisfactory (Figure 7) (Petrasheuskaya et al. 2022).

Thus, it can be shown that the presence of the estrone and estradiol moieties, as well as the variations at N-4 of the thiosemicarbazone and alterations at C-17, did not result in actual

increases in antitumor activity, following the same trend as the hybrids discussed by Janković et al. (2024), with all derivatives exhibiting moderate or unsatisfactory biological activity against the tested cell lines. Unlike the trend observed for the previous hybrids, which all exhibited reduced antitumor activity, the hecogenin derivatives (**126**, **127**, and **128**) stood out, with IC_{50} values < 10 μM for the tested cell lines, demonstrating the importance of this steroid nucleus for the design of antitumor prototypes (Figure 7).

This relationship is evident in the study proposed by Elsayed et al. (2017), who developed semisynthetic analogs of hecogenin with inhibitory potential against MEK (Mitogen-Activated Protein Kinase), with the aim of treating breast cancer. Hybridization was performed between the steroidal core of hecogenin and thiosemicarbazone groups, primarily at the C-12 position, and the compounds were evaluated against various breast tumor cell lines, notably the MDA-MB-231 line. Compound **126**, corresponding to hecogenin-12-(3'-methylphenyl)thiosemicarbazone, was the most promising compound, with an IC_{50} of 1.9 ± 0.3 μM. Furthermore, in selectivity assays conducted with the non-tumor human breast epithelial cell line MCF-10A, it was observed that compound **126**, at concentrations between 1 and 20 μM, did not affect cell viability. The ability of compound **126** to induce the release of LDH (lactate dehydrogenase), a marker of cytotoxicity, in MDA-MB-231 cells was also evaluated, with cytotoxicity of only 5.94% observed at the maximum concentration of 10 μM. In the evaluation of the metastatic capacity of MDA-MB-231 cells using a wound healing assay, compound **126** promoted dose-dependent inhibition of cell migration, with an IC_{50} of 2.5 μM (Figure 7) (Elsayed et al. 2017).

When the ability of MDA-MB-231 cells to invade through the extracellular matrix was investigated, compound **126** achieved 92.4% inhibition of invasion at a concentration of 5 μM. The ability of compound **126** to inhibit MEK and ERK (Extracellular Signal-Regulated Kinase) was also evaluated, demonstrating a reduction in the expression of these kinases at both concentrations analyzed (1.5 μM and 4 μM). Molecular docking studies revealed a strong interaction between the compound and MEK (PDB ID: 3EQF), with a binding energy of -9.00 $kcal.mol^{-1}$, mediated by hydrogen bonds and hydrophobic interactions with residues such as Ser194, Cys207, and Phe209. Finally, in the *in vivo* evaluation, mice received intraperitoneal doses equivalent to 10 $mg.kg^{-1}$, administered three times a week for 28 days. No evident signs of toxicity or significant changes in body weight were observed. Furthermore, at the end of treatment, tumor inhibition of 78.1% was observed (Figure 7) (Elsayed et al. 2017).

Similarly, Bai et al. (2021) developed hecogenin-thiosemicarbazone hybrids containing different substitutions at the N-4 (R) position of the thiosemicarbazone moiety and evaluated their antitumor potential against the MCF-7, MDA-MB-231, HT-29, A549, and the non-tumor HUVEC cells. Compounds **127** (R= phenyl) and **128** (R = hydrogen) stood out for their high activity against the MCF-7 cell lines, with IC_{50} values of 2.16 μM and 1.59 μM, respectively, and against the A549 cell line, with IC_{50} values of 7.68 μM and 5.44 μM, respectively. However, against the MDA-MB-231 and HT-29 cell lines, compound **128** exhibited IC_{50} values below 10 μM, corresponding to 2.67 μM and 6.72 μM, respectively (Figure 7) (Bai et al. 2021).

Furthermore, the authors investigated whether the antitumor mechanism of compound **128** was related to the induction of apoptosis in MDA-MB-231 cells. A significant, time-dependent

increase was observed in the population of cells in early apoptosis, from 5.9% to 7.8% after 6 hours, and in late apoptosis, from 9.5% to 15.2%, also after 6 hours, using a concentration of 10 μM. In cell cycle progression studies, it was found that compound **128**, at concentrations between 10 and 40 μM, promoted a significant increase in the cell population in the sub-G1 phase in both MCF-7 and MDA-MB-231 cells, rising from 3.25% and 3.04% to 54.95% and 67.72%, respectively, indicating intense induction of cell death. Furthermore, in cell migration assays using the MDA-MB-231 cell line, compound **128** was able to significantly reduce migration at a concentration of 20 μM, also decreasing the number of cells capable of invading the Matrigel-coated Transwell chamber membrane, demonstrating its antimetastatic potential (Figure 7) (Bai et al. 2021).

Various Aromatic Compounds

As the study progresses, it becomes evident that various aromatic compounds are needed as preferred structures for the hybridization process with thiosemicarbazone. Thus, in addition to acting as secondary groups and spacers, they exhibit significant activity, functioning as pharmacophore groups that influence antitumor activity. Notable examples in this context include benzamidine, iminodiacetate, bromophenol, benzylidene, 3-aryl-2-cyanoacrylates, cinnamic acid, chalcone, thymol, and salicylaldehyde (Nepali et al. 2014).

Initially, for compounds containing benzamidine, iminodiacetate, and thymol rings linked to thiosemicarbazone, slight variations at the N-4 position of the TSC can be observed. As reported by Vijayan et al. (2015), who synthesized a benzamidine-thiosemicarbazone hybrid (N-4: methyl). Using molecular fluorescence spectroscopy assays, the binding affinity of the hybrid **129** to ct-DNA (calf thymus DNA) was evaluated, and it was found that the compound exhibited hypochromism (2.41%) at 304 nm, along with a slight red shift, indicating that the hybrid binds to DNA via intercalation (Kb= $4.3x10^3$). The ethidium bromide displacement assay and viscosity measurements corroborated the previous findings regarding how the hybrid interacts with DNA. Furthermore, the authors state that the compound under study has an affinity for BSA (Kbin= $6.05x10^7$). In the *in vitro* tests, hybrid **129** exhibited low cytotoxic activity against the tested cell lines: Vero (IC_{50}= 165.44 ± 6.05 μM), A375 (IC_{50}= 128.54 ± 3.83 μM), HeLa (IC_{50}= 190.95 ± 2.01 μM), and Hep3B (IC_{50}= 146.51 ± 2.81 μM), results inferior to cisplatin (A375: 40.32 ± 1.99 μM; HeLa: 43.32 ± 6.69 μM), the positive control (Figure 7) (Vijayan et al. 2015).

The presence of a methyl group as a substitution at N-4 was also observed in thymol hybrids (**130**) by Laamari et al. (2023), which were evaluated against different tumor lines and stood out for their good IC_{50} results (HT-1080: 7.10 ± 1.23 μM; A549: 14.40 ± 0.36 μM; MCF-7: 19.64 ± 1.45 μM; MDA-MB-231: 17.80 ± 2.74 μM). In the investigation of the type of programmed cell death induction, the HT-1080 and A549 cell lines were treated with 10 μM of the compound; for the HT-1080 cell line, there was an increase in apoptotic events (early and late apoptosis) from 1.45 ± 1.12% to 26.64 ± 2.32% compared to the control, and in the A549 cell line, there was an increase in apoptosis from 1.78 ± 1.52% to 28.32 ± 2.14% compared to the control. To understand the mechanism underlying the antitumor effect, caspase assays were performed, which showed that, with the use of compound **130**, caspase-3 and caspase-7 activity increased from 6.17 ± 1.86% and 5.23 ± 2.18% to 26.62 ± 2.71% and 27.92 ± 3.61% in HT-1080 and A549 cells, respectively. Finally, in the assessment of changes in the cell cycle progression of the HT-1080 cell line following treatment with 10 μM, an increase in cells in the

G2/M phase was observed, from 11.6% to 49.7%, and a decrease in the G0/G1 phase, from 73.5% to 27.9%, while the S phase showed no significant change (Figure 7) (Laamari et al. 2023).

Furthermore, Zaltariov et al. (2017) present thiosemicarbazone hybrids with the iminodiacetate group, which at the N-4 position contain N,N-dimethyl (**131**) and N-pyrrolidine (**132**). When also evaluated against different cell lines, **131** (HeLa - IC_{50}= 4.2 μM; K-562 - IC_{50}= 4.8 μM; A549 - IC_{50}= 5.4 μM; LS-174 - IC_{50}= 4.7 μM) and **132** (HeLa - IC_{50}= 3.9 μM; K-562 - IC_{50}= 6.1 μM; A549 - IC_{50}= 8.5 μM; LS-174 - IC_{50}= 4.7 μM) yielded good and similar results. In addition to demonstrating good selectivity, with IC_{50} values of 99.1 μM and 84.7 μM against the MRC-5 cell line, respectively. In the cell cycle assay, it was observed that after 24 hours of treatment, compound **132** was able to induce a slight increase in the sub-G1 and G1 populations of the treated K-562 cells. After 48 h, compound **131** increased the sub-G1 population — which may indicate a fraction of cells undergoing apoptosis and/or necrosis — and also caused an S-phase arrest, suggesting a possible binding to the DNA of K-562 cells; this corroborates the results of the apoptosis assay, in which a percentage increase in the number of dead cells was observed. Furthermore, a subsequent test found that, among the compounds evaluated, **131** exhibited the greatest inhibitory effect against ribonucleotide reductase (Figure 7) (Zaltariov et al. 2017).

However, there has been research into larger substitutions at the N-4 position, with Mohammed et al. (2021) and Mourad et al. (2021) investigated the synthesis of new thiosemicarbazone hybrids with the 3-aryl-2-cyanoacrylate group, presenting variations in the *para* position of the aryl group; furthermore, both authors evaluated cytotoxic activity against the same human cancer cell lines. In the study by Mohammed et al. (2021) on the MCF-7 cell line, compounds **133** (unsubstituted), **134** (methoxy), and **135** (acetyloxy) stood out, with IC_{50} values of 3.72 ± 0.23, 4.85 ± 0.29, and 3.69 ± 0.22 μM, respectively, which were lower than that of 5-FU (IC_{50}= 31.2 ± 1.65 μM). For the A549 tumor cell line, none of the compounds exhibited activity superior to that of 5-FU. However, the acetyloxy-substituted compound (**135**) showed better performance and underwent further investigation, such as cell cycle analysis, in which it caused an increase in the cell population in the G0/G1 (from 52.96% to 56.01%) and S (from 38.65% to 42.41%) phases. A decrease in the cell population in the G2/M phase (from 8.39% to 1.58%) was also observed compared to untreated cells. Furthermore, the authors found that MCF-7 cells underwent total (1.73%), early (0.54%), and late (0.13%) apoptosis when exposed to compound **135**, compared to untreated cells. The apoptosis-inducing activity of compound **135** was demonstrated by an increase in caspase-3/7 activity from 0.69% to 14.29% relative to the untreated control, as well as by the upregulation of Bax (factor of 6.054) and p53 (factor of 4.503), along with the downregulation of Bcl-2 protein expression (by a factor of 0.302). In molecular docking studies, the compounds were evaluated against TOPO IIβ (PDB ID: 3QX3), yielding binding energy values ranging from -6.99 to -9.81 kcal.mol^{-1}. Compound **135** (-9.81 kcal.mol^{-1}) stood out for forming interactions with residues Lys739 and Glu870, which are responsible for the interaction with TOPO IIβ (Figure 7) (Mohammed et al. 2021).

Among the hybrids highlighted by Mourad et al. (2021) are compound **136** (*p*-methoxyphenyl), which achieved an IC_{50} of 8.42 μM against MCF-7, and **137** (*p*-dimethylaminophenyl), which, unlike the compounds obtained by Mohammed et al. (2021), exhibited significant activity against A549, with an IC_{50}= 1.94 μM, and was also evaluated against the normal MCF-10a cell line and HEL-299 (IC_{50}= 29.25 ± 1.52 and 27.06 ± 0.31

μM, respectively). To understand the antitumor effect, a cell cycle analysis of A549 cells treated with compound **137** at a concentration of 1.94 μM revealed a reduction in the percentage of cells in the G0/G1 (from 45.8% to 38.31%) and G2/M phases (from 12.93% to 5.46%), accompanied by a notable increase in DNA content in the S phase (to 56.23%) compared to control cells; this demonstrates the interference of compound **137** with the cell cycle, leading to cell death by apoptosis. Furthermore, the early and late apoptosis rates for compound **137** at 1.94 μM were 3.15% and 14.12%, respectively, compared to untreated A549 cells, indicating a significant concentration-dependent increase in the number of apoptotic cells (Figure 7) (Mourad et al. 2021).

In addition, the mRNA expression of apoptosis-related genes was observed in the A549 cell line, revealing that compound **137** at 1.94 μM downregulates Bcl-2 gene expression (0.361-fold decrease) and upregulates the expression of the Bax and p53 genes (5.046- and 3.291-fold increases, respectively) compared to the control. In the analysis of caspase 3/7 activity in MCF-7 cells treated with compound **137** at 1.94 μM, there was a 6.27-fold upregulation compared to the control A549 cells. Finally, the compound at a concentration of 1.94 μM was also evaluated for its ability to inhibit β-tubulin polymerization and TOPO IIβ activity, showing inhibition rates of 63.4% and 55.7%, respectively. Finally, in molecular docking tests, compound **137** was tested against β-hydroxysteroid dehydrogenase (PDB ID: 3HB5) and the Kelch-like ECH-associated protein 1 (PDB ID: 1X2R), yielding docking scores of -4.70 $kcal.mol^{-1}$ and -5.89 $kcal.mol^{-1}$, respectively; regarding amino acids, with the 3HB5 receptor, it interacted with Ser12, Thr190, Arg37, Thr190, Ala196, Leu93, Ile14, and Ala91, and with the 1X2R receptor, it interacted with Val606, Ile559, Gly367, Thr560, Ala607, Cys513, Ala466, and Val369 (Mourad et al. 2021).

Furthermore, Assaleh et al. (2022) stood out for producing a series of twelve cinnamic acid-thiosemicarbazone hybrids, subdivided into four distinct series based on substitutions on the azomethine carbon, aromatic groups at R_1, and possible minor variations in R. In addition, the series also feature substitutions (R_2) on the aromatic ring derived from the cinnamic acid moiety. Among the hybrids, **138** (R= H, R_1= 2-pyridyl, R_2= H), **139** (R= H, R_1= 2-phenol, R_2= H), and **140** (R= H, R_1= 8-hydroxyquinolin-2-yl, R_2= H) proved to be the most active against A549 cells, in which they reduced the viable cell population by more than 50% at a concentration of 100 μM (49 ± 7%, 49 ± 4%, and 49 ± 4% viable cells, respectively). Compound **141** (R= methyl, R_1= 2-pyridyl, R_2= H) demonstrated that the introduction of the methyl group at the C7 position significantly reduced antitumor activity in all cell lines (when compared to compound **138**). The addition of a chlorine atom at the *meta* or *para* positions of the cinnamoyl ring resulted in analogs with distinct activities, notably compounds **139** and **140**, in which derivative **142** (R= H, R_1= 2-phenol, R_2= *m*-chloro) was more potent (Sk-OV-3: 21 ± 8 μM; A549: 39 ± 3 μM) than derivative **143** (R= H, R_1= 2-phenol, R_2= *p*-chloro) (Sk-OV-3: 72 ± 5 μM; A549: 58 ± 6 μM) and compound **139**, which has no substitution on the aromatic ring (Sk-OV-3: 67 ± 9 μM; A549: 48 ± 4 μM), which exhibited similar activity (Figure 7) (Assaleh et al. 2022).

The opposite was observed for hybrid **140** (Sk-OV-3: 65 ± 5 μM; A549: 48 ± 4 μM), in which the substitution at the *meta* position (compound **144** - R= H, R_1= 8-hydroxyquinolin-2-yl, R_2= *m*-chloro) reduced anticancer activity, whereas the substitution (compound **145** - R= H, R_1= 8-hydroxyquinolin-2-yl, R_2= *p*-chloro) exhibited activity against four of the five tested cell lines (LoVo: 43 ± 5 μM; SK-OV-3: 43 ± 3 μM; A549: 38 ±

2 μM; MCF-7: 35 ± 3 μM). None of the derivatives had substantial effects on the AsPC-1 cell line. However, the viability of MCF-7 cells was reduced by compounds **142** and **145**, which also stood out in relation to SK-OV-3 cells, exhibiting a notable incidence of cell death only at a concentration of 100 μM. For LoVo cells, compound **145** was the only one to exert a substantial effect on cell survival. Finally, A549 cells demonstrated greater susceptibility to cinnamic acid hydrazides, but only compounds **142** and **145** reduced cell survival to less than 50% at concentrations below 100 μM (Figure 7) (Assaleh et al. 2022).

Finally, another structural pattern that also yielded good results corresponds to structures in which modifications were made only to the azomethine carbon, without any substitutions at the N-4 position of the thiosemicarbazone. This is the case with the bromophenol-thiosemicarbazone hybrid **146** (R_1= 2,3-dibromo-4,5-dimethoxyphenyl) by Guo et al. (2019) and **147** (R_1= 2,3,6-dibromo-4,5-dimethoxyphenyl) by Guo et al. (2020). Initially, compound **146** exhibited selective inhibitory activity against polymerase-1 (IC_{50} = 29.5 μM) and potential antitumor activity against the SK-OV-3, Bel-7402, and HepG-2 cancer cell lines (IC_{50}= 2.39; 5.45, and 4.60 μM, respectively). Furthermore, compound **146**, at doses of 25 and 50 $mg.kg^{-1}$, inhibited tumor growth in the *in vivo* SK-OV-3 cell xenograft model (70.02% and 58.87%, respectively), while inhibition by the positive control olaparib was 55.73% (25 $mg.kg^{-1}$). Furthermore, other tests demonstrated that compound **146** exerts an antitumor effect by inducing apoptosis and cell cycle arrest, causing DNA double-strand breaks, alterations in DNA repair, inhibition of PARylation, and antiproliferative effects resulting from the production of reactive oxygen species (Figure 7) (Guo et al. 2019).

In addition, the compound **147** showed good results against various cell lines, the results against HCC-1937, Capan-1, MDA-MB-231, and MCF-7 with IC_{50} values of 2.13 ± 0.67 μM, 3.88 ± 1.01 μM, 4.78 ± 1.70 μM, and 5.01 ± 1.97 μM, respectively. For central nervous system tumor cell lines, the IC_{50} values were 7.01 ± 2.23 μM for A172 and 7.78 ± 1.68 μM for U-87 MG. Finally, for other cell lines, such as PANC-1, SK-OV-3, and HepG-2, the IC_{50} values were 7.28 ± 2.09 μM, 8.39 ± 0.83 μM, and 18.25 ± 1.55 μM, respectively. Thus, compound **147** proved to be less effective than compound **146** against the SK-OV-3 and HepG-2 cell lines. Regarding the non-tumor cell line HELF, compound **147** exhibited an IC_{50} was 12.29 ± 0.70 μM, and selectivity for tumor cells was observed, particularly those deficient in BRCA. Compound **147** demonstrated potent inhibition of PARP-1 (IC_{50} of 79.79 ± 2.16 μM). Furthermore, it was able to induce cell apoptosis and cell cycle arrest at the G2/M phase in HCC-1937 cells, with these results primarily related to PARP-1 inhibition. In the *in vivo* studies, the compound **147** reduced tumor growth in the HCC-1937 xenograft by 49.56% (Figure 7) (Guo et al. 2020).

Another aromatic nucleus investigated was 2,4,6-trimethylphenylsulfonyl, which is linked to thiosemicarbazone via a methoxyphenyl group (**148**), as reported by Zhang et al. (2024). Among the series obtained by the author, compound **148** was the only one that stood out in the analysis of PARP-1 (at 100 nM) and PARP-2 inhibition potential, exhibiting the highest inhibition values, equal to 42.51% and 46.68%, respectively. The author explained the low potency of the other compounds in the series by noting that the thiosemicarbazone group has poor binding affinity at the nicotinamide (NI) binding site. This is because, although it can only partially mimic NAD^+, forming important hydrogen bonds with the Ser904 and Gly863 residues of PARP-1, the absence of essential aromatic structures prevents the formation of

π-π stacking interactions with Tyr907 and/or Tyr896 (Figure 7) (Zhang et al. 2024).

Finally, Campos et al. (2023) and Awaji et al. (2024) also synthesized interesting molecules containing the thiosemicarbazone unit, proposing thiosemicarbazone-chalcone (**149**) and bis-azo-salicylaldehyde-thiosemicarbazone (**150**) hybrids, respectively. Initially, compound **149** exhibited low toxicity (LD_{50} > 100 μM) in toxicity tests using *Artemia salina*. In addition to reducing the viability of MT-2 cells infected with HTLV-1, it exhibited an IC_{50} of 47.06 μM, compared to cisplatin (IC_{50}= 2.29 μM). In the cell death assay, the results indicated that 50 μM of compound **149** exerted a pro-apoptotic effect after 24 hours of incubation, resulting in 36.1% apoptotic cells. It was also found that the compound reduced the expression of CD25 by approximately 30%. Furthermore, through fluorescence emission assays, it was confirmed that the compound can interact with DNA. To better understand this, interaction studies were conducted using molecular docking with DNA (PDB ID: 1BNA), in which compound **149** established interactions with DG04, DA05, DA06, DT20, and DG22, yielding a score of 40.1 in the major groove and a score of 58.5 in the minor groove. The authors suggested that compound 158 could interact with DNA primarily through the minor grooves (Figure 7) (Campos et al. 2023).

Compound **150** from Awaji et al. (2024) was investigated for its efficacy and safety against the A431 cell line. Based on cytotoxicity studies using the MTT assay, bis-azo-salicylaldehyde-thiosemicarbazone demonstrated selectivity for A431 tumor cells (IC_{50}= 126.58 ± 3.75 μM) compared to HSF cells (IC_{50}= 151.77 ± 4.37 μM). In gene expression studies, treatment with compound **150** resulted in a significant decrease in phosphatidylinositol 3-kinase (PI3K) activity. However, the other compounds, also reported in the study, showed better results (Figure 7) (Awaji et al. 2024).

Promising Thiosemicarbazone Hybrids Against Cancer Cell Lines and Molecular Targets

Figure 8 shows a structure-activity relationship, and Table I summarizes the IC_{50} results for the thiosemicarbazone hybrids highlighted in this review. It shows that only 20 hybrids exhibited a good inhibition profile in tumor cell lines. Among them, thiosemicarbazone hybrids with nitrogen-containing groups yielded the highest number of promising results, with nine molecules exhibiting IC_{50} values below 2 μM, including hybrids containing indole, quinoline, pyridine, and pyrazole moieties.

Among the nitrogen heterocycles, it can be observed that the lowest results are related to a hybrid of thiosemicarbazone with the pyrazole fragment (**65** - IC_{50}= 0.16 ± 0.02 μM against SR) and indole (**13** - IC_{50}= 0.19 μM against A431). The good inhibition profile of hybrids containing the quinoline fragment is also evident, such as **34** and **35**, which expressed results below 1

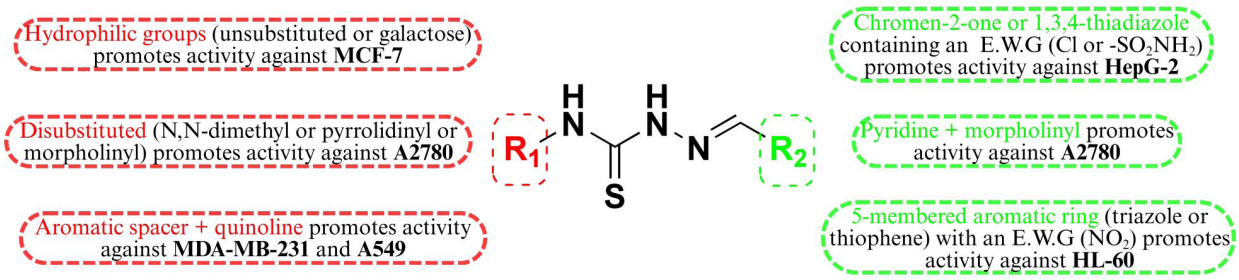


Figure 8. Main structural features of thiosemicarbazone-based hybrids associated with antitumor activity against different cancer cell lines.

μM, ranging from 0.21 ± 0.02 μM to 0.82 ± 0.21 μM against A549, HT-29, and MKN-45. However, it is noteworthy that compound **34**, which has a phenyl group in the azomethine of the thiosemicarbazone, showed slightly better results than compound **35** (Table I).

Furthermore, hybrids containing oxygenated heterocycles also stood out, with three coumarin hybrids and four morpholine hybrids showing results below 2 μM. However, it is evident that thiosemicarbazone hybrids with the morpholine group obtained the best results in this review, with inhibition concentration values below 0.1 μM. These are compounds **102**, **103**, and **104**, in which **103**, which has a pyrrolidinyl group at N-4, showed the best IC_{50} results against A2780 (0.008 ± 0.002 μM) and A2780cisR (0.028 ± 0.006 μM). Meanwhile, hybrids **85** and **86**, which contain the coumarin fragment, showed values ranging from 1.28 μM to 1.82 μM against HepG-2, MCF-7, LU-1, and SK-MEL-2 (Table I).

Regarding the other groups, sulfur heterocycles, various heterocycles, and various aromatics, each presented only one hybrid with biological activity below 2 μM, namely thiophene (**80**), thiadiazole (**112**), and 3-aryl-2-cyanoacrylates (**137**), tested against HL-60 (IC_{50}= 1.54 μM), HepG-2 (IC_{50}= 0.53 ± 0.01 μM) and A549 (IC_{50}= 1.94 μM), respectively. Meanwhile, the steroid analogues had two hybrids with results below 2 μM, namely compounds **126** and **128**, evaluated against MCF-7 (IC_{50}= 1.59 μM) and MDA-MB-231 (IC_{50}= 1.9 ± 0.3 μM) (Table I).

In addition, we observed the substitution pattern of the N-4 position of thiosemicarbazones among the compounds highlighted in Table I. It is noted that 17 hybrids have substitutions in the N-4 position of thiosemicarbazone, with the presence of the phenyl group being verified in seven molecules, with modifications in the *meta* and *para* positions, with the presence of methyl, hydroxyl, nitro, and amino groups, as well as bromine, chlorine, and fluorine atoms. There are also structures that had N-4 composing cyclic frameworks ranging from 5 to 7 members, with other nitrogen and oxygen atoms composing the cycle, in addition to the interposition of a phenyl group and carbonyls, as occurs with **43**. In addition, three frameworks had monosaccharides in N-4, and to a lesser extent, the presence of methyl groups and indirect bonding with quinoline and ethyl cyanoacrylate groups were verified as substitutions.

Upon analyzing the data extracted from Table I, several structural observations can be made regarding the strains in which at least three hybrids exhibited activity. When examining compounds **85** and **86**, which contain a *D*-galactose group at N-4, and compound **128**, in which that position is unsubstituted, a contribution from hydrophilic groups can be observed against the MCF-7 cell line. Additionally, for the A2780 cell line, it is evident that the N,N-dimethyl, pyrrolidinyl, and morpholinyl groups found in compounds **102**, **103**, and **104**, respectively, were the N-4 substitutions that yielded the best results. Furthermore, the presence of a spacer (phenoxy group) between N-4 and the quinoline moiety (compounds **34** and **35**) or a substituted aromatic group (compounds **126** and **137**) were the ones that stood out in the MDA-MB-231 and A549 cell lines.

Regarding the benzylidene moiety, some observations were also made. For compounds **85** and **86** (chromen-2-one) and **112** (1,3,4-thiadiazole), it can be observed that these aromatic structures were substituted with electron-withdrawing groups (-Cl or $-SO_2NH_2$) and that this fact may be associated with activity against the HepG-2 cell line. In turn, the combination of the 2-pyridine and morpholine moieties appears to have enhanced

Table I. Notable compounds reported in the articles included in this review that exhibited IC_{50} values below 2 μM.

Authorship	Cancer cell line	Hybrid	IC_{50}
Ohui et al. (2019)	A2780	**102**	0.010 ± 0.001 μM
		103	0.008 ± 0.002 μM
		104	0.07 ± 0.01 μM
	A2780cisR	**102**	0.035 ± 0.006 μM
		103	0.028 ± 0.006 μM
		104	0.76 ± 0.06 μM
Chaudhary et al. (2024)	A431	**13**	0.19 μM
Milunovic et al. (2024)	MES-SA	**108**	0.25 ± 0.05 μM
Zhai et al. (2016)	A549	**34**	0.33 ± 0.02 μM
		35	0.23 ± 0.02 μM
	HT-29	**34**	0.21 ± 0.02 μM
		35	0.42 ± 0.09 μM
	MKN-45	**34**	0.71 ± 0.08 μM
		35	0.82 ± 0.21 μM
	MDA-MB-231	**34**	1.2 ± 0.17 μM
		35	1.4 ± 0.15 μM
Bondock et al. (2023)	HepG-2	**112**	0.53 ± 0.01 μM
	Caco2	**112**	1.01 ± 0.10 μM
	MCF-7	**112**	1.12 ± 0.10 μM
Blázquez-Tapias et al. (2024)	HeLa	**50**	1.06 ± 0.21 μM
		51	1.49 ± 0.46 μM
Othman et al. (2022)	HL-60	**64**	0.47 ± 0.03 μM
		66	1.09 ± 0.01 μM
	SR	**65**	0.16 ± 0.02 μM
Marques et al. (2019)	HL-60	**80**	1.63 μM
Toan & Thanh (2021)	HepG-2	**85**	1.53 μM
		86	1.75 μM
	MCF-7	**85**	1.28 μM
		86	1.81 μM
Bai et al. (2021)	MCF-7	**128**	1.59 μM
Elkafoury et al. (2024)	MDA-MB-468	**43**	1.83 μM
Elsayed et al. (2017)	MDA-MB-231	**126**	1.9 ± 0.3 μM
Mourad et al. (2021)	A549	**137**	1.94 μM

the pharmacological potential against the A2780 cell line, as observed in compounds **102**, **103**, and **104**, respectively. Finally, the presence of the bioisosteric heterocycles 1,2,3-triazole or thiophene — when directly or indirectly substituted by the nitro group (NO_2) — may have been crucial for the activity demonstrated by compounds **64**, **66**, and **80** against the HL-60 cell line.

By analyzing the results of the extracted articles, based on the observation of molecular docking results, one can understand the author's interest in investigating the interaction of the molecules presented throughout the review with 23 calls for molecular targets, as shown in Table II. Among them, the most frequently addressed targets were VEGFR-2 and topoisomerases. For VEGFR-2, the use of three different PDB codes was understood, with ID 4ASD and 2OH4 evaluated against hybrids containing indole (**11** and **13**) and hybrids containing quinoline (**41** and **42**), respectively. Meanwhile, 3WZE was evaluated only with a hybrid containing pyrazole (**66**), as shown in Figure 9.

Among the hybrids studied, the lowest bond energy value was presented by **42** (-12.85 $kcal.mol^{-1}$), which consists of a hybrid of thiosemicarbazone with quinoline, similar to **41**, which also had a good result presented by its bond energy, as shown in Figure 9. The difference between the compounds is evident in the N-2 position of quinazolin-4(3H)-one, with an ethyl group present in **42** and a *p*-methylphenyl group in **41**. Furthermore, both compounds showed IC_{50} values below 10 μM against the HepG-2, HCT-116, and MCF-7 cell lines. However, in the evaluation of *in vitro* inhibition of VEGFR-2, **42** obtained an IC_{50} value of 2.67 μM, while **41** reached 4.1 ± 0.06 μM, as shown in Table II.

In addition, compound **13** also had an interesting interaction energy value (-11.1 $kcal.mol^{-1}$), which corroborates the results found in *in vitro* tests against A431, in which it obtained a low IC_{50} value (0.19 μM). Derivative **11** obtained a binding energy result of -6.31 $kcal.mol^{-1}$, and despite being a lower result, it achieved IC_{50} values lower than 5 μM against strains A431, A549, and MCF-7. Finally, compound **66** had an interaction energy value of -7.33 $kcal.mol^{-1}$ and obtained one of the best IC_{50} values against the HL-60 strain (1.09 ± 0.01 μM) and *in vitro* inhibition against the VEGFR-2 enzyme (IC_{50}= 0.067 ± 0.028 μM), as shown in Table II.

Furthermore, the differences between the co-crystallized targets used in each study, as well as the limitations of the results — such as the absence of macromolecule-ligand complexes for some of the hybrids (**41** and **42**) — make it difficult to conduct an in-depth analysis of the interaction profile with VEGFR-2. Overall, it can be assumed that the inclusion of a heterobicyclic system in the azomethine moiety of the thiosemicarbazone, as evidenced in compounds **11** and **13**, appears to favor hydrogen bonding with the Lys868 amino acid residue. When we specifically examine the indole ring at C-5 substituted with a hydrogen-bonding donor group (**13**), the stability of the complex is enhanced by promoting interaction with Val899. Replacing the bicyclic system with a *p*-nitrophenyl-substituted triazole ring at the azomethine portion, as seen in compound **66**, alters the profile of interactions with the target, favoring hydrogen bonding with the Asp1046 residue. Finally, the absence of substituents at N-4 of the thiosemicarbazone (compounds **41** and **42**), does not appear to directly impact affinity for the target, maintaining a binding energy similar to that of the previous compounds.

However, it should be noted that it is not possible to precisely identify in which region of VEGFR-2 (hinge-binding element, linker, and/or allosteric pocket) the thiosemicarbazone moiety makes a specific contribution, since the

Table II. Biological targets of interest for thiosemicarbazones reported in the articles included in this review.

Biological Target	PDB ID	Authorship	Hybrid	Interaction Energy	Interaction regions	*In vitro* inhibitions
VEGFR-2	4ASD	Chaudhary et al. (2023)	**11**	-6.31 kcal.mol^{-1}	Ile1025 and Arg1027	-
		Chaudhary et al. (2024)	**13**	-11.1 kcal.mol^{-1}	Lys868, Val899, Glu885, Leu889 Val848, Val899, Val916, Cys1045, Phe1047	-
	2OH4	Mahdy et al. (2020)	**41**	-53.80 kJ.mol^{-1}	-	IC_{50}= 4.1 ± 0.06 µM
		El-Adl et al. (2021)	**42**	-47.72 kJ.mol^{-1}	-	IC_{50}= 1.00 ± 0.13 µM
	3WZE	Othman et al. (2022)	**66**	-7.33 kcal.mol^{-1}	Cys919, Cys1045, Glu885, and Val899	IC_{50}= 0.067 ± 0.028 µM
VEGFR-2 kinase	3VHE	Chaudhary et al. (2024)	**13**	-10.10 kcal.mol^{-1}	Leu840, Leu840, Lys868, Val899, Cys1045, and Phe1047	-
	5GWK	Sousa et al. (2024)	**56**	Score= 95.33	Arg487 and Asp463	% Inhibition (100 µM) = 95%
TOPO IIα	1ZXM	Bakherad et al. (2019)	**6**	Score= 59.61	Leu248 e Lys254, Ala317, Lys352, Asn12, Ile141, Ser148, Ala167, and Lys168	-
TOPO IIβ	3QX3	Mohammed et al. (2021)	**135**	-9.81 kcal.mol^{-1}	Lys739 and Glu870	-
TOPO-I	1T8I	Elkafoury et al. (2024)	**43**	-	Asn722, Arg364, Lys532, and His632	IC_{50}= 46.2 ± 3.3 nM
AKR1C3	1ZQ5	Janković et al. (2024)	**120**	-9.90 kcal.mol^{-1}	Trp227, Arg226, Tyr24, Ser118, and Asn167	% Inhibition (33 µM) = 79.85%
			121	-10.04 kcal.mol^{-1}	Asn167, Tyr319, Tyr219, Tyr24, and Arg226	% Inhibition (33 µM) = 76.48%
β-hydroxysteroid dehydrogenase	3HB5	Mourad et al. (2021)	**137**	-4.70 kcal.mol^{-1}	Ser12, Thr190, Arg37, Thr190, Ala196, Leu93, Ile14, and Ala91	-
Caspase-3	3GJQ	Bimoussa et al. (2024)	**99**	-4.96 kcal.mol^{-1}	-	-
CDK2	6GUH	Kassem et al. (2024)	**47**	-6.40 kcal.mol^{-1}	Ile10, Asp86, and Gln131	IC_{50}= 16.73 µM
		Bakherad et al. (2019)	**7**	-9.20 kcal.mol^{-1}	Ile10, Val18, Val64, Phe80, Lys89, Leu134, Ala144, and Gln131	-
cIAP	-	Laamari et al. (2025a)	**97**	-30.66 kJ.mol^{-1}	Ser130, Val108, and Phe109	-
bCAII	-	Laamari et al. (2025a)	**97**	-23.94 kJ.mol^{-1}	Asp163, Leu222, and Lys223	-

Table II. Continuation.

bTNAP	-	Laamari et al. (2025a)	**97**	-29.82 kJ.mol^{-1}	His434, Glu435, His321, and His324	-
DHFR	1KSM	Aftab et al. (2024)	**69**	-	Ser59, Val115, Ile7, Phe34, and Leu22	IC_{50}= 12.37 ± 0.48 µM
EGFR	4HJO	Toan & Thanh (2021)	**85**	-6.84 kcal. mol^{-1}	Asp831, Thr830, Thr766, Cys773, and Gly772	IC_{50}= 0.512 µM
			86	-6.80 kcal. mol^{-1}	Asp831, Thr830, Cys773, Arg817, and Gly772	IC_{50}= 0.258 µM
DNA	1BNA	Marques et al. (2019)	**80**	-	DC23 and DG2	-
		Campos et al. (2023)	**149**	-	DG04, DA05, DA06, DT20, and DG22	-
HDAC4	2VQJ	Paneth et al. (2023)	**113**	-25.40 kcal. mol^{-1}	His158, His159, Gly331, Pro156, His159, Phe168, and Gly330.	-
			114	-27.00 kcal. mol^{-1}		-
			115	-27.80 kcal. mol^{-1}		-
HDAC4c	4CBY	Paneth et al. (2023)	**113**	-18.50 kcal. mol^{-1}	-	-
			114	-18.50 kcal. mol^{-1}	-	-
			115	-18.00 kcal. mol^{-1}	-	-
HDAC8	3SFF	Paneth et al. (2023)	**113**	-21.90 kcal. mol^{-1}	Tyr306, His143, Gly151, Phe152, His180, Phe208, Ile34, Trp141, Gly303, and Gly304	-
			114	-20.10 kcal. mol^{-1}		-
			115	-21.10 kcal. mol^{-1}		-
IGF-1	1JQH	Kumar et al. (2018)	**17**	-6.70 kcal. mol^{-1}	Leu22, Val30, Ala48, Ser26, Lys176, Lys50, Gly167, and Met99	-
Kelch-like ECH-associated protein 1	1X2R	Mourad et al. (2021)	**137**	-5.89 kcal. mol^{-1}	Val606, Ile559, Gly367, Thr560, Ala607, Cys513, Ala466, and Val369	-
Kinase 2	2VTA	Chaudhary et al. (2024)	**13**	-10.40 kcal. mol^{-1}	Glu81, Leu83, Asp145, Ile10 Val18, Ala31, Phe82, Ala134, and Leu144	-
Kinase CK2α	6TGU	Abolibda et al. (2025)	**54**	-5.17 kcal. mol^{-1}	His161	-

Table II. Continuation.

MEK kinase	3EQF	Elsayed et al. (2017)	**126**	-9.00 kcal. mol^{-1}	Ser194, Cys207, and Phe209	-
mR2 RNR	1W68	Milunovic et al. (2024)	**108**	Score= 65.1	Try324, Glu335, Asp272, Phe241, Val328, and Phe237.	-
PARP-1	7AAD	Elkafoury et al. (2024)	**43**	-	Ser904, Gly863, Ser864, Glu763, and Tyr907	IC_{50}= 32.2 ± 3.26 nM
PI3K	4TV3	Mushtaq et al. (2024)	**26**	-10.30 kcal. mol^{-1}	His670, Met811, Ile633, Leu632, and Cys838	-
			27	-8.60 kcal. mol^{-1}	Gln630, Gln815, Lys271, Leu755, His670, Phe666, Leu814, Glu849, and Ser629	-
			28	-8.90 kcal. mol^{-1}	Lys548, Asn575, Tyт361, Leu367, Cys368, Pro366, Asp454, and Pro458.	-
PPARγ LBD	6DGR	Paneth et al. (2023)	**113**	-25.80 kcal. mol^{-1}	Tyr473, Phe282, Gln286, Ser289, His323, His449 and Leu469	-
			114	-25.50 kcal. mol^{-1}		-
			115	-28.50 kcal. mol^{-1}	Tyr327, Met364, Lys367, Leu340, Ile341, and Phe264	-
ROCK-1	3TWJ	Alqahtani & Bayazeed (2020)	**49**	-6.76 kcal. mol^{-1}	Asp374 and Arg84	-
Tyrosinase	2Y9W	Batool et al. (2024)	**8**	-5.15 kcal. mol^{-1}	Asp357, Ser364, Tyr311, Phe368, Val37, and Trp358.	IC_{50}= 12.40 ± 0.26 µM
	2Y9X	Azimi et al. (2024)	**62**	-	His61, His259 and His296, Cys83, and Asn81	IC_{50}= 2.09 ± 0.32 µM

interaction depends on the overall architecture of the hybrids and their respective conformations. This is reflected in the heterogeneous profile of interactions with the amino acid residues Asp1046, Glu885, Lys868, and Cys1045, depending on the compound involved. Furthermore, these studies may suggest a possible application of this moiety to mimic the HBA/HBD pharmacophore of type II inhibitors.

Relevant to the tests involving topoisomerases, the authors' interest in detecting the interaction of their ligands with different subtypes of the enzyme was understood, as shown in Figure 10. TOPO-I (PDB ID: 1T8I), at first, in analyses with the quinoline hybrid **43**, no detailed binding energy values were verified, but as presented by the author, it would be close to -42.4321 kcal.mol^{-1}. Furthermore, in *in vitro* enzyme inhibition studies, the IC_{50} result was 46.2

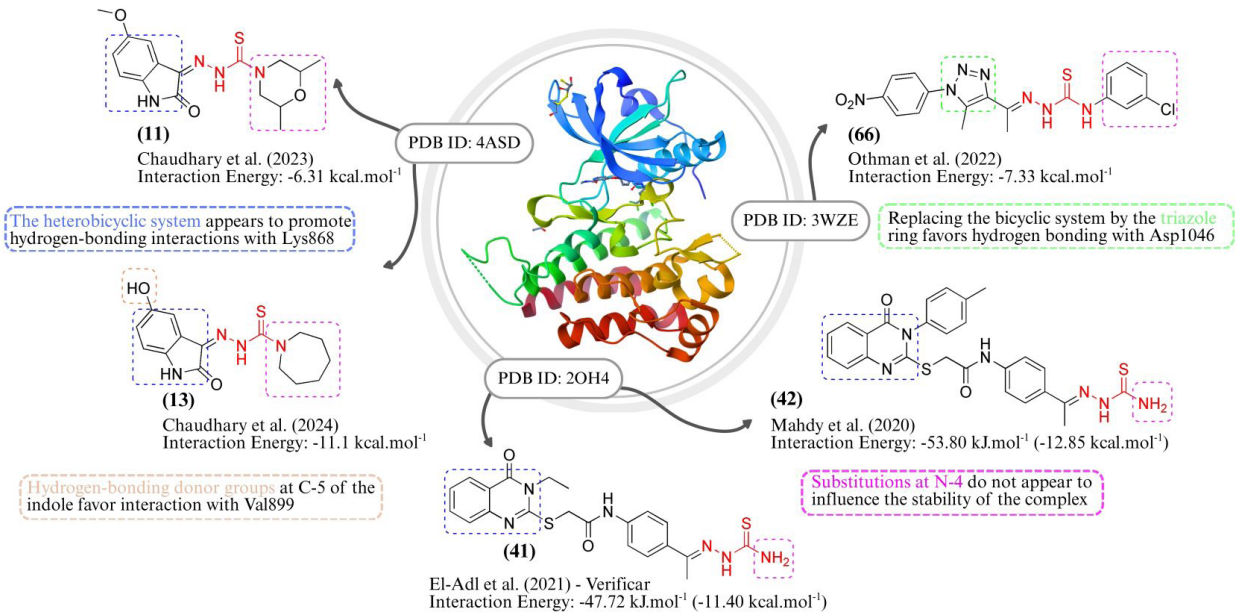


Figure 9. Illustration showing the VEGFR-2 target with the main thiosemicarbazone-based hybrids highlighted by the respective authors as promising in the interaction.

± 3.3 nM, while in MDA-MB-468 lineage inhibition tests, the IC_{50} was 1.83 µM. Furthermore, TOPO IIα was evaluated against a hybrid containing indole (**6**) and acridine (**56**), using PDB ID 1ZXM and 5GWK, respectively. Among them, hybrid **56** had the highest interaction score, equal to 95.33, and in *in vitro* evaluations, it achieved 95% enzyme inhibition at 100 µM and an IC_{50} of 10.69 µM against Lucena-1. In relation to **6**, a score of 59.61 was verified, and an IC_{50} result equal to 12.50 ± 1.00 µM against A-549. Finally, TOPO IIβ (PDB ID: 3QX3) was anchored with the hybrid of thiosemicarbazone with 3-aryl-2-cyanoacrylate **135**, with a binding energy result of -9.81 kcal. mol^{-1}, and an IC_{50} value against MCF-7 equal to 3.69 ± 0.22 µM.

Molecular Hybridization and Translational Challenges

Although the molecular hybridization strategy appears promising, certain difficulties can be identified as barriers to translating the results into clinical practice. Among these, the physicochemical properties of the compounds stand out; since they are obtained by combining pharmacophore subunits, they can lead to a considerable increase in molecular weight and, consequently, lipophilicity, resulting in hybrids with unfavorable pharmacokinetic characteristics, such as low oral bioavailability (Gediya & Njar 2009, Arya et al. 2025).

In addition, research is largely based on *in vitro* cytotoxic assays and/or *in silico* predictions, with uncertain forecasts or results that rarely correlate with clinical efficacy. Furthermore, factors such as metabolic stability, toxicity, synthetic complexity, and other limitations may also be called into question. As a result, few hybrids advance to the *in vivo* and clinical trials, highlighting the gaps that need to be addressed in drug design. This fact is also evident in the case of thiosemicarbazone hybrids, none of which have, to date, been approved for clinical use as antineoplastic agents by regulatory agencies (Gediya & Njar 2009, Arya et al. 2025).

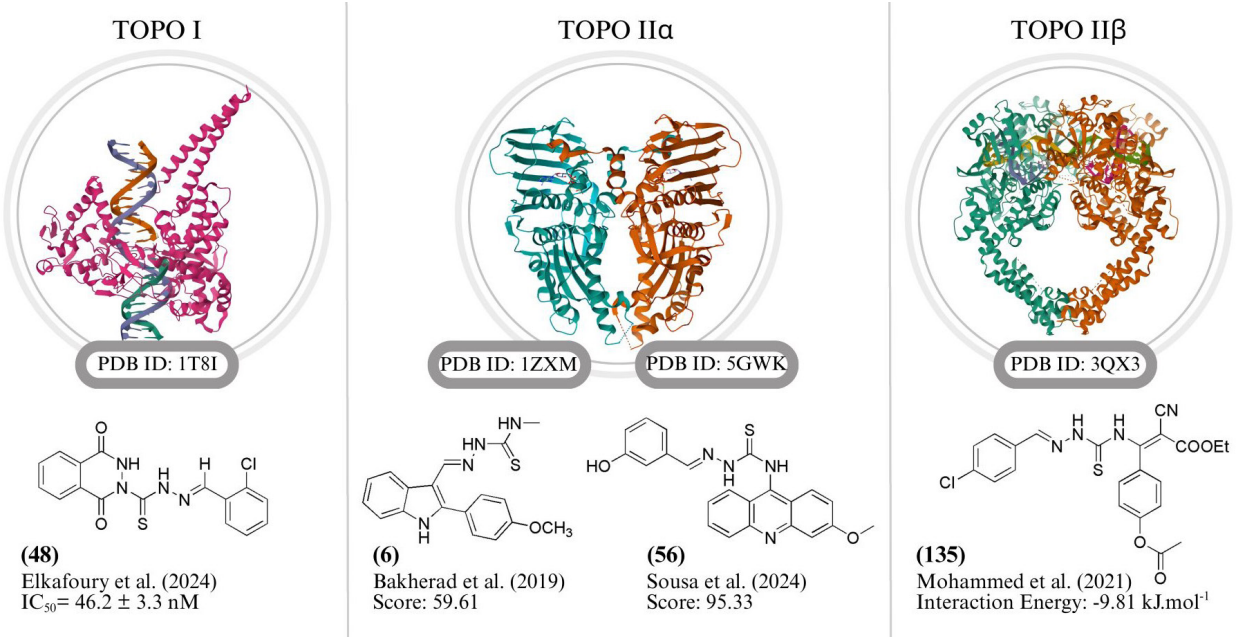


Figure 10. Illustration showing the topoisomerase target with the main thiocarbazone-based hybrids highlighted by the respective authors as promising in their interaction with the different isoforms of the enzyme.

CONCLUSIONS

In the last decade (2015-2025), there has been considerable interest in designing hybrids containing the thiosemicarbazone fragment in their structures for antitumor activity. This fact can be evidenced by the large number of publications contained in this review that comprise the synthesis of these hybrids, as well as *in silico*, *in vitro*, and/or *in vivo* evaluations showing compounds that are potential candidates for antitumor drugs.

This study highlighted the main substitutions found in the benzylidene and N-4 portions of the thiosemicarbazone fragment, presenting experiments in which the results were promising. In addition, cases of failure were also presented. Thus, the relevance of nitrogenous heterocycles in the composition of prominent hybrids is indisputable, given the large number of publications related to this fragment, as well as the outstanding performance presented in the described assays. In addition, this review also showed the notoriety that other molecular frameworks, such as oxygenated heterocycles, develop in the construction of leading compounds aimed at the activity of interest, considering the promising results obtained at both testing levels.

At the molecular level, this review highlighted the main pharmacological targets explored (VEGFR-2 and topoisomerases) in tests with thiosemicarbazone hybrids, using either computational methods or *in vitro* assays. One point worth noting is that few studies included *in vitro* experiments to validate the *in silico* findings regarding the mechanism of action of these hybrids. Thus, this gap can be addressed in future studies to provide greater robustness to the scientific findings at this discovery phase.

The range of tumor cell lines highlighted in the *in vitro* evaluation of thiosemicarbazone hybrids and their pharmacological potential against these lines is well known. However, the large number of *in vitro* cytotoxic assays is not accompanied by validation methods in animal models. In the early phase of lead compound discovery, a wide variety of validation assays

are necessary to establish a stronger scientific foundation.

Therefore, considering the biological potential of thiosemicarbazones, coupled with their ease of obtaining, the search for antitumor drugs finds a promising field that is still to be explored for the research and development of lead compounds. In short, this review consolidates a decade of advances in the hybridization of thiosemicarbazones, providing a rational basis for researchers to guide the synthesis of new antitumor prototypes, reduce costs, and optimize the selection of targets and cell lines in the preclinical stages.

Acknowledgments

The authors would like to thank the Conselho Nacional de Desenvolvimento Científico e Tecnológico (CNPq) (Process 306865/2020-3-PQ-3) for funding the research and the University of International Integration of Afro-Brazilian Lusophony for its support.

REFERENCES

ABDALLAH AM, GOMHA SM, ZAKI MEA, ABOLIBDA TZ & KHEDER NA. 2023. A green synthesis, DFT calculations, and molecular docking study of some new indeno[2,1-b]quinoxalines containing thiazole moiety. J Mol Struct 1292: 136044.

ABOLIBDA TZ, EL-SAYED AAAA, FARAG B, ZAKI MEA, ALREHAILY A, ELBADAWY HM, AL-SHAHRI AA, ALSENANI SR & GOMHA SM. 2025. Novel thiazolyl-pyrimidine derivatives as potential anticancer agents: Synthesis, biological evaluation, and molecular docking studies. Results Chem 13: 102008.

ABUSAIF MS, RAGAB A, FAYED EA, AMMAR YA, GOWIFEL AMH, HASSANIN SO, AHMED GE & GOHAR NA. 2025. Exploring a novel thiazole derivatives hybrid with fluorinated-indenoquinoxaline as dual inhibitors targeting VEGFR2/AKT and apoptosis inducers against hepatocellular carcinoma with docking simulation. Bioorg Chem 154: 108023.

AFIFI OS, SHAABAN OG, RAZIK HAAE, EL-DINE S, ASHOUR FA, EL-TOMBARY AA & ABU-SERIE MM. 2019. Synthesis and biological evaluation of purine-pyrazole hybrids incorporating thiazole, thiazolidinone or rhodanine moiety as 15-LOX inhibitors endowed with anticancer and antioxidant potential. Bioorg Chem 87: 821-837.

AFTAB H ET AL. 2024. Synthesis, *in vitro* biological evaluation and *in silico* studies of novel pyrrolidine derived thiosemicarbazones as dihydrofolate reductase inhibitors. RSC Adv 14: 31409-31421.

ALDHAHRANI A, ALSHAYE NA, ALSHAYA DS, MOHAMED DA, FAYAD E, SOPHY MAE, AL-ASHGER NA, SALEM MG & FAROUK NA. 2025. In Vitro biological evaluation of some hybrid molecules bearing 2-quinoline as anti-inflammatory and anti-cancer agents. J Mol Struct 1326: 141060.

ALQAHTANI AM & BAYAZEED AA. 2020. Synthesis and antiproliferative activity studies of new functionalized pyridine linked thiazole derivatives. Arab J Chem 14: 102914.

AMIN A, QADIR T, SHARMA PK, JEELANI I & ABE H. 2022. A Review on The Medicinal And Industrial Applications of N-Containing Heterocycles. Open Med Chem J 16: 1874-1045.

ARYA GC, MEHLA S & SINGH L. 2025. Hybrid anticancer agents: Design, development, and therapeutic potential. Lett Drug Des Discov 22: 100265.

ASSALEH MH, BJELOGRLIC SK, PRLAINOVIC N, CVIJETIC I, BOZIC A, ARANDJELOVIC I, VUKOVIC D & MARINKOVIC A. 2022. Antimycobacterial and anticancer activity of newly designed cinnamic acid hydrazides with favorable toxicity profile. Arab J Chem 15: 103532.

AWAJI AA, ALHAMDI HW, ALSHEHRI KM, ALFAIFI MY, SHATI AA, ELBEHAIRI SEI, RADWAN NAF, HAFEZ HS, ELSHAARAWY RFM & WELSON M. 2024. Bio-molecular Fe(III) and Zn(II) complexes stimulate the interplay between PI3K/AKT1/EGFR inhibition and induce autophagy and apoptosis in epidermal skin cell cancer. J Inorg Biochem 262: 112720.

AZIMI F, MAHDAVI M, KHOSHNEVISZADEH M, SHAFIEE F, AZIMI M, HASSANZADEH F & ASHRAFEE FH. 2024. Kinetic studies, molecular docking, and antioxidant activity of novel 1,3-diphenyl pyrazole-thiosemicarbazone with anti-tyrosinase and anti-melanogenesis properties. Bioorg Chem 152: 107722.

BABAHAN-BIRCAN I, EMIRDAĞ S, ÖZMEN A, ABBAK M, UJAM OT, DEMIRKAYA I & GÜNAY ME. 2022. A new hybrid ligand and its metal complexes from a natural plant (*Styrax officinalis*) bearing egonol, thiosemicarbazone and oxime units, and their anti-cancer activities. Appl Organomet Chem 36: e6784.

BACHER F, DÖMÖTÖR O, CHUGUNOVA A, NAGY NV, FILIPOVIĆ L, RADULOVIĆ S, ENYEDY ÉA & ARION VB. 2015. Strong effect of copper(II) coordination on antiproliferative activity of thiosemicarbazone–piperazine and thiosemicarbazone–morpholine hybrids. Dalton Trans 44: 9071-9090.

BAI C, WU S, REN S, ZHU M, LUO G & XIANG H. 2021. Synthesis and evaluation of novel thiosemicarbazone and semicarbazone analogs with both anti-proliferative and anti-metastatic activities against triple negative breast cancer. Bioorg Med Chem 37: 116107.

BAKHERAD Z, SAFAVI M, FASSIHI A, SADEGHI-ALIABADI H, BAKHERAD M, RASTEGAR H, GHASEMI JB, SEPEHRI S, SAGHAIE L & MAHDAVI M. 2019. Anti-cancer, anti-oxidant and molecular docking studies of thiosemicarbazone indole-based derivatives. Res Chem Intermed 45: 2827-2854.

BATOOL Z, ULLAH S, KHAN A, SIDDIQUE F, NADEEM S, ALSHAMMARI A, ALBEKAIRI NA, TALIB R, AL-HARRASI A & SHAFIQ Z. 2024. Design, synthesis, and *in vitro* and *in silico* study of 1-benzyl-indole hybrid thiosemicarbazones as competitive tyrosinase inhibitors. RSC Adv 14: 28524-28542.

BAYAZEED A, ALNOMAN RB, ALATAWI K, ALATAWI OM, ALQAHTANI AM, MOJALLY M, ALENAZI NA & EL-METWALY NM. 2023. Synthesis, molecular modeling and bioactivity of new bis-thiazole, thiazole-pyrazole, and thiazole-pyridine analogues. J Saudi Chem Soc 27: 101754.

BIMOUSSA A, HACHIM ME, KHATABI KE, LAAMARI Y, OUBELLA A, ALAJMI MF, AUHMANI A, AJANA MA, MORJANI H & ITTO MYA. 2024. Semicarbazone, thiosemicarbazone tailed isoxazoline-pyrazole: synthesis, DFT, biological and computational assessment. Future Med Chem 16: 2073-2086.

BLÁZQUEZ-TAPIAS B, HALDER S, MENDIOLA MA, ROY N, SAHU N, SINHA C, JANA K & LÓPEZ-TORRES E. 2024. New Tin (IV) and Organotin (IV) Complexes with a Hybrid Thiosemicarbazone/Hydrazone Ligand: Synthesis, Crystal Structure, and Antiproliferative Activity. Bioinorg Chem Appl 2024: 1-16.

BONDOCK S, ALBARQI T, ABBOUD M, NASR T, MOHAMED NM & ABDOU MM. 2023. Tail-approach based design, synthesis, and cytotoxic evaluation of novel disubstituted and trisubstituted 1,3-thiazole benzenesulfonamide derivatives with suggested carbonic anhydrase IX inhibition mechanism. RSC Adv 13: 24003-24022.

CAMPOS MC, BARBOSA IR, GUEDES GP, ECHEVARRIA A, ECHEVARRIA-LIMA J & CHAVES OA. 2023. Novel Zn(II)-complex with hybrid chalcone-thiosemicarbazone ligand: Synthesis, characterization, and inhibitory effect on HTLV-1-infected MT-2 leukemia cells. J Inorg Biochem 245: 112239.

CARDOSO MVDO ET AL. 2015. Design, synthesis and structure–activity relationship of phthalimides endowed with dual antiproliferative and immunomodulatory activities. Eur J Med Chem 96: 491-503.

CHAUDHARY U, DAWA D, BANERJEE I, SHARMA S, MAHIYA K, RAUF A, POKHAREL YR & YADAV PN. 2023. Anticancer potency of N(4)-ring incorporated-5-methoxyisatin thiosemicarbazones. J Mol Struct 1274: 134549.

CHAUDHARY U, KUMAR P, SHARMA P, CHIKARA A, BARUA A, MAHIYA K, SUBIN JA, YADAV PN & POKHAREL YR. 2024. Synthesis of 5-hydroxyisatin thiosemicarbazones, spectroscopic investigation, protein-ligand docking, and in vitro anticancer activity. Bioorg Chem 153: 107872.

DOBROVA A, PLATZER S, BACHER F, MILUNOVIC MNM, DOBROV A, SPENGLER G, ENYEDY ÉA, NOVITCHI G & ARION VB. 2016. Structure–antiproliferative activity studies onL-proline- and homoproline-4-N-pyrrolidine-3-thiosemicarbazone hybrids and their nickel(II), palladium(II) and copper(II) complexes. Dalton Trans 45: 13427-13439.

DZITKO K, KAPROŃ B, PANETH A, BEKIER A, PLECH T, PANETH P & TROTSKO N. 2023. TZD-Based Hybrid Molecules Act as Dual Anti-Mycobacterium tuberculosis and Anti-Toxoplasma gondii Agents. Int J Mol Sci 24: 2069.

EL MALAH T, FARAG H & SHAMROUKH AH. 2024. Synthesis, Characterization, and Molecular Docking of Novel Isatin-thiosemicarbazone Containing 1,2,3-triazole Derivatives as Potential Anti-cancer Agents. Curr Org Chem 29: 1050-1056.

EL-ADL K ET AL. 2021. Design, synthesis, and anti-proliferative evaluation of new quinazolin-4(3H)-ones as potential VEGFR-2 inhibitors. Bioorg Med Chem 29: 115872.

ELKAFOURY EM, EL-HAMAMSY MH, EL-BASTAWISSY EA, AFARINKIA K & ABOUKHATWA SM. 2024. Synergy trap for guardian angels of DNA: Unraveling the anticancer potential of phthalazinone-thiosemicarbazone hybrids through dual PARP-1 and TOPO-I inhibition. Bioorg Chem 153: 107924.

ELSAYED HE, EBRAHIM HY, HAGGAG EG, KAMAL AM & EL SAYED KA. 2017. Rationally designed hecogenin thiosemicarbazone analogs as novel MEK inhibitors for the control of breast malignancies. Bioorg Med Chem 25: 6297-6312.

ESAM Z, AKHAVAN M, MIRSHAFA A & BEKHRADNIA A. 2023. Green synthesis, anti-proliferative evaluation, docking, and MD simulations studies of novel 2-piperazinyl quinoxaline derivatives using hercynite sulfaguanidine-SA as a highly efficient and reusable nanocatalyst. RSC Adv 13: 25229-25245.

FARGHALY TA, ABO ALNAJA AM, EL-GHAMRY HA & SHAABAN MR. 2020. Synthesis and DNA binding of novel bioactive thiazole derivatives pendent to N-phenylmorpholine moiety. Bioorg Chem 102: 104103.

FAYED EA, AMMAR YA, RAGAB A, GOHAR NA, MEHANY AB & FARRAG AM. 2020. In vitro cytotoxic activity of thiazole-indenoquinoxaline hybrids as apoptotic agents, design, synthesis, physicochemical and pharmacokinetic studies. Bioorg Chem 100: 103951.

FREITAS LAB ET AL. 2024. Thiazolyl-isatin derivatives: Synthesis, in silico studies, in vitro biological profile against breast cancer cells, mRNA expression, P-gp modulation, and interactions of Akt2 and VIM proteins. Chem-Biol Interac 394: 110954.

GAZIEVA GA, ANIKINA LV, PUKHOV SA, KARPOVA TB, NELYUBINA YV & KRAVCHENKO AN. 2016. Substituted N-aminothioglycolurils containing thiosemicarbazone moiety and their cytotoxic activity in vitro. Mol Divers 20: 837-846.

GEDIYA LK & NJAR VC. 2009. Promise and challenges in drug discovery and development of hybrid anticancer drugs. Expert Opin Drug Discov 4: 1099-1111.

GOMHA SM, ZAKI MEA, MALIWAL D, PISSURLENKAR RRS, IBRAHIM MS, FATHALLA M & HUSSEIN AM. 2023. Synthesis, in-silico studies, and biological evaluation of some novel 3-thiazolyl-indoles as CDK2–inhibitors. Results Chem 6: 101209.

GUO C ET AL. 2019. Discovery of Novel Bromophenol–Thiosemicarbazone Hybrids as Potent Selective Inhibitors of Poly(ADP-ribose) Polymerase-1 (PARP-1) for Use in Cancer. J Med Chem 62: 3051-3067.

GUO C, ZHANG F, WU X, YU X, WU X, SHI D & WANG L. 2020. BTH-8, a novel poly (ADP-ribose) polymerase-1 (PARP-1) inhibitor, causes DNA double-strand breaks and exhibits anticancer activities in vitro and in vivo. Int J Biol Macromol 150: 238-245.

HAMAD HT. 2025. The anti-cancer effectiveness of some heterocyclic compounds containing sulfur atom. Results Chem 15: 102182.

HASSAN EA, EBRAHIUM MM, AL-HAKIMI AN, MORSY NA & EBRAHIUM AM. 2025. Azo-thiosemicarbazone transition metal complexes: synthesis, structural characterization, theoretical insights, and anticancer and antimicrobial activities. J Mol Struct 1341: 142610.

JAMPILEK J. 2019. Heterocycles in Medicinal Chemistry. Heterocycles Med Chem 24: 3839.

JANKOVIĆ ĐD, ŠESTIĆ TLj, BEKIĆ SS, SAVIĆ MP, ĆELIĆ AS, SCHOLDA J, KOPP F, MARINOVIĆ MA, PETRI ET & AJDUKOVIĆ JJ. 2024. Development of new steroid-based hydrazide and (thio) semicarbazone compounds with anticancer properties. J Steroid Biochem Mol Biol 242: 106545.

KARP JE, GILES FJ, GOJO I, MORRIS L, GREER J, JOHNSON B, THEIN M, SZNOL M & LOW J. 2008. A Phase I study of the novel ribonucleotide reductase inhibitor 3-aminopyridine-2-carboxaldehyde thiosemicarbazone (3-AP, Triapine®) in combination with the nucleoside analog fludarabine for patients with refractory acute leukemias and aggressive myeloproliferative disorders. Leuk Res 32: 71-77.

KASSEM AF, SEDIEK AA, OMRAN MM, FODA DS & AL-ASHMAWY AAK. 2024. Design, synthesis and *in vitro* anti-proliferative evaluation of new pyridine-2,3-dihydrothiazole/thiazolidin-4-one hybrids as dual CDK2/GSK3β kinase inhibitors. RSC Adv 14: 31607-31623.

KOÇYIĞIT ÜM, DOĞAN M, MUĞLU H, TASLIMI P, TÜZÜN B, YAKAN H, BAL H, GÜZEL E & GÜLÇIN İ. 2022. Determination of biological studies and molecular docking calculations of isatin-thiosemicarbazone hybrid compounds. J Mol Struct 1264: 133249.

KUMAR S, SAHA ST, GU L, PALMA G, PERUMAL S, SINGH-PILLAY A, SINGH P, ANAND A, KAUR M & KUMAR V. 2018. 1*H*-1,2,3-Triazole Tethered Nitroimidazole–Isatin Conjugates: Synthesis, Docking, and Anti-Proliferative Evaluation against Breast Cancer. ACS Omega 3: 12106-12113.

LAAMARI Y, BIMOUSSA A, FAWZI M, OUBELLA A, ROHAND T, MEERVELT LV, ITTO MYA, MORJANI H & AUHMANI A. 2023. Synthesis, crystal structure and evaluation of anticancer activities of some novel heterocyclic compounds based on thymol. J Mol Struct 1278: 134906.

LAAMARI Y ET AL. 2025a. Exploration of new thiazolidinones derived from natural verbenone: Design, synthesis, characterization, and in silico evaluation of alkaline phosphatase and carbonic anhydrase-II inhibition activity. J Mol Struct 1322: 140332.

LAAMARI Y ET AL. 2025b. New isoxazoline-linked 1,3,4-thiadiazole derivatives: Synthesis, antiproliferative activity, molecular docking, molecular dynamics and DFT. J Mol Struct 1319: 139368.

LEATH CA ET AL. 2025. Incorporation of triapine (T) to cisplatin chemoradiation (CRT) for locally advanced cervical and vaginal cancer: Results from NRG-GY006, a phase III randomized trial. Gynecol Oncol 195: 122-133.

MAHDY HA ET AL. 2020. Design, synthesis, molecular modeling, in vivo studies and anticancer evaluation of quinazolin-4(3H)-one derivatives as potential VEGFR-2 inhibitors and apoptosis inducers. Bioorg Chem 94: 103422.

MAHMOUD HK, ABDELHADY HA, ELAASSER MM, HASSAIN DZH & GOMHA SM. 2022. Microwave-Assisted One-Pot Three Component Synthesis of Some Thiazolyl(Hydrazonoethyl) Thiazoles as Potential Anti-Breast Cancer Agents. Polycycl Aromat Compd 42: 7232-7246.

MAHMOUD HK, FARGHALY TA, ABDULWAHAB HG, AL-QURASHI NT & SHAABAN MR. 2020. Novel 2-indolinone thiazole hybrids as sunitinib analogues: Design, synthesis, and potent VEGFR-2 inhibition with potential anti-renal cancer activity. Eur J Med Chem 208: 112752.

MARQUES KM ET AL. 2019. 5-Nitro-Thiophene-Thiosemicarbazone Derivatives Present Antitumor Activity Mediated by Apoptosis and DNA Intercalation. Curr Top Med Chem 19: 1075-1091.

MARSHALL CM, FEDERICE JG, BELL CN, COX PB & NJARDARSON JT. 2024. An Update on the Nitrogen Heterocycle Compositions and Properties of U.S. FDA-Approved Pharmaceuticals (2013–2023). J Med Chem 67: 11622-11655.

MCDEVITT MA ET AL. 2011. Final Results From a Phase II Trial of Triapine® Plus Fludarabine for Adults with Aggressive Myeloproliferative Disorders. Blood 118(21): 1755.

MILUNOVIĆ MNM, DOBROVA A, NOVITCHI G, GLIGORIJEVIĆ N, RADULOVIĆ S, KOŽIŠEK J, RAPTA P, ENYEDY EA & ARION VB. 2017. Effects of Terminal Substitution and Iron Coordination on Antiproliferative Activity of L-Proline-salicylaldehyde–Thiosemicarbazone Hybrids. Eur J Inorg Chem 2017: 4773-4783.

MILUNOVIC MNM ET AL. 2024. Copper(II) Complexes with Isomeric Morpholine-Substituted 2-Formylpyridine Thiosemicarbazone Hybrids as Potential Anticancer Drugs Inhibiting Both Ribonucleotide Reductase and Tubulin Polymerization: The Morpholine Position Matters. J Med Chem 67: 9069-9090.

MOHAMED DM, KHEDER NA, SHARAKY M, NAFIE MS, DAWOOD KM & ABBAS AA. 2024. Synthesis of novel piperazine-based bis(thiazole)(1,3,4-thiadiazole) hybrids as anti-cancer agents through caspase-dependent apoptosis. RSC Adv 14: 24992-25006.

MOHAMMED FZ, RIZZK YW, EL DEEN IM, MOURAD AAE & EL BEHERY M. 2021. Design, Synthesis, Cytotoxic Screening and Molecular Docking Studies of Novel Hybrid Thiosemicarbazone Derivatives as Anticancer Agents. Chem Biodivers 18: e2100580.

MOURAD AAE, RIZZK YW, ZAKI I, MOHAMMED FZ & EL BEHERY M. 2021. Synthesis and cytotoxicity screening of some synthesized hybrid nitrogen molecules as anticancer agents. J Mol Struct 1242: 130722.

MUSHTAQ A, ASIF R, HUMAYUN WA & NASEER MM. 2024. Novel isatin–triazole based thiosemicarbazones as potential anticancer agents: synthesis, DFT and molecular docking studies. RSC Adv 14: 14051-14067.

NEPALI K, SHARMA S, SHARMA M, BEDI PMS & DHAR KL. 2014. Rational approaches, design strategies, structure activity relationship and mechanistic insights for anticancer hybrids. Eur J Med Chem 77: 422-487.

OHUI K ET AL. 2019. New Water-Soluble Copper(II) Complexes with Morpholine–Thiosemicarbazone Hybrids: Insights into the Anticancer and Antibacterial Mode of Action. J Med Chem 62: 512-530.

OLIVEIRA AR, DOS SANTOS FA, FERREIRA LPDL, PITTA MGDR, SILVA MVDO, CARDOSO MVDO, PINTO AF, MARCHAND P, RÊGO MJBR & LEITE ACL. 2021. Synthesis, anticancer activity and mechanism of action of new phthalimido-1,3-thiazole derivatives. Chem Biol Interact 347: 109597.

OLIVEIRA GP ET AL. 2025. Palladium(II) and platinum(II) thiophene-based thiosemicarbazones: Synthesis, properties, and anticancer studies. J Mol Struct 1322: 140306.

OLIVEIRA JF ET AL. 2015. Synthesis of thiophene-thiosemicarbazone derivatives and evaluation of their *in vitro* and *in vivo* antitumor activities. Eur J Med Chem 104: 148-156.

OTHMAN EM, FAYED EA, HUSSEINY EM & ABULKHAIR HS. 2022. The effect of novel synthetic semicarbazone- and thiosemicarbazone-linked 1,2,3-triazoles on the apoptotic markers, VEGFR-2, and cell cycle of myeloid leukemia. Bioorg Chem 127: 105968.

OUBELLA A, BYADI S, BIMOUSSA A, FAWZI M, AUHMANI A, PODLIPNIK C, MORJANI H, RIAHI A, ROBERT A & ITTO MYA. 2022. Novel isoxazoline-linked 1,3,4-thiadiazole hybrids as anticancer agents: Design, synthesis, biological evaluation, molecular docking, and molecular dynamics simulation. Arch Pharm (Weinheim) 355: e2200066.

PANETH A, KAPROŃ B, PLECH T, PADUCH R, TROTSKO N & PANETH P. 2023. Combined In Silico and In Vitro Analyses to Assess the Anticancer Potential of Thiazolidinedione–Thiosemicarbazone Hybrid Molecules. Int J Mol Sci 24: 17521.

PATHANIA S, NARANG RK & RAWAL RK. 2019. Role of sulphur-heterocycles in medicinal chemistry: An update. Eur J Med Chem 180: 486-508.

PETRASHEUSKAYA TV ET AL. 2022. Estradiol-Based Salicylaldehyde (Thio)Semicarbazones and Their Copper Complexes with Anticancer, Antibacterial and Antioxidant Activities. Molecules 28: 54.

PETRASHEUSKAYA TV, KISS MA, DÖMÖTÖR O, HOLCZBAUER T, MAY NV, SPENGLER G, KINCSES A, ČIPAK GAŠPAROVIĆ A, FRANK É & ENYEDY ÉA. 2020. Salicylaldehyde thiosemicarbazone copper complexes: impact of hybridization with estrone on cytotoxicity, solution stability and redox activity. New J Chem 44: 12154-12168.

PETRASHEUSKAYA TV, WERNITZNIG D, KISS MA, MAY NV, WENISCH D, KEPPLER BK, FRANK É & ENYEDY ÉA. 2021. Estrone–salicylaldehyde N-methylated thiosemicarbazone hybrids and their copper complexes: solution structure, stability and anticancer activity in tumour spheroids. JBIC J Biol Inorg Chem 26: 775-791.

PINHEIRO P, FRANCO LS, MONTAGNOLI TL & FRAGA CAM. 2024. Molecular hybridization: a powerful tool for multitarget drug discovery. Expert Opin Drug Discov 19: 451-470.

SANTOS TAR, DA SILVA AC, SILVA EB, GOMES PATDM, ESPÍNDOLA JWP, CARDOSO MVDO, MOREIRA DRM, LEITE ACL & PEREIRA VRA. 2016. Antitumor and immunomodulatory activities of thiosemicarbazones and 1,3-Thiazoles in Jurkat and HT-29 cells. Biomed Pharmacother 82: 555-560.

SASHIDHARA KV, SINGH LR, SHAMEEM M, SHAKYA S, KUMAR A, LAXMAN TS, KRISHNA S, SIDDIQI MI, BHATTA RS & BANERJEE D. 2016. Design, synthesis and anticancer activity of dihydropyrimidinone–semicarbazone hybrids as potential human DNA ligase 1 inhibitors. MedChemComm 7: 2349-2363.

ŠESTIĆ TL ET AL. 2025. Heterocyclic androstane derivatives targeting hormone-related cancers: Synthesis, bioactivity and docking studies. Eur J Med Chem 296: 117850.

SHALINI & KUMAR V. 2021. Have molecular hybrids delivered effective anti-cancer treatments and what should future drug discovery focus on? Expert Opin Drug Discov 16: 335-363.

SINGH AK ET AL. 2022. Concept of Hybrid Drugs and Recent Advancements in Anticancer Hybrids. Pharmaceuticals 15: 1071.

SINGH H & AGRAWAL DK. 2022. Recent advances in the development of active hybrid molecules in the treatment of cardiovascular diseases. Bioorg Med Chem 62: 116706.

SINGH PK & SILAKARI O. 2018. The Current Status of O-Heterocycles: A Synthetic and Medicinal Overview. ChemMedChem 13: 1071-1087.

SOUSA GLS ET AL. 2024. Design, synthesis and antiproliferative evaluation of new acridine-thiosemicarbazone derivatives as topoisomerase IIα inhibitors. Results Chem 7: 101371.

STEPANENKO I, BABAK MV, SPENGLER G, HAMMERSTAD M, POPOVIC-BIJELIC A, SHOVA S, BÜCHEL GE, DARVASIOVA D, RAPTA P & ARION VB. 2021. Coumarin-Based Triapine Derivatives and Their Copper(II) Complexes: Synthesis, Cytotoxicity and mR2 RNR Inhibition Activity. Biomolecules 11: 862.

TOAN VN & THANH ND. 2021. Synthesis and antiproliferative activity of hybrid thiosemicarbazone derivatives bearing coumarin and d-galactose moieties with EGFR inhibitory activity and molecular docking study. Med Chem Res 30: 1868-1885.

UCAR O, OZTURK II, GRZEŚKIEWICZ AM, KUBICKI M, BANTI C & HADJIKAKOU SK. 2025. Synthesis, structural characterization, and biological evaluation of novel antimony(III) thiosemicarbazone complexes with uncommon geometries. Inorg Chim Acta 581: 122627.

VIEGAS-JUNIOR C, DANUELLO A, BOLZANI VS, BARREIRO EJ & FRAGA CAM. 2007. Molecular Hybridization: A Useful Tool in the Design of New Drug Prototypes. Curr Med Chem 14: 1829-1852.

VIJAYAN P, VISWANATHAMURTHI P, VELMURUGAN K, NANDHAKUMAR R, BALAKUMARAN MD, KALAICHELVAN PT & MALECKI JG. 2015. Nickel(II) and copper(II) complexes constructed with N_2S_2 hybrid benzamidine–thiosemicarbazone ligand: synthesis, X-ray crystal structure, DFT, kinetico-catalytic and in vitro biological applications. RSC Adv 5: 103321-103342.

YAKAN H, AZAM M, KANSIZ S, MUGLU H, ERGUL M, TASLIMI P, KOÇYİĞİT ÜM, KARAMAN M, AL-RESAYES SI & MIN K. 2023. Isatin/thiosemicarbohydrazone hybrids: Facile synthesis, and their evaluation as anti-proliferative agents and metabolic enzyme inhibitors. Bull Chem Soc Ethiop 37: 1221-1236.

YEE EMH, BRANDL MB, BLACK DS, VITTORIO O & KUMAR N. 2017. Synthesis of isoflavene-thiosemicarbazone hybrids and evaluation of their anti-tumor activity. Bioorg Med Chem Lett 27: 2454-2458.

ZALTARIOV MF ET AL. 2017. New Iminodiacetate–Thiosemicarbazone Hybrids and Their Copper(II) Complexes Are Potential Ribonucleotide Reductase R2 Inhibitors with High Antiproliferative Activity. Inorg Chem 56: 3532-3549.

ZHAI X, BAO G, WANG L, CHENG M, ZHAO M, ZHAO S, ZHOU H & GONG P. 2016. Design, synthesis and biological evaluation of novel 4-phenoxy-6,7-disubstituted quinolines possessing (thio)semicarbazones as c-Met kinase inhibitors. Bioorg Med Chem 24: 1331-1345.

ZHANG Y ET AL. 2024. Design of Selective PARP-1 Inhibitors and Antitumor Studies. J Med Chem 67: 8877-8901.

CAIO VICTOR S. SOARES[1]
https://orcid.org/0009-0000-1184-6405

JOÃO PEDRO P. GOMES[1,2]
https://orcid.org/0009-0003-8744-3583

ANTONIO MIGUELSINHO M. DE SOUSA FILHO[1,2]
https://orcid.org/0009-0009-2562-9378

LUIZ VITOR O. LIMA[1]
https://orcid.org/0009-0005-1226-2053

CIDLA S. MARINHO[1]
https://orcid.org/0009-0005-4612-1056

ANA KAROLINE R. NOVAIS[1]
https://orcid.org/0000-0001-5004-9687

MARIA DO CARMO A. DE LIMA[3]
https://orcid.org/0000-0002-8277-3458

JAMERSON F. DE OLIVEIRA[1,2]
https://orcid.org/0000-0001-9606-8154

[1]Universidade da Integração Internacional da Lusofonia Afro-Brasileira (Unilab), Instituto de Ciências da Saúde, R. José Franco de Oliveira, s/n, Zona Rural, 62790-970 Redenção, CE, Brazil

[2]Universidade Federal do Ceará (UFC), Programa de Pós-Graduação em Ciências Farmacêuticas, R. Capitão Francisco Pedro, 1210, Rodolfo Teófilo, 60430-370 Fortaleza, CE, Brazil

[3]Universidade Federal de Pernambuco (UFPE), Centro de Biociências, Av. Professor Moraes Rego, 1235, Cidade Universitária, 50670-901 Recife, PE, Brazil

Correspondence to: Jamerson Ferreira de Oliveira
E-mail: jamerson@unilab.edu.br

Author contributions

All authors researched data for the article, contributed substantially to discussion of the content, wrote the article and reviewed and edited the manuscript before submission. The authors declare that they have no known competing financial interests or personal relationships that could have appeared to influence the work reported in this paper.

How to cite

SOARES CVS, GOMES JPP, DE SOUSA FILHO AMM, LIMA LVO, MARINHO CS, NOVAIS AKR, DE LIMA MCA & DE OLIVEIRA JF. 2026. Thiosemicarbazone-based Molecular Hybrids as Prototypes for Antitumor Drugs: Recent Advances in the Last Decade. An Acad Bras Cienc 98: e20260029. DOI 10.1590/0001-3765202620260029.

Manuscript received on January 23, 2026;
accepted for publication on August 3, 2026

Handling editor

Yraima Cordeiro

Data availability

As this is a review article, no new data were generated during this study.

CC BY